Science
AAAS

Supplementary Materials for

Multi-omics landscape and molecular basis of radiation tolerance in a tardigrade

Lei Li *et al*.

Corresponding authors: Guangyi Fan, fanguangyi@genomics.cn; Lizhi Wang, rj_wl@126.com; Dong Yang, yangdong@ncpsb.org.cn; Lingqiang Zhang, zhanglq@nic.bmi.ac.cn

Science **386**, eadl0799 (2024)
DOI: 10.1126/science.adl0799

The PDF file includes:

Other Supplementary Material for this manuscript includes the following:

Materials and Methods

Materials
Materials are listed in tables S15 and S16.

Methods

Tardigrade culture
A tardigrade culturing system has been successfully established in 2020 in our laboratory (*30*) by modifying the culturing methods for *Ramazzottius varieornatus* and *Hybsibius exemplaris* (*92, 93*) [the tardigrade *Hypsibius dujardini* Z151 strain and/or sourced from Sciento in studies prior to 2018 was actually *Hypsibius exemplaris*, not *Hybsibius dujardini* (*12, 94*)]. In brief, mosses in which tardigrades live were collected from Laojieling area of the Funiu Mountain in Henan Province, China (33°38′56.90" N, 111°46′30.95" E) at 1200 m a.s.l. Mosses were rehydrated to let the animals recover from cryptobiosis. The moss samples were immersed in pure water (Milli-Q, likewise below) for several hours to let the animals recover from cryptobiosis; and active tardigrades were extracted from the samples, picked up with a pipette, and transferred to culture dishes under a stereomicroscope (Nikon, SMZ745T). Animals were reared on a Petri dish (35 mm in diameter) that contained approximately 2mL pure water. Approximately 2 mL 1.5% agar gel was layered at the bottom of the dishes. The green alga *Chlorococcum humicola* was added to the dishes as a food source. Culture dishes were covered with lids, placed in an incubator with 20℃ and 80% relative humidity, and kept with a photoperiod of 12 hours of light and 12 hours of darkness each day. Animals were transferred to new culture dishes by a pipette every 1 to 2 weeks. In our established rearing system, the tardigrades grew successfully and produced further generations. After that, a laboratory population was founded by a single animal with the established rearing system. All the tardigrades used in this study originate from this laboratory population.

Detailed morphological and molecular analysis in this study indicated that the tardigrade reared in our lab was *Hypsibius henanensis* **sp. nov.**, a new tardigrade species of the *Hypsibius dujardini* morphogroup (see the following methods and the supplementary text for detailed information).

For large-scale culture, tardigrades were cultured in in Petri dishes (150 mm in diameter) with pure water and no agar gel was layered at the bottom. The green alga *Chlorococcum humicola* was added to the dishes as a food source.

Microscopy and imaging for tardigrades
Specimens for light microscopy were picked directly from Petri dishes under a stereomicroscope and were mounted in Hoyer's medium (*95*). 20 adults and 6 eggs were collected. A Nikon 90i microscope equipped with phase contrast objectives and a Nikon DS-Fil digital camera was used for observation, capturing images and measurement.

Specimens for imaging in the scanning electron microscope (SEM) were prepared according to Stec *et al.* (*81*) with minor modifications. Briefly, tardigrades were placed in warm water (60℃). Then specimens were dehydrated in a water/ethanol series (from 0% to 100% ethanol, with 10% increments), critical point dried in CO_2, mounted on SEM stubs covered with double-sided conductive tape and sputter coated with a thin layer of gold. A EVOLS10 + Suttle & find (ZEISS) Scanning Electron Microscope were used for observations.

Morphometrics

Measurements were made using the imbedded measurement software NIS-Elements (D, Nikon). Measurements, in micrometers (μm), were made only if the body or structures were in the proper orientation. Body length was measured from the rostral end to the terminal end of the body, excluding hind legs. Buccal tube widths were measured as the external diameters at the level of the stylet support insertion point. Lengths of the claw branches were measured from the base of the claw to the top of the branch, including accessory points. The *pt* index is the percent ratio of the length of a given structure to the length of the buccal tube measured from the stylet sheath opening to the end of the buccal tube(*96*).

Genotyping

After 2 days starvation and antibiotics treatment, tardigrades were extensively cleansed and genomic DNA was extracted individually using a Quick-gDNA MicroPrep kit. The cleaned animal was transferred to a low-binding PCR tube with minimal water (< 5 μL), to which a 200 μL genomic lysis buffer with 0.5% beta-mercaptoethanol was added immediately. The animal was lysed using three freeze-thaw cycles of −80℃ and 37℃ incubation, and genomic DNA was extracted following manufacturer's protocol.

Genotyping was performed according to the methods described (*12, 81*). We sequenced four DNA fragments for genotyping: a small ribosome subunit (18S rRNA), a large ribosome subunit (28S rRNA), an internal transcribed spacer (ITS-2) and cytochrome oxidase subunit I (COI). Both 18S rRNA and 28S rRNA are nuclear markers that can be applied in phylogenetic analyses to investigate high taxonomic levels (*12, 81, 97, 98*). ITS-2 is a non-coding nuclear fragment with high evolution rates that is suitable for both intra-specific comparisons and comparisons between closely related species (*12, 81, 98, 99*). COI is a protein-coding mitochondrial marker that is widely used as a standard barcode gene of intermediate effective mutation rate (*12, 81, 98, 100*). Primers and specific PCR programs were described in previous reports (*12, 81*). PCR products were sequenced. The obtained sequences were trimmed to delete ambiguous regions and primers using SnapGene (v3.1.1). The four marker sequences were uploaded in GenBank database and their accession numbers were listed in table S3.

The pairwise p-distance among the *H. henanensis* **sp. nov.** and other 4 known species (table S4) in the genus *Hypsibius* were calculated using MEGA (v11.0.13) software (*101*). The aligned sequences were then trimmed to 558 and 443 bp (for the COI and ITS-2 fragments, respectively). For COI, codon positions included were 1st+2nd+3rd.

For the phylogeny analysis, the *H. henanensis* **sp. nov.** and other 45 known species in the family Hipsibiidae were involved (table S4), with *Ramazzottius varieornatus* as an outgroup. As for the species selection, we referenced a recently published article about the systematics of Hipsibiidae (*98*). The nucleotide sequences of them were downloaded from GenBank (table S4). 18S rRNA, 28S rRNA, and ITS-2 sequences were aligned via MAFFT (v7.407) (*102*) with the G-INS-I method (*86, 103*). COI sequences were first translated with the invertebrate mitochondrial code to check pseudogene, and then aligned with the MAFFT with '-auto' option. All sequences were trimmed with trimAl (v1.4.1) (*104*). Sequences were concatenated with phyloSuite (v1.2.3) (*105*), and model selection for each alignment partition (6 in total: 18S, 28S, ITS-2, and three COI codons) was performed with PartitionFinder (v2.1.1) (*106*). Maximum likelihood (ML) tree reconstruction using concatenated sequences was constructed with IQ-TREE (v2.1.4) (*107*). Then we used iTOL (https://itol.embl.de/) software to draw the phylogenetic tree.

For species delimitation, Bayesian Poisson tree processes (bPTP) (*82*), Bayesian Phylogenetics and Phylogeography (BPP) (*83, 84*) and Assemble Species by Automatic Partitioning (ASAP) (*85*) were used. Sequences representing four markers (18S rRNA, 28S rRNA, ITS-2, and COI) were concatenated and then used to bulid maximum likelihood (ML) phylogenetic tree, which was

treated as guide tree in BPP analysis (*Hypsibius* sp., taxonomy ID 2961725, was used as outer group). Sequences of four markers were downloaded from GenBank or produced *de novo* (tables S3 and S4). The methods utilized for sequence alignment, concatenation, partitioning, and tree building were identical to those described in the previous section for phylogeny analysis. COI sequences were used for BPP analysis (v4.0) (*83*) (thetaprior = 3 0.002 e, tauprior = 3 0.030), and two independent runs were carried out to confirm consistency between runs. For bPTP, a tree-based (bPTP) method was performed on COI tree (*Hypsibius* sp. was outer group), single gene alignments and ML tree were produced as described above. Then, bPTP analysis were performed with 100,000 generations, a thinning of 100 generations and 10% burn in (*86*). COI alignments were uploaded to the ASAP webpage (https://bio.tools/asap-assemble) and analyzed with default parameters.

Anhydrobiotic induction and recovery

Anhydrobiotic induction and recovery was performed according to the protocols described by Hengherr *et al.* (*108*). Briefly, after thoroughly washed with pure water, 30 animals were transferred into 0.2 mL tubes and residual water was removed using a micropipette. The open tubes were then exposed to 85% relative humidity (RH) in a small chamber containing a saturated solution of KCl for 48 hours and then dried at 35% RH for an additional 5 days in a chamber containing a saturated solution of $MgCl_2$. Anhydrobiotic tardigrades were rehydrated by adding 100 μL pure water to the microliter tubes. The animals required 20-30 min to resume motility. Rehydration was monitored using a stereomicroscope. Tardigrades were assumed to be dead if there was no movement visible.

Radiation treatment

For heavy ion irradiation, the samples were irradiated with carbon ions $^{12}C^{6+}$ (80 MeV/u, with an LET of ~50 keV/μm) at the doses 200 and 2,000 Gy. These irradiations were made at the Heavy Ion Research Facility in Lanzhou (HIRFL) at the Institute of Modern Physics (IMP), Chinese Academy of Sciences (CAS). Control samples (0 Gy) were kept in the HIRFL facility without irradiation. γ-ray irradiation was performed in a ^{137}Cs source (Beijing Institute of Radiation Medicine) at a dose rate of 8 Gy/min at room temperature. X-ray irradiation was delivered by an X-RAD 160 X-ray irradiator (Precision X-ray Inc.) at a dose rate of 1.9 Gy/min at room temperature. In all irradiation campaigns, three samples per dose were prepared.

In order to evaluate the effect of γ-ray irradiation on survival of adults, groups of 20 adults were selected and placed in 6-well plates with 2 mL of pure water. Irradiation of the samples was performed at room temperature at the following doses: 0, 200, 500, 1000, 2000, 3000, 4000, and 5000 Gy with γ-rays. All irradiations were made on active hydrated animals. After irradiation the animals were transferred to new 6-well plates with 2 mL of distilled water and green alga *Chlorococcum humicola*. Effects of irradiation on animal survival were estimated according to the methods described (*92*, *109*). Survival of animals was monitored daily until all the tardigrades were dead.

Genome sequencing

The tardigrades were picked out from the culture medium under a stereomicroscope, animals were extensively washed with pure water and starved for 2 days in pure water with 1% penicillin streptomycin to clear the gut content and remove surface microbes. After 2 days, the tardigrades were thoroughly washed again with pure water and picked out one by one.

Genomic DNA for Oxford Nanopore Technologies (ONT) sequencing was extracted using MagAttract HMW DNA Kit (Qiagen) from approximately 10,000 individuals of *H. henanensis* **sp. nov.** according to the standard operating procedure provided by the manufacturer. The degradation and contamination of the extracted DNA was monitored on 1% agarose gels. DNA purity was then tested using NanoDrop™ One UV-Vis spectrophotometer (Thermo Fisher Scientific, USA). DNA concentration was further measured by Qubit® 3.0 Fluorometer (Invitrogen, USA). Next, the ends of DNA fragments were repaired and A-ligation reaction were conducted with NEBNext Ultra II End Repair/dA-tailing Kit. The adapter in the LSK109 kit was used for further ligation reaction and Qubit® 3.0 Fluorometer (Invitrogen, USA) was used to quantify the size of library fragments. Sequencing was then performed on a Nanopore PromethION sequencer (Oxford Nanopore Technologies, UK) instrument at Nextomics (Wuhan, China). The Flow cell version was R9.4.1. Nanopore sequencers generate FAST5 files that contain signal data. Basecalling was first performed to convert the FAST5 files to FASTQ format with Guppy software (v3.2.2) with the 'Fast' mode. The raw reads of FASTQ format with mean_qscore_template < 7 were then filtered resulting in pass reads.

For the WGS short-reads sequencing, genomic DNA for MGISEQ 2000 sequencing (BGI-Shenzhen, Shenzhen, China) was extracted using Quick-gDNA MicroPrep kit (Zymo Research) from approximately 300 individuals of *H. henanensis* **sp. nov.** The SOAPnuke was used for adapter removal according to the following criterion: if the sequencing read matches 50% or more of the adapter sequence, delete the entire read.

Chromatin conformation capturing (Hi-C)

To anchor hybrid scaffolds onto the chromosome, genomic DNA was extracted for the Hi-C library from 17,000 individuals of *H. henanensis* **sp. nov.** Then, we constructed the Hi-C library. In brief, freshly harvested tardigrades were vacuum infiltrated in nuclei isolation buffer supplemented with 2% formaldehyde. Crosslinking was stopped by adding glycine and additional vacuum infiltration. Fixed tardigrades were then grounded to powder before re-suspending in nuclei isolation buffer to obtain a suspension of nuclei. The purified nuclei were digested with 100 units of DpnII and marked by incubating with biotin-14-dCTP. Biotin-14-dCTP from non-ligated DNA ends was removed owing to the exonuclease activity of T4 DNA polymerase. The ligated DNA was sheared into 300-600 bp fragments, and then was blunt-end repaired and A-tailed, followed by purification through biotin-streptavidin-mediated pull down. Finally, the Hi-C libraries were quantified and sequenced using the DNBSEQ-T7 platform at Nextomics (Wuhan, China).

Genome assembly based on the ONT sequencing results

For de novo genome assembly (by Nextomics), a ONT-only assembly was constructed by using an OLC (overlap layout-consensus)/string graph method with NextDenovo (v2.3.1, https://github.com/Nextomics/NextDenovo). Considering the high error rate of ONT raw reads, the original subreads were first self-corrected using NextCorrect, thus obtained consistent sequences (CNS reads). Comparing CNS were then performed with NextGraph module to capture correlations of CNS. Based on the correlation of CNS, the preliminary genome was assembled. To improve the accuracy of the assembly, the contigs were refined with Racon (v1.3.1, https://github.com/isovic/racon.git) using ONT long reads and Nextpolish (v1.3.0, https://github.com/Nextomics/NextPolish) using short reads with default parameters that sequenced by MGISEQ 2000. To discard possibly redundant contigs and generate a final assembly, similarity searches were performed with the parameters "identity 0.8-overlap 0.8".

The completeness of genome assembly was assessed using BUSCO (Benchmarking Universal Single Copy Orthologs, v4.0.5) (*110*). To evaluate the accuracy of the assembly, all the short reads

sequenced by MGISEQ 2000 were mapped to the assembled genome using BWA (Burrows-Wheeler Aligner, v0.7.12-r1039) and the mapping rate as well as genome coverage of sequencing reads were assessed using SAMtools (v0.1.1855). Besides, base accuracy of the assembly was calculated with bcftools (v1.8.0, http://samtools.github.io/bcftools/).

GC-depth analysis was performed using minimap2 (r41) (*111*). The third-generation genome reads were mapped back to the genome, and the reads alignment rate, depth, GC content were statistically analyzed. Then, use a sliding window of 10 kb to calculate the average GC content and average sequencing depth of each contig and the GC-depth plot was obtained. Due to the specificity of GC content among species, if GC depth is concentrated and enriched in the same region, it indicates that there is no contamination in the genome. On the contrary, there may be exogenous contamination. To determine the contamination source, align the assembled genome sequence (segmenting sequences by 50 kb if the contig length greater than 1 Mb) with the NT (nucleotide sequence database), and calculate the sequence alignment results (the optimal alignment for unsegmented sequences is the final alignment result, while the maximum number of species in bin alignment is the final alignment result) then determine sequence origination. After removing the contamination sequences, GC-depth analysis was performed again to check the result.

The coverage of expressed genes of the assembly was examined by aligning all the RNA-seq reads against the assembly using HISAT (v2.1.0, http://ccb.jhu.edu/software/hisat/index.shtml) with default parameters. To avoid including mitochondria sequences in the assembly, the draft genome assembly was submitted to the NT library and aligned sequences were eliminated.

Hi-C assisted genome assembly

In total, 370 million paired-end reads were generated from the libraries. Then, quality controlling of Hi-C raw data was performed using Hi-C-Pro as former research. First, low-quality sequences (quality scores < 20), adaptor sequences and sequences shorter than 30 bp were filtered out using fastp (v0.12.6), and then the clean paired-end reads were mapped to the draft assembled sequence using bowtie2 (v2.3.2) (-end-to-end --very-sensitive -L 30) to get the unique mapped paired-end reads. Valid interaction paired reads were identified and retained by HiC-Pro (v2.8.1) from unique mapped paired-end reads for further analysis. Invalid read pairs, including dangling-end, self-cycle, re-ligation, and dumped products were filtered by HiC-Pro (v2.8.1). The scaffolds were further clustered, ordered, and oriented scaffolds onto chromosomes by LACHESIS (https://github.com/shendurelab/LACHESIS), with parameters CLUSTER_MIN_RE_SITES = 100, CLUSTER_MAX_LINK_DENSITY = 2.5, CLUSTER NONINFORMATIVE RATIO = 1.4, ORDER MIN N RES IN TRUNK = 60, ORDER MIN N RES IN SHREDS = 60. Finally, placement and orientation errors exhibiting obvious discrete chromatin interaction patterns were manually adjusted.

Karyotype analyses

Karyotyping was performed as described by Gabriel *et al.* (*112*). Embryos were removed from the parental exuvia by slicing with 25-gauge hypodermic needles and then fixed in absolute methanol for 20 min at 4℃, followed by a 90%-70%-50% methanol series at room temperature. Embryos were then post-fixed in 4% paraformaldehyde in 0.5 × PBT (0.5 × phosphate buffered saline with 0.05% Triton X-100) for 10 min at room temperature. Embryos were then washed 5 min each in 0.5 × PBT with 5 times. DAPI (5 μg/μL) was added to the next wash of 20 min, followed by two subsequent washes of 5 min each. Embryos were then mounted on slides. Finally, Image was acquired using microscope (Nikon A1R).

Genome annotation

We used GMATA (v2.2) (*113*) to identify the simple sequence repeats (SSR), and TRF (v4.07b) (*114*) to analyze tandem repeats in genome with default parameters. The software RepeatMasker (v1.331) (*115*) (www.repeatmasker.org) was used to predict transposable element (TE) repeat sequences.

The gene models in the genome of *H. henanensis* **sp. nov.** were predicted via three methods including homology-based or transcriptome-based prediction, and the ab initio prediction. 1) For homology-based prediction, we mapped the protein sequences of two published tardigrade genomes, *R. varieornatus* (*8*) and *H. exemplaris* (*9*), onto the genome of *H. henanensis* **sp. nov.** through GeMaMo (v1.6.1) (*116*), determined the position information of the corresponding protein alignment, and then obtained gene information based on homologous gene annotation. 2) The transcriptome sequence generated in this study was compared to the genome by GMAP (in PASA v2.3.3) (*117*) back to get the transcript location information, and then the transcript reassembled based on PASA (v2.3.3) (*118*) was used to find the most appropriate open reading frame (ORF) by GeneMark ST (v5.1) (*119*) to get the gene location information. 3) Ab initio prediction. Based on the gene information obtained by PASA (v2.3.3) using transcriptome sequence annotation, the gene model was semi-supervised and self-training using GeneMark ST (v5.1) (*119*), and then predicted. Compare the predicted genes with the Swissport database through BLASTP (v2.7.1), and then filter the results (identity ≥ 95%). Based on the filtered results, select the 3,000 genes with the highest score in GeneMark ST as the training set for the AUGUSTUS (v3.3.1) (*120*) model training. Finally, based on the prediction model, AUGUSTUS (v3.3.1) was used to predict the genes in the genome. The different predicted gene sets obtained from the above three methods were integrated through Evidence Modeler (EVM) software EVidenceModeler (v1.1.1) (*118*) to obtain a non-redundant exon set, thus defining a more reliable gene structure.

Data and methods for synteny analysis

The basic principle of genome synteny analysis is based on sequence alignment of gene sequences. We selected the published genomes of three tardigrades, *H. exemplaris* (*13*), *R. varieornatus* (*8*), and *Paramacrobiotus metropolitanus* (*11*), as closely related species, and compared *H. henanensis* **sp. nov.** with them respectively using MCscan in JCVI software package (v1.2.9) (*121*). The comparison results of MCscan were divided into two parts, one was the high-quality synteny block, after filtering tandem repeats and low score comparison results; the other part was the final synteny block with additional anchors added and then simply simplified anchors file. In order to gain a more comprehensive understanding of the synteny results, these two parts were both analyzed and shown. When creating the circus diagram, the scaffolds with a length greater than 500,000 bp for *H. exemplaris*, greater than 1,000,000 bp for *R. varieornatus* or *P. metropolitanus* were selected.

Horizontal gene transfer (HGT) analysis in *H. henanensis* **sp. nov.**

To evaluate proportion of HGT genes in *H. henanensis* **sp. nov.** Protein sequence alignment was performed against the non-redundant protein database in National Centre for Biotechnology Information (NCBI, https://www.ncbi.nlm.nih.gov/) using diamond 0.8 (k = 0). Several taxa subsets, including Metazoa, Viridiplantae, Fungi, other Eukaryota, Bacteria, Archea, and Virus, were set for further HGT analyses. Species annotation was based on taxonomy database, the best five hits of each protein against each taxon were collected as described in previous researches (*8, 122*). Proteins that did not have any match with at least one taxa subset with an E-value ≤ 10^{-5} were excluded, and tardigrade proteins were excluded either (*8, 122*). HGT indices were calculated by subtracting the best bit score of the metazoan hit from that of the non-metazoan hit in diamond alignment results. Proteins which got HGT indices (≥ 30) were identified as putative HGT candidates, and ones with HGT indices (< 30) were identified as indeterminate (*8*). As for

taxonomic origin of other proteins, best hits were collected. The proteins with E-value larger than 10^{-5} and proteins that got no taxonomic data were classified as "No specific taxonomy". Metazoan origin was identified when the species of best hit annotated as "Metazoan". HGT candidates were further identified by phylogenetic analysis.

To test the phylogenetic results for all HGT candidates, we retrieved the 1,000 most similar homologs of different species from the NCBI database. Putative HGT proteins with too few homologues (< 5) were excluded from later phylogenetic analysis. Homologues proteins were aligned by MAFFT (v7.407) (*102*), with '-auto' option, and trimmed ambiguously aligned regions using trimAl (v1.4.1) (*104*), ML trees were built using IQ-TREE (v2.1.4) (*107*) and fasttree(v2.1.11) (*123*), with best-fitting model of amino acid evolution and 1,000 ultrafast bootstrapping replicates. Each ML tree was rooted at the midpoint in Itol (https://itol.embl.de/) and manually inspected ("metazoan" was set as inner group). The phylogenetic tree of HhDODAs (fig. S12) was rooted using the ape (*124*) and phangorn (*125*) R packages. In addition, HGT candidates were supported by at least two layers of over 80% bootstrap in the donor cluster.

To check connection positions of HGT candidates during assembling, Nanopore raw reads (20 ×) were mapped back to *H. henanensis* **sp. nov.** genome using minimap2 (v2.17) (*111*), connection position checks were visualized and performed in IGV software (v2.15.2) (*126*). Then, "one by one" BLASTP was performed against the non-redundant database of NCBI for every HGT candidate with all latest available data to recheck HGT index. Proteins which got HGT indices (≥ 30) considered as "well-supported" HGT genes, and the remaining putative HGT genes were considered as "weakly-supported" HGT genes.

Sample preparation for omics experiments

The thoroughly washed and starved samples of *H. henanensis* **sp. nov.** were generated on 3.5 cm plates. 9,000 individuals (3 groups, 3,000 individuals per group) were used for the omics experiments. The heavy ion irradiation was carried out with carbon ions (see 'Radiation' section for detailed information). As the control, the unirradiated samples were placed in the same environment as the irradiation source, and were collected together with the irradiated samples 4 hours after irradiation. Each experiment group was divided into 6 equal fractions as three replicates for the transcriptome and proteome experiment, *i.e.*, 500 individuals for each experiment.

Transcriptome identification and quantification

The individuals were lysed in 400 μL TRIzol reagent using three freeze-thaw cycles of liquid nitrogen and 37℃ incubation, and RNA was extracted using a Direct-zol RNA kit (Zymo Research) following the manufacturer's instructions. RNA purity was checked using the NanoPhotometer spectrophotometer (IMPLEN, CA, USA). RNA integrity was assessed using the RNA Nano 6000 Assay Kit of the Bioanalyzer 2100 system (Agilent Technologies, CAUSA). RNA was amplified with SMARTer® Ultra® Low RNA kit (Takara, Janpan, Cat#634936). The RNA with polyA tail was primed with oligo-dT primer carrying a known sequence at the 5'-end. Reverse transcription was performed until the enzyme has reached to the 5'-end of mRNA transcript. Meanwhile, 2-5 cytosines were introduced to 3'-end of the first cDNA strand. By adding the ISPCR primers, the second strand of cDNA was synthesized by LD-PCR. Subsequently, the double-strand cDNA was fragmented, followed by end repair, A-tailing, adapter ligation, size selection and amplification. The libraries were checked with QPCR for quantification and Agilent 5400 system (Agilent, USA) for size distribution detection. Qualified libraries were pooled and sequenced on Illumina NovaSeq 6000 with PE150 strategy in Novogene Bioinformatics Technology (Beijing, China). We chose Salmon software (v1.5.2) (*127*) and the transcript sequence of protein-coding genes inferred in this study for transcriptomics quantitative analysis, including two main steps: index building and

sample quantification. Subsequent gene expression file generation was performed using the R package tximport.

Proteomic identification and database searching

UA solution (8 M urea in 0.1 M Tris-HCl, pH 8.5) containing 1 × protease and phosphatase inhibitor (Thermo Fisher Scientific, USA) was added to the bacterial precipitation for cell lysis and placed on ice for 30 min. Per sample was extracted by 15 min of sonication (1-s on and 1-s off, amplitude 20%) in lysate (BRANSON, USA). Peptide segments were isolated by FASP (filter-aided sample preparation) digestion method with trypsin. Each sample was subjected to reversed phase nLC-MS/MS analysis using high-precision mass spectrometry (Thermo Fisher Scientific Orbitrap Exploris 480). In detail, 500 ng peptides were loading onto 20-cm columns packed in-house with C18 particles (1.9 μm). The polypeptide samples were dissolved in 10 μL of solvent A (0.1% FA in water), injected with 5 μL, loaded onto the pre-column at the flow rate of 3 μL/min on the EASY-nano-LC chromatography system, and then separated on the column at the flow rate of 300 nL/min. The gradient was as follows: solvent B (0.1% FA in 80% ACN) increased linearly from 7% to 12% (0-6 min); solvent B rose linearly from 12% to 45% (6-67 min); 95% solvent B (67-75 min). The mass spectrum data was collected by FAIMSPro equipped with the specific parameters were set as follows: the spray voltage of ion source was set to 2.1 kV. FAIMSPro adopts two voltages of −45 V and −65 V, each cycle time was set to 1.3 s. Data dependent acquisition with MS method was used in which one full scan (350-1,500 *m/z*, R = 60,000 at 120 *m/z*, maximum injection time 50 ms) at a target of 3×10^6 ions was first performed, followed by 10 data-dependent MS/MS scans with higher-energy collisional dissociation (AGC target 7.5×10^4 ions, maximum injection time at 22 ms, isolation window 1.6 *m/z*, normalized collision energy 27%, and R = 15,000 at 120 *m/z*). Dynamic exclusion of 45 s was enabled.

The proteome data (raw files) were searched using Maxquant (v2.0.3.0) (*128*) against the protein sequence database inferred in this study. Carbamidomethyl (C) was set as fixed modifications. Variable modifications included Oxidations (M); Acetyl (Protein N-term); MS/MS match tolerance was 20 ppm; Min. razor peptides: 1; Peptide and protein FDR < 0.01; Pollution and reverse library results were removed. The "match between runs" parameter was selected.

Identification of differential expression genes (DEGs)

R package "DESeq2" was used for the DEG identification from transcriptome data (TPM values). For the proteome data, the iBAQ (intensity-based absolute quantification) data were normalized by divided to the median value in each sample data. Proteins detected in more than 2/3 of the samples in at least one group were kept for the further analysis. If the protein was detected in less than 2/3 of the samples in the other group, the missing values were interpolated with the global minimum value. For the calculation of $\log_2$FC and FDR values, R package "limma" was used. Cutoff for DEG determination: |log2FC| > 1 and adjust *P*-value < 0.05; highly upregulated: FC > 10 and adjust *P*-value < 0.05.

Gene age inference

Referring to reference species with complete genome sequences in the UniProt database, we selected a representative species for each genus, removed species with protein coding genes below 500, and retained 3,376 species for the further analysis. We did reciprocal sequence alignment of all *H. henanensis* **sp. nov.** protein sequences with the protein sequences of the 3,376 species mentioned above using Diamond BLASTP (*129*). The matches with both E-values less than 1×10^{-5} were regarded as the homologous genes. The number of homologous genes in each species

for each gene were calculated. We then determined the evolutionary age of each gene based on the phylostratigraphy approach (*130-132*).

Intrinsic disorder prediction

Intrinsically disordered regions were identified using SPOT-D (*133, 134*) (default parameters), which is based on deep recurrent and convolutional neural networks. SPOT-D was used to calculate the structural disorder value of each amino acid residue. The amino acid residue with the disorder value larger than 0.426 was defined as disordered residue. The proportion of disordered residues in one protein was calculated, named as structural disorder ratio (SDR). According to a previous study (*135*), proteins were divided into three categories according to SDR: 0~10%, 'highly structured'; 10~30%, 'moderately disordered'; 30~100%, 'highly disordered'.

Gene expansion and contraction analysis

In addition to the protein sequence data of *H. henanensis* **sp. nov.** (produced in this study) and the other three tardigrades with complete genome annotation (*H. exemplaris*, *R. varieornatus*, *P. metropolitanus*), the protein sequences of other 9 representative bilaterians (*Drosophila melanogaster*, *Araneus ventricosus*, *Penaeus monodon*, *Caenorhabditis elegans*, *Ancylostoma ceylanicum*, *Crassostrea gigas*, *Lamellibrachia satsuma*, *Strongylocentrotus purpuratus*, *Mus musculus*) were downloaded from National Center for Biotechnology Information (NCBI) as reference species for gene family analysis. The longest transcripts of each gene were selected. The selected species are shown in figure S28. Using OrthoFinder (v2.5.4, https://github.com/davidemms/OrthoFinder), the orthologous gene and species tree were inferred. Using MCMCTree (v4.9) to estimate species divergence time and obtain a super metric tree (species tree with differentiation time); CAFE (computational analysis of gene family evolution) (v4.2.1) was used to estimate the number of gene family members of ancestors of each branch through the "birth-death model", so as to predict the contraction and expansion of the gene family relative to the ancestors. In addition, to fully infer the tardigrade-specific expanded gene families, a gene family with more than 10 genes in each species of tardigrades and less than 10 genes in other species, if omitted by the CAFE process, was also considered an expanded gene family in tardigrades.

Gene ontology (GO) annotation and the over-representation analysis

We used the InterproScan software (v5.32-71.0) (base on protein domain) (*136*) and the EggNOG database (base on BLASTP) (*137*) to annotate the GO annotation of the genome of the *H. henanensis* **sp. nov.**, and the default parameters were used. A total of 9,848 genes were annotated.

The over- or under-representation analysis is based on hypergeometric distribution model, and the *P* values were corrected using the Benjamini-Hochberg method. The over- or under-representation strengths are represented by $-\log(P)$ or $\log(P)$ respectively. When the heatmaps were used to represent the over/under-representation strengths, the values of $-/+\log(P)$ were transformed into 11 grades (−5~5): -5, $\log(P) \leq -4$; -4, $-4 < \log(P) \leq -3$; -3, $-3 < \log(P) \leq -2$; -2, $-2 < \log(P) < \log(0.05)$; -0.5, $\log(0.05) \leq \log(P) < 0$; 0, $\log(P) = 0$; 0.5, $0 < -\log(P) \leq -\log(0.05)$; 2, $-\log(0.05) < -\log(P) < 2$; 3, $2 \leq -\log(P) < 3$; 4, $3 \leq -\log(P) < 4$; 5, $-\log(P) \geq 4$.

Weighted gene co-expression network analysis (WGCNA)

All the genes quantified in the transcriptome under three irradiation doses were selected for the WGCNA and was then conducted according to the WGCNA package in R (v4.2.1) (*120*). A hierarchical clustering dendrogram was built and similar gene expressions were divided into 24 different modules. Then the expression profiles of each module were summarized by the module

eigengene (ME) and the correlation between the ME and irradiation doses was calculated. Finally, the modules with high correlation coefficient with irradiation features were focused and the genes in these modules were selected for subsequent analyses. The hub genes were screened for network graph, total and hub genes matching GO annotations were analyzed for functional enrichment respectively (FDR < 0.05).

Construction of plasmids

The coding sequences of *DODA1* (H.Henanensis.Chr4.1382), *NDUFB8* (H.Henanensis.Chr6.152) were amplified by PCR from cDNA of *H. henanensis* **sp. nov.**, *BCS1a* (H.Henanensis.Chr1.760) and *RvDsup* (GenBank accession number, LC050827) were chemically synthesized directly, they were all inserted into pLVX-IRES-puro vector for expression with a C-terminal Flag tag. PCR amplification was performed using GoldenStar T6 Super PCR Mix according to the manufacturer's instructions. Specially, the sequence of the H.Henanensis.Chr4.1382 was used as a template to design primers for PCR amplification of *DODA1*. This amplification yielded a 430-bp product, and its length coincides with that of the entire *DODA1* gene plus the overlap sequences for Gibson assembly. The GST-HhDODA1 and His-HhDODA1 were subcloned into pGEX-6p-1 and pET28a vector respectively. All the HhDODA1 mutants were constructed by standard site-directed mutagenesis. The GST-GdDODA and pLVX-FLAG-GdDODA were synthesized and inserted into pGEX-6p-1 and pLVX-IRES-puro vector respectively according to *GdDODA* sequence (gi 501179334) in NCBI database. The His-GdDODA was constructed by subcloning full-length of GdDODA into pET28a vector. For TRID1-WT-GFP(A206K)-GST plasmid, the coding sequence of *TRID1* (H.Henanensis.Chr4.1468) was amplified from cDNA of *H. henanensis* **sp. nov.** by PCR, the GFP fragment was amplified from pEGFP-N1 vector plasmid. The resulting PCR products were ligated into pGEX-6p-1 plasmid. To eliminate the impact of GFP dimerization on phase separation experiments, the alanine at position 206 of the GFP was mutated to lysine (*138*) by standard site-directed mutagenesis. The fragments of TRID1-ΔPrLD and GFP(A206K) were amplified from TRID1-WT-GFP(A206K)-GST and ligated into pGEX-6p-1 vector. The TRID1-WT-pLVX was constructed by subcloning full-length of TRID1-WT into pLVX-IRES-Puro vector with a C-terminal Flag tag. The TRID1-ΔPrLD-pLVX was constructed by subcloning from TRID1-ΔPrLD-GFP(A206K)-GST into pLVX-IRES-Puro vector with a C-terminal Flag tag. The TRID1-WT-GFP was constructed by subcloning full-length of TRID1 into pEGFP-N1 vector. The TRID1-ΔPrLD-GFP was constructed by subcloning into pEGFP-N1 vector. The vectors pEGFP-C1-PARP1 was a gift from Prof. Xingzhi Xu (Shenzhen University Medical School, China). DsRed-53BP1 was a gift from Prof. Lei Shi (Tianjin Medical University, China). The primer sequences were listed in table S15. All clones were confirmed by DNA sequencing.

DODA expression and purification

The HhDODA1 and GdDODA proteins derived from plasmid pGEX-6p-1 and pET-28a were expressed in TSBL21 (DE3) pLysS (Tsingke Biotechnology) and induced with 1 mM isopropyl-1-thio-β-D-galactopyranoside (IPTG) at 20℃ for 12 hours.

For Glutathione-S-transferase (GST) tagged protein purification, cells were harvested by centrifugation and resuspended in phosphate buffered solution PBS with 1% Nonidet P-40 supplemented with protease inhibitors. Then the cells were subjected to sonication and centrifugation. The lysate was incubated with glutathione Sepharose 4B beads (Santa Cruz) for 2 hours and then washed five times with lysis buffer. DODA proteins were freed from its GST-fusion by cleavage using the PreScission protease followed by ultrafiltration.

For His-tagged protein purification, cells were harvested by centrifugation and resuspended in phosphate buffered solution PBS with 1% Nonidet P-40 supplemented with protease inhibitors.

Cells were harvested by centrifugation and resuspended in phosphate buffered solution (PBS) with 1% Nonidet P-40 supplemented with protease inhibitors. Then the cells were subjected to sonication and centrifugation. The lysate was incubated with His-tag purification resin for 4 hours and then washed five times with lysis buffer. DODA proteins were eluted by elution buffer contain 500 mM imidazole followed by ultrafiltration.

Proteins were quantified using the Bradford protein assay and then used in enzyme assays, gel filtration, or resolved on SDS-PAGE followed by Coomassie brilliant blue staining.

Enzymatic assays

The reaction was initiated by adding the enzyme to a solution of L-DOPA (1 mM) and ascorbic acid (10 mM) in sodium phosphate buffer (50 mM, pH 7.0) unless otherwise stated. The mixture was incubated at 25°C. Enzyme activity was determined using a continuous spectrophotometric method by measuring the absorbance due to betalamic acid and muscaflavin appearance at a λ of 414 nm (*139*). Measurements were performed at 25°C in 96-well plates in a Multiskan Sky plate reader (Thermo Fisher Scientific, USA). The final sample volume was 200 µL. The molar extinction coefficient at 424 nm, with an ε of 24,000 M^{-1} cm^{-1}, was taken for the quantification of betalamic acid (*140*). The specific activity at each substrate concentration (L-DOPA, 0.005 to 2 mM range) was plotted and the values of K_m and V_{max} were calculated by the non-linear fitting of the data to the Michaelis-Menten equation, without considering substrate inhibition. All regressions were carried out using the GraphPad Prism 9.5. The reaction mixture was centrifuged for 15 min (12,000 g) at 4°C. The supernatant was subjected to HPLC analysis.

Production of betalains

The betalains were produced by adapting a biotechnological procedure in bacterial cell factories following a previously described method (*141*, *142*). Briefly, the betalains was obtained by microbial factories containing *E. coli* (expressing His-HhDODA1). The bacterial culture was performed in 2 × yeast extract and tryptone (2 × YT) growth medium supplemented with kanamycin (10 µg/mL). The culture was incubated at 37°C under shaking until an optical density at 600 nm (OD_{600}) of 0.8-1.0 was obtained. Subsequently, IPTG (50 µg/mL) was added to the culture and kept under shaking at 20°C for 12 hours. The culture was then centrifuged at 4,000 rpm for 20 min. The supernatant was discarded and the bacterial pellet obtained was resuspended in the prepared reaction solution at a volume similar to that used for bacterial growth in 2 × YT medium. For the reaction solutions, L-DOPA (7.6 mM), sodium ascorbate (15 mM), and the corresponding amino acid (38 mM) or phenylethylamine (38 mM) were added separately in pure water, the pH of the solution were adjusted to 6.3~6.5 and monitored every day. For the production of dopaxanthin, only L-DOPA and sodium ascorbate, at the same concentrations as above, were added. The reaction solutions were incubated at 20°C under constant shaking (120 rpm) kept in the dark until the maximum production of betaxanthin was reached. After incubation, the contents were centrifuged at 4,000 rpm for 20 min and the bacterial pellets were discarded, keeping the supernatants at −80°C until the beginning of the purification stage.

Purification of betaxanthins

The samples were analyzed by HPLC/MS on a Waters Auto Purification LC/MS system (3100 Mass Detector, 2545 Binary Gradient Module, 2767 Sample Manager, and 2998 Photodiode Array (PDA) Detector). The system was equipped with a Waters C18 5 µm SunFire separation column (150 × 4.6 mm), equilibrated with HPLC grade water with 0.1% formic acid (solvent A) and HPLC grade acetonitrile (solvent B) with a flow rate of 0.3 mL/min at room temperature. Preparative HPLC-MS on a Waters Auto Purification LC/MS system (3100 Mass Detector, 2545 Binary

Gradient Module, 515 HPLC pump, 2767 Sample Manager, and 2998 Photodiode Array (PDA) Detector). The system was equipped with a Waters C18 5 μm X-bridge separation column (150 × 4.6 mm).

The yellow fractions further purified using a Waters C18 5 μm X-bridge separation column (150 × 4.6 mm) by HPLC grade water with 0.1% formic acid (solvent A) and HPLC grade acetonitrile (solvent B) following a stepwise elution program at 20 mL/min: 100% A for 0-5 min; 0-15% acetonitrile in A for 5-20 min; and 35% acetonitrile in A for 25-30 min.

Preparation of deuterated betaxanthins

The d_1-betalamic acid and d_2-dopaxanthin were synthesized by stirring the non-deuterated substrate in deuterated water with 0.1% deuterated formic acid for 1 hour, followed by freeze-drying. The reaction mechanism is shown in fig. S17C.

Dopaxanthin undergoes hydrogen-deuterium exchange in deuterated water, so we only provide deuterated NMR of dopaxanthin. This compound had poor solvency or decomposed in other solvents, so no other non-deuterated dopaxanthin NMR was obtained.

Deuterated betalamic acid can only exist stably in deuterated water, it will be quickly exchanged back to non-deuterated betalamic acid in water. Deuterated dopaxanthin exchange much slower in water, so we choose it for mass spectrometry experiments.

NMR spectra

^{1}H NMR spectra were recorded on a Brucker 400 MHz or 600 MHz spectrometer at ambient temperature with D_2O as the solvent unless otherwise stated. ^{13}C NMR spectra were recorded on a Brucker 151 MHz spectrometer (with complete proton decoupling) at ambient temperature. Chemical shifts are reported in parts per million relatives to D_2O (1H, δ 4.79 ppm) and DMSO-d_6 (6H, δ 2.50 ppm). Data for ^{1}H NMR are reported as follows: chemical shift, integration, multiplicity (s = singlet, d = doublet, t = triplet, q = quartet, m = multiplet) and coupling constants.

Metabolite extraction

For betalains analysis in tardigrades, the tardigrades were picked out from the culture medium under a stereomicroscope, animals were extensively washed with pure water and starved for 2 days in pure water with 1% penicillin streptomycin to clear the gut content and remove surface microbes. Then, the tardigrades were thoroughly washed again with pure water and collected one by one. The tardigrades pellets were added with pre-cooled methanol/water (80:20, v/v), 100 mM ascorbic acid, disrupted by bead beating with silica beads at 4℃, homogenized by sonification on ice, incubate at −20℃ for 1 hour, and centrifuged. The supernatants were evaporated. The dry extracts were reconstituted with water before analysis. For betalains in human cells, the extraction method was the same as above, without the bead beating step.

Untargeted mass spectrometry analysis of betalains

Ultra Performance Liquid Chromatography (UPLC)-Vion ion mobility spectrometry (IMS) QTOF (Waters) with an electrospray ionization (ESI) source was used for untargeted metabolites analyses. Chromatographic separation of metabolites was performed with an Acquity UPLC-HSS T3 column (100 × 2.1 mm i.d., 1.8 μm), applying a flow rate of 0.3 mL/min with a column temperature of 35℃. A linear gradient was performed using water with 0.1% FA as solvent A and acetonitrile with 0.1% FA as solvent B. The linear gradient was performed for 18 min from 5% solvent B to 100% solvent B (0 min, 5% B; 0.5 min, 5% B;12 min, 20% B; 15 min, 100% B; 18 min, 5% B). Fresh samples were analyzed after enzymatic reactions. Metabolites were detected in positive ion mode within a mass range from 50 to 1,200 *m/z*. The source temperature was set at

100℃. The desolvation temperature was set at 450℃. MS conditions were: capillary voltage, 1 kV; scan time, 0.2 s; low collision energy, 6 eV; collision energy (HDMSE) starting at 10.00 eV and ending at 45.00 eV; desolvation gas flow, 800 L per hour; Lock mass correction was carried out with leucine enkephalin every 0.5 min. Data were analyzed by Progenesis QI software (v2.4, Waters).

Targeted mass spectrometry analysis of betalains in HeLa cells

For targeted mass spectrometry analysis of betalains, QTRAP® 5500 mass spectrometer (Applied Biosystems-SCIEX Scientific, Concord, Canada) equipped with a Kinetex® F5 LC column (100 × 2.1mm, 2.6 μm) (Phenomenex, USA) were used. A binary solvent system was used (mobile phase A: 0.1% formic acid in water; mobile phase B: 0.1% formic acid in acetonitrile) for target compounds separation. The gradient elution program was as below: 98-98% A (0-0.8 min), 98-70% A (0.8-8 min), 70-1% A (8-10 min), 1-1% A (10-12 min), 1-98% A (12-12.1 min), 98-98% A (12.1-15 min). The total run time was 15 min for each sample. Mass spectrometry was operated in positive electrospray ionization mode, and multiple reaction monitoring (MRM) mode was applied for identification of betalains. The temperature of the electrospray ionization (ESI) ion source was set at 550℃. Curtain gas flow was set as 20 psi, collisionally-activated dissociation (CAD) gas was set as a medium, and the ion spray voltage was (+) 5500 V, with ion gas l and 2 set as 50 psi. The MRM transitions for 11 compounds are shown in table S11.

Targeted mass spectrometry analysis of betalains in *H. henanensis* **sp. nov.**

Chromatographic separation was performed on an ExionLC™ AD system (Shimadzu, Kyoto, Japan) equipped with an on-line degasser, a multiplate autosampler, and a column temperature compartment. Mass spectrometric detector was performed on SCIEX Triple Quad™ 7500 (Applied Biosystems-SCIEX Scientific, Concord, Canada) under positive ionization mode. The ionization source is Turbo V™, which belongs to the ESI ion source.

Qualitative analysis was performed using the targeted scan mode MRM (multiple reaction monitoring. Chromatographic peaks were separated on a Kinetex® F5 column (150 × 2.1 mm, 2.6 μm, Phenomenex, USA). The mobile phase for chromatographic separation is comprised of 0.1% (v/v) aqueous formic acid in water (A) and 0.1% aqueous formic acid in acetonitrile (B). The gradient elution was as follows: 0-1.5 min, 5% B; 1.5-2 min, 5-10% B; 2-5 min, 10-30% B; 5-7 min, 30-95% B; 7-8 min, 95% B; and 8.01-10 min, 5% B. The column temperature was set at 40℃ with a flow rate of 0.3 mL/min. The injection volume was 5 μL. The optimized parameters of mass spectrometry are illustrated below for MRM: curtain gas (CUR), 40 psi; ion source gas 1 (Gas1), 35 psi; ion source gas 2 (Gas2), 70 psi; temperature (TEM), 550℃; ion-spray voltage (IS), 1500 V; CAD gas, 9. A composite scanning mode MRM was used to identify the betalains, the MRM transitions for 11 compounds are shown in table S12.

Gel filtration

Pure recombinant HhDODA1 proteins were applied to a Superdex 200 10/300 GL column equilibrated with sodium phosphate buffer (50 mM, pH 7.5) with 150 mM NaCl. The protein was eluted with the same buffer at a flow rate of 0.5 mL/min. Elutions were performed in an Äkta purifier apparatus (GE Healthcare) and monitored at 280 nm. Column calibration was performed with the following protein markers: cytochrome c (12.4 kDa), ovalbumin (44 kDa), conalbumin (75 kDa), aldolase (158 kDa), ferritin (440 kDa), and thyroglobulin (669 kDa).

Structure analysis

HhDODA1 and GdDODA structures were predicted by AlphaFold2 (https://colab.research.google.com/github/sokrypton/ColabFold/blob/main/AlphaFold2.ipynb). Potential active sites of HhDODA1 were predicted by PyMOL (v2.5.4, http://www.pymol.org). All structural figures were generated in PyMOL software.

Cell culture and transfection

HeLa, U2OS, and HEK293T cells were maintained in Dulbecco's modified Eagle's medium (DMEM) supplemented with 10% fetal bovine serum (FBS, Gemini). Transfections were carried out using Lipofectamine 2000 (Invitrogen) according to the manufacturer's instructions.

Lentiviral production and infection

The pLVX-IRES-puro constructs, as well as assistant vectors psPAX2 and pMD2.G, were co-transfected into HEK293T cells. Viral supernatants were collected, clarified by the filtration through 0.45 μm filters. The viruses were used to infect cells in a 6-well dish with 8 μg/mL polybrene. Infected cells were selected with 1.5 μg/mL puromycin.

Co-immunoprecipitation

HEK293T were transfected with these indicated plasmids and 48 hours after the transfection, cells were lysed with HEPES lysis buffer (20 mM HEPES (pH 7.2), 150 mM NaCl, 0.5% Triton X-100, 1 mM NaF and 1 mM dithiothreitol) with the protease inhibitor (MedCHemExpress) and PhosSTOP (Solarbio). Immunoprecipitation was performed using the indicated primary antibody and protein A/G agarose beads (Santa Cruz) at 4℃, which were then washed with HEPES buffer three times. The lysates and immunoprecipitates were analyzed by immunoblotting.

Western blotting

Cell lysates boiling in SDS-PAGE sample buffer were resolved by SDS-PAGE followed by immunoblot analysis using the indicated primary antibodies followed by detection with the related secondary antibody and the SuperSignal West Pico PLUS chemiluminescent Detection Reagent.

Immunofluorescence

Cells were washed with PBS, fixed in 4% paraformaldehyde for 10 min. Then the cells were washed with cold PBS, permeabilized with 0.2% Triton X-100 and incubated with appropriate primary antibodies and secondary antibodies coupled to Alexa Fluor 488 or 594. The cells were then washed for four times, and a final concentration of 0.1 mg/mL DAPI was included in the final wash to stain nuclei. Images were acquired with a Nikon A1R confocal system. γH2AX foci were analyzed by Foci Counter (https://www.biologie.uni-konstanz.de/bioimaging-centre/service/image-analysis/bic-macro-toolkit/foci-counter/).

Colony formation assays

Cells were plated in 12-well plates in triplicates (400 cells per well) and were subsequently treated with IR and let to grow in colonies for 10-14 days. After 10-14 days, the cells were washed with PBS, fixed with 4% formaldehyde for 10 min and stained with crystal violet (0.1% wt/vol) for 20 min. The number of colonies per well was counted, and the plating efficiency and surviving fraction for given treatments were calculated on the basis of the survival rates of nonirradiated cells.

Single-Cell Gel Electrophoresis (SCGE)/Comet assay

The experimental approach was used as described previously (*143*). Briefly, the media was removed, and then 0.005% trypsin was added to the cells after irradiation immediately. Next, the cells were suspended in cold PBS for later use. Thereafter, 0.5 mL of 1.5% normal melting agarose (NMA) was added to the frosted glass slides. Then the glass slides were placed flat at 4℃ for 10 min. 2×10^6 cells were mixed with 120 μL of 0.5% low-melting agarose (LMA), covering the coverslips, placing them flat at 4℃ for 10 min, and carefully removing them. The slides were placed overnight in fresh cell lysis buffer at 4℃. Next, the glass slides were rinsed with ddH_2O and then were placed in precooled alkaline electrophoresis buffer for 20 min, followed by electrophoresis at 4℃ for 1 hour at 17 V and 300 mA. The slides were then neutralized twice with neutralization buffer for 10 min each time. Thereafter, the glass slides were removed and stained with SYBR Gold Nucleic Acid Gel Stain for 20 min in the dark. The slides were washed with ddH_2O, and comet formation was observed under a fluorescence microscope (Nikon nie). The pictures were analyzed using CASP software (http://casplab.com/).

ROS detection

For ROS detection, cells were treated with or without 10 Gy X-ray irradiation, 4 hours post irradiation, the cells were stained with 2,7-dichlorodihydrofluorescein diacetate (DCFH-DA, in green) and incubated at 37℃ for 1 hour. Images were acquired with a Nikon A1R confocal system. The mean fluorescence intensity of the DCFH-DA fluorescence was calculated using Cellpose (v2.0) (*144*) and ImageJ software (v1.53e, https://imagej.nih.gov/). Intracellular ROS have also been detected with CM-H2DCFDA by flow cytometry. Briefly, cells were trypsinized and loaded with 10 μM CM-H2DCFDA (Invitrogen), incubated at 37℃ for 45 min, and immediately analyzed by flow cytometry. For MitoSOX Red (Invitrogen) experiments, cells were trypsinized and loaded with 5 μM MitoSOX Red at 37℃ for 30 min.

Raman spectroscopy and imaging measurements

For sample preparation, tardigrades were anesthetized in 0.12% avertin (Sigma-Aldrich). Animals became largely im-mobile within 10 min. An appropriate amount of 0.4% (w/v) agarose (BIOWEST, Spain) was dropped onto a Raman aluminum slide (Shanghai D-band Co., Cat#1001, 75 mm × 25 mm), then the anesthetized tardigrade suspension was dropped onto the solidified agarose. When the water is about to evaporate and dry, another layer of agarose was applied to embedding the sample. After solidification, the slides were placed in 10 cm Petri dishes and immersed in ~50 mL of water.

Raman spectra were collected using a confocal Raman microscope (Alpha 300R, WITec, Germany) equipped with a piezoelectric stage (UHTS 300, WITec, GmbH.), 63 × water immersive objective lens (Zeiss W Plan Apochromat 63 ×, N.A = 1), green solid-state excitation laser (λ = 532 nm, WITec, GmbH.), and an imaging spectrograph (Newton, Andor Technology Ltd. UK) equipped with a 600 groove/mm grating and a thermoelectrically cooled (60℃) charged-coupled detector (CCD) optically connected to the objective through a 10 μm diameter single mode silica fiber-optic cable. The laser excitation spot size is ~350 nm. This setup enabled acquisition of spectral data across a wavenumber range from 0-3600 cm^{-1}. In all cases, the excitation laser intensity was kept constant between sample scans.

For single-spectrum Raman measurements. The spectra were recorded with an integration time of 8 s, a laser power of 15 mW on a point and one accumulation in the range of 400–3200 cm^{-1}. For each sample, Raman spectra were collected randomly.

For Raman imaging, single tardigrade mapping to obtain a spatially resolved spectral map was acquired with an integration time of 3 s per point with a step size of 2 μm between adjacent points. Laser power was 15 mW. Each sample map took ~1-4 hours to acquire depending on the tardigrade

size. The spectral range of was from 400 cm^{-1} to 3200 cm^{-1}. Confocal Raman mapping was performed on at least 3 individuals per group.

Raman imaging images were preprocessed using WITec Project FIVE (v5.2.3.78). Single-cell Raman spectra were preprocessed using LabSpec software (v6.6.2.7). Comic ray correction was first performed. Polynomial baseline fitting and subtraction were performed on all spectra (degree: 10, max points: 64; noise points: 10), which attempted to estimate the background via user-defined polyline points and effectively abolished sloped baseline (*145*). The entire spectrum region was vector normalized (*146*) so that the sum of all intensity values of a spectrum squared equals one. Quantification of biomolecules was done by integrating the area of the corresponding Raman bands.

siRNA soaking

The experimental approach was used as described previously (*147*). Tardigrades were soaked in 40 μL siRNA or siNC (negative control siRNA) in a PCR tube. The final concentration of siDODA1 and siTRID1 were 75 ng/μL and 100 ng/μL, respectively. The soaked tardigrades were cultured in an incubator with 20℃ for several days without food supply.

Quantitative Real-time PCR (qPCR)

After soaking in siRNA for 5 days, RNA was extracted from single tardigrade by using the Direct-zol RNA MicroPrep Kit (Zymo Research) after three repeated freeze-thaw cycles between liquid nitrogen and 37℃, oscillating vortices were carried out during the process. Then, RNA was reverse transcribed with the ReverTra Ace qPCR RT Master Mix (TOYOBO, Japan). qPCR reaction was performed on qTOWER 3G System (Analytik jena, Germany) with the Taq Pro Universal SYBR qPCR Master Mix (Vazyme) according to the manufacturer's protocol, including amplification cycle conditions. The β-tubulin gene (gene ID: H.Henanensis.Chr6.262) of *H. henanensis* **sp. nov.** was used as the internal control. The primer sequences were listed in table S15. According to the cycle threshold (Ct) value and the dissolution curve, the $2^{-\Delta\Delta Ct}$ method was used to estimate the relative expression level of the target gene and verify the interference efficiency

Survival curve assays

Tardigrades soaked in siRNA for 5 days or DODA1 inhibitor for 3 days were treated with or without X-ray radiation in the indicated dose. After irradiation, the tardigrades continued to be cultured under the same conditions as described earlier. Survival was checked daily and scored as alive (movement or curled-up) or dead (straight and transparent) over the course of 5-6 days. This data was converted to Kaplan-Meier survival curves in GraphPad Prism 9.5 and subjected to simple survival analysis with log-rank test to determine significant differences in survival between groups.

TRID1 purification and phase separation assays

The full-length TRID1 protein containing 267 amino acids shows a predicted molecular weight of 30.1 KDa, PrLD is a domain containing 27 amino acids (RQASQSNNQAKAATALFSSSQSNN QAK). The TRID1-ΔPrLD protein containing 240 amino acids shows a predicted molecular weight of 27.3 KDa. TRID1-ΔPrLD-GFP(A206K)-GST and TRID1-ΔPrLD-GFP(A206K)-GST were expressed and purified from *E. coli* strain BL21 induced with 50 μg/mL IPTG at 25℃. Bacteria were collected by centrifugation and lysed by sonication in lysis solution (PBS with 1% Triton X-100, 1% β-mercaptoethanol and 1 mM PMSF). After centrifugation, clear lysate was incubated with glutathione Sepharose 4B beads, washed with washing buffer (PBS with 1% Triton X-100, 150 mM NaCl, 1% β-mercaptoethanol and 1 mM PMSF). After centrifugation, the

supernatant was removed and added to the enzyme digestion buffer (50 mM Tris-HCl, 50 or 150 mM NaCl, 1 mM EDTA, 1 mM DTT, pH 7.5), and then add 5 μL PreScission Protease to incubate at 4℃ overnight. Purified proteins were concentrated by ultra-centrifugal filter unit (10 K MWCO, Millipore) and estimate protein concentration by using Coomassie Brilliant Blue staining.

The *in vitro* phase separation assays of TRID1-WT-GFP(A206K)-GST and TRID1-ΔPrLD-GFP(A206K)-GST were performed in 50 mM Tris-HCl, pH 7.4 and different concentrations (50, 150, or 300 mM) NaCl at room temperature. Phase separated droplets were imaged by using Nikon A1R confocal microscope with 60 × oil objective. Time lapse images of phase separation were captured over a 20 min time course with 1 minute interval. For cellular phase separation assay, HeLa cells transfected with TRID1-WT-GFP and TRID1-ΔPrLD-GFP for 48 hours were grown on a dish with thin glass bottom and imaged by using Nikon A1R confocal microscope with 60 × oil objective in a constant temperature table at 37℃ and 5% CO_2.

Fluorescence recovery after photobleaching (FRAP)

The experimental approach was used as described by M. Du *et al.* (*148*). *In vitro* FRAP experiments were performed on Nikon A1R confocal microscope at room temperature. A rectangular area in droplets were photobleached with 100% laser power for 15 s using 405-nm laser. Time lapse images were acquired over a 5 min time course after bleaching with 15 s interval. For cellular FRAP experiments, cells were grown on a dish with thin glass bottom, a heated stage with an objective lens heater was used to keep the cells at the appropriate temperature (37℃) and 5% CO_2 during imaging. A rectangular area in droplets were photobleached with 100% laser power for 15 s using 405-nm laser. Time lapse images were acquired over a 3 min time course after bleaching with 30 s interval. Fluorescence intensities of phase separated droplets were quantified using Nikon NIS-Elements AR (Advanced Research) software (v4.40.00).

Cell flow cytometry

For measurement of repair efficiency, Cell flow cytometry assays were performed as described previously (*63*). HEK293T cells were transfected with TRID1-WT, or TRID1-ΔPrLD, plus DR-GFP or EJ5-GFP, I-SceI, and a mCherry empty plasmid. Then, cells were trypsinized and washed with PBS, collected with LSRFortessa SORP (BD) finally. For intracellular ROS analysis, cells were trypsinized and loaded with 10 μM CM-H2DCFDA (Invitrogen), incubated at 37℃ for 45 min, and immediately analyzed by flow cytometry. For MitoSOX Red (Invitrogen) experiments, cells were trypsinized and loaded with 5 μM MitoSOX Red at 37℃ for 30 min. The data were analyzed by FlowJo (v10.8.1).

Laser microirradiation

Laser microirradiation were performed as described previously (*63*). HeLa cells were transfected with indicated plasmids. The cell medium was replaced by DMEM with 0.5 μg/mL Hoechst before irradiation. Cells of interest were microirradiated with 100% laser power for 15 s using 405-nm laser. Time lapse images were acquired over a 5 min time course after bleaching with 30 s interval. Fluorescence intensities were quantified using Nikon NIS-Elements AR software (v4.40.00). For quantification of protein accumulations at laser-generated DSBs, the mean fluorescence intensity within the regions of interest (ROI) was measured for each time point. The intensity values were background subtracted, and the ratio of intensity within the microirradiated nuclear area to non-microirradiated area was calculated.

Mitochondrial and cytosol NAD^+/NADH ratio detection

Mitochondrial and cytosol NAD^+/NADH ratio detection was performed according to previous studies (*149, 150*). Hela or HEK293T cells cultured in 96-well plates were tranfected with vectors, including iNapc-mito, SoNar-mito, iNapc-cyto and SoNar-cyto for 48 hours. Then the fluorescence intensities of 96-well plates were monitored by SpectraMax i3x (Molecular Devices).The relative changes in NAD^+/NADH ratio was calculated as follows: (1) the ratios of fluorescence emission at 488 nm excitation over that of 405 nm excitation for SoNar (R488/405 for SoNar) or for iNapc (R488/405 for iNapc) were calculated; (2) R488/405 for SoNar was normalized by R488/405 for iNapc to calculate NAD^+/NADH ratio; (3) the NAD^+/NADH ratio at baseline condition (Control or before the addition of 10 μM rotenone) was used to further normalize the NAD^+/NADH ratios after treatment. iNapc-mito, SoNar-mito, iNapc-cyto and SoNar-cyto vectors were purchased from Probiotic SOLUTIONS.

Isolation of mitochondria

Isolation of mitochondria was carried out at 4℃ according to the previous study (*151*). Cells were harvested and suspended by buffer-A (100 mM Tris pH 7.4, 225 mM sorbitol, 60 mM KCl, 1 mM EGTA and 0.1% BSA). The suspension was homogenized by a soft blender for 150 s and the homogenate was centrifuged at 3,000 g for 10 min. Supernatant was further centrifuged at 20,000 g for 30 min to obtain the crude mitochondria. The pellet was suspended in buffer-B (20 mM HEPES, pH 7.4, 150 mM NaCl). Mitochondria were extracted by 1% (w/v) digitonin for 1 hour with slow stirring at 4℃ in buffer-B. The digitonin/protein ratio was 6:1 (*152*). The extraction was centrifuged at 13,000 g for 30 min at 4℃ and the supernatant was used for Blue Native PAGE (BN PAGE).

Blue Native PAGE

Blue Native PAGE technique was used to determine native respiratory supercomplexes masses. Samples were mixed with 10 × loading buffer (0.1% (w/v) Ponceau S, 50% (w/v) glycerol) and subjected to 4%-13% blue native PAGE gel for electrophoresis at 4℃ based on the Blue native PAGE Nature protocol (*152*).

Immunoaffinity purification and immunodectection of mitochondrial proteins

For immunoaffinity purification, the mitochondria suspended in buffer-B were extracted by 1% (w/v) digitonin for 1 hour, the supernatant were incubated with anti-FLAG-G1 Affinity Resin for 1 hour, washed with wash buffer (20 mM HEPES, pH 7.4, 150 mM NaCl, 0.1% digitonin) 5 times, then eluted with 1mg/ml FLAG peptide. The elutes were mixed with 10 × BN PAGE loading buffer or SDS-loading buffer and subjected to BN PAGE or SDS-PAGE respectively. For immunodetection of proteins, primary antibodies are listed in the Key materials table. Chemiluminescence of the HRP-conjugated secondary antibody was detected using the SuperSignal West Pico PLUS chemiluminescent Detection Reagent.

Statistics

The quantified data with statistical analysis were performed using GraphPad Prism 9.5 (https://www.graphpad.com/). Data are shown as mean ± SD or median, unless otherwise designated. One-way ANOVA was used for analysis of multiple groups with a single independent variable. The Tukey and Dunnett tests were used as post-hoc tests to the ANOVA, where the Tukey test was used to compare every mean with every other mean, and the Dunnett test was used when comparing every mean to a control mean. Specially, for analysis of tail length of comet assays, γH2AX foci number, and mean fluorescence intensities of DCFH-DA, a Kruskal-Wallis test followed by Dunn's multiple comparisons test was used. For semi-quantitative analysis of

threonine-betaxanthin by their Raman bands, Mann-Whitney U test was used. $P > 0.05$, not significant (ns); * $P < 0.05$; ** $P < 0.01$; *** $P < 0.001$; **** $P < 0.0001$.

Supplementary Text

Desiccation and radiation tolerance of *H. henanensis* sp. nov.

As the reared tardigrades were originally collected from dried moss, the animals should have retained their tolerance to desiccation. To confirm this, we examined the survival rates after desiccation and rehydration (fig. S3A). Survival rates following 7 days of desiccation was 85.65% (fig. S3B). Thus, desiccation tolerance was highly maintained in *H. henanensis* **sp. nov.** Several species (*Richtersius* aff. *coronifer*, *Milnesium inceptum*, *R. varieornatus*, *etc.*) that are tolerant to rapid desiccation also have a high radiation tolerance. So, we want to know whether *H. henanensis* **sp. nov.** can also tolerate ultra-high dose radiation. We evaluated the effect of gamma radiation on survival of adults (fig. S3D, data S10). The survival rate of different dose groups has been maintained at 100% in the first 4 days. After day 7, there were significant difference in survival rate among different does groups. Doses of γ-ray up to 500 Gy did not affect the survival of *H. henanensis* **sp. nov.** There were no significant differences observed between 0, 200, and 500 Gy. Survival for all doses above 500 Gy gradually decreases as the irradiation dose increases. A dose of 1,000 Gy reduced the survival to 50% after 22.5 days and survival then declined relatively linearly. For doses of 4,000 and 5,000 Gy the survival was reached 50% after 10 days post-irradiation, and there was no significant difference between them. Together, these results suggested that *H. henanensis* **sp. nov.** can tolerate ultra-high dose radiation.

Evaluation of the genome assembly

The amount of original pass ONT reads was 64.14 Gb, the pass read number was 15078167, and N50 of the read length was 10.95 Kb. The assembly has longer contig N50 (4.6 Mb) and scaffold N50 (19.07 Mb) values than other tardigrade genome assemblies (table S6), indicating that we obtained a high-quality assembly. BUSCO evaluation (*110*) was based on the single copy homologous genes in eukaryota_odb10 OrthoDB database. About 83.92% of the complete gene elements can be found in the genome, indicating that most of the conservative genes are assembled completely, which reflects the high reliability of the assembly results from the side (table S6). After genome assembly, possible bacterial sequence contamination was removed (18 contigs, about 3.75% total contig length) (fig. S4).

Karyotype analyses

When females laying eggs, the embryo will undergo meiosis to produce haploid chromosomes, then it restores a diploid chromosome number by reduplicating chromosomes (automixis), rather than by fertilization, which is consistent with the reproductive strategy of *H. exemplaris (94, 112)*. We collected exuvia of *H. henanensis* **sp. nov.** that contained developing eggs (embryonic stages) for karyotype analyses. Both haploid (n = 6) and diploid (2n = 12) chromosome were observed (fig. S5C). The assembled genome in our results have revealed that *H. henanensis* **sp. nov.** is a diploid organism and has 6 pairs of chromosomes (fig. S5, A and B). The results of karyotype analyses were consistent with the results in Hi-C.

The genomic synteny analysis

Synteny analysis between chromosomes revealed that chromosome 6 lacks synteny with the other chromosomes (fig. S5A), indicating that this chromosome may have evolved relatively independently. Synteny analysis among differ between *H. henanensis* **sp. nov.** (Hh) and the other three tardigrades with available genome sequence revealed that there are more synteny regions between Hh and *H. exemplaris* (He) (fig. S6), consistent with their closest relationship in

phylogeny. The results of synteny analysis reflect a good correspondence between the chromosomes of Hh and He (fig. S6A): Chr. 1 (Hh) corresponds to Chr. 2 (He), Chr. 2 (Hh) corresponds to Chr. 5 (He), Chr. 13 (Hh) corresponds to Chr. 3 (He), Chr. 4 and 6 (Hh) corresponds to Chr. 1 (He), Chr. 5 (Hh) corresponds to Chr. 4 (He). The synteny regions between Hh and other tardigrades, are mainly matched in a 1:1 pattern, indicating the matched synteny regions are relatively reliable.

Description of the transcriptome and proteome data and quality control

In each experiment groups, more than 12,000 transcripts were quantified. As for the proteome identification, between ~10,000 and ~14,000 peptides were identified, which resulted in the overall identification of 3,366 quantified proteins across the 9 samples (fig. S7A, data S5). The repeated experiments showed high reproducibility (fig. S7, B and C). The correlation between the abundance of identified transcripts and proteins in the same sample yielded consistent results with previous similar analyses (with a correlation coefficient of around 0.55) (fig. S7D). The above results indicate that the transcriptome and proteome data are of high quality.

The detailed functional interpretation of the DEGs obtained from the combined analysis of transcriptome and proteome

We filtrated 1,007 DEGs that were that were differential in transcriptome or proteome (fig. S8, A and B). Terms related to DNA damage repair, especially the NHEJ pathway, were significantly enriched in Quadrants I (fig. S8C). This indicates that the damage repair program is rapidly activated after exposure to heavy ion irradiation, the expression of target genes (*LIG1*, *LIG4*, *XRCC1*, *Ku70*, *Ku80*, *PARP1*, *PNKP* and so on) increased at both transcriptome and proteome levels. In response to DNA damage, XRCC1 interacts with PNKP, DNA ligase and DNA polymerase form protein complexes, and they are immediately recruited to DNA damage sites and participate in base excision repair and single strand break repair (*153-155*). Ku70-Ku80 dimer can recruit downstream NHEJ core factors to efficiently repair DNA double strands breaks (*156*). It is noteworthy that membrane transport related proteins are also activated, which might be associated with the membrane repair after radiation (ESCRT-I, ESCRT-III, SEC62, LIMS1, AP1M1, ATOX1, GOT1B) (fig. S8C).

HGT analysis in *H. henanensis* sp. nov.

HGT index method (*8, 122*) were used to measure putative HGT genes, 459 putative HGT genes were found. Among them, 101 HGT candidates were further identified by phylogenetic analysis (fig. S10A). In the subsequent analysis, we checked connection positions of adjacent genes, and performed "one by one" BLASTP for every HGT candidate with all latest available data to recheck HGT index. As the result, 75 genes can span their connection positions smoothly (coverage $\geq$ 10) and get HGT index of at least 30, then were considered as "well-supported" HGTs (0.5% of total genes) (fig. S10, A and B, and data S6). The remaining 384 genes (2.6% of total genes) were considered as "weakly-supported" HGTs. All well-supported HGTs were encoded in scaffolds containing metazoan-origin genes, and 92% (69/75 genes) were adjacent to at least one metazoan gene (data S6). We checked for bacterial contamination (fig. S10C), compared the sequencing coverage and GC content of HGT candidates with native genes (fig. S10D), and checked the expression level of HGT genes (fig. S10E). All these results confirmed the credibility of HGTs.

Phylogenetic analysis of DOPA dioxygenase

DOPA dioxygenase mainly contain two types. One type contains a DOPA_dioxygen domain (PF08883), and another type contains a LigB domain (PF02900). We performed BLASTP (cutoff:

Evalue < 1E-5) based on five HhDODAs (containing DOPA_dioxygen domain) and the known 17 DOPA dioxygenase sequences containing LigB domain (fig. S13B) to get the currently available squences of DOPA dioxygenase. In total, 10706 protein sequences from 5,437 species were remained for the subsequent phylogenetic analysis. The results revealed a distinct division of the two types of DOPA dioxygenase into two clusters, attributable to the absence of sequence homology between them, even though they both belong to the DOPA dioxygenases. Within the cluster of type 1, a pronounced segregation of HhDODA1-4 from HhDODA5 is evident, indicating that HhDODA1-4 constitutes an independent subfamily and underwent separate evolutionary trajectories from HhDODA5 (fig. S12).

Three-dimensional structures of DODAs

Three-dimensional structure models of HhDODA1 and DOPA 4,5-dioxygenase from the bacteria *Gluconacetobacter diazotrophicus* (GdDODA), which has been shown to possess DOPA dioxygenase activity (*45*), were generated with high confidence using AlphaFold2 (*157*) (fig. S11). Comparison of these two proteins revealed similar structural features (fig. S11B), indicating that HhDODA1 possesses DOPA dioxygenase activity.

In addition, HhDODA1 was determined to be a dimer with a molecular mass estimated at 23.5 kDa under native conditions (fig. S15F), which is consistent with DODAs from betalain-producing bacteria and fungi (*45, 158, 159*). The optimum pH for the DOPA dioxygenase activity of HhDODA1 was determined to be pH 7.0 (fig. S15G), and this pH was used to characterize the kinetic parameters of HhDODA1 (fig. S15H).

Function analysis for the tardigrade specific genes

Since tardigrade gene function annotation is mainly based on the homologous mapping to the species of other phyla, there is only a few functional annotated tardigrade-specific genes. Therefore, we inferred their functions based on the old genes that have similar expression pattern. To this end, weighted gene co-expression network analysis (WGCNA) was performed on genes identified by the transcriptome (12,629 genes), resulting in 24 distinct modules. As shown in fig. S26A, blue module (1,556 genes) is most significantly correlated with upregulated in 2,000 Gy group (correlation coefficient = 0.97, FDR = 1×10^{-5}) and green module (552 genes) is correlated with upregulated in 200 Gy group. Functional analysis of genes indicated that tardigrade specific genes in the blue module might be involved in DNA repair, nucleic acid metabolism and proteolysis, while those in the green module might participate in chitin catabolic process and various enzyme activities (fig. S26B). In addition, more than 42.8% of the genes in the blue module encode the proteins locating in the nucleus, far more than the overall level (35.3%). Furthermore, a network of the top 50 weighted hub genes was mapped, which included 8 tardigrade-specific genes and 42 relatively older genes (fig. S26C). These genes are enriched in nuclear localization and might be involved in DNA-related processes such as DNA recombination, DNA repair and cell meiosis. (fig. S26D)

Gene family expansion and contraction

There are 477 expanded gene families and 2,609 contracted gene families in tardigrades based on CAFE results (fig. S28A, and data S8). In addition, two gene families (OG0000110 and OG0000141) were also added as the expanded gene family according to the additional standard (see Method section). Further analysis of representative gene families revealed four main points (figs. S28B and S29): 1) the extensive contraction of gene families in tardigrades is concentrated in biological processes such as tissue/organ development, chromatin remodeling, and transcription regulation, suggesting that tardigrades may have a simplified organism structure and

transcriptional regulation mechanism that might be beneficial for tolerating extreme environments; 2) the expansion of genes related to oxidative stress in tardigrades indicates this classic protective mechanism may be intensified in tardigrades; 3) Expansion of the GPCR family in the tardigrade genome may relate to more complicated signaling in response to various extreme environmental conditions; 4) the UDP-glucuronosyltransferase (UGT) family is expanded in tardigrades, sharing the highest sequence identity with the UGT family in plants. Interestingly, multiple UGT family molecules in plants are associated with stress resistance (*160*, *161*), indicating that the UGT family may play an important role in tardigrades' tolerance to extreme environments.

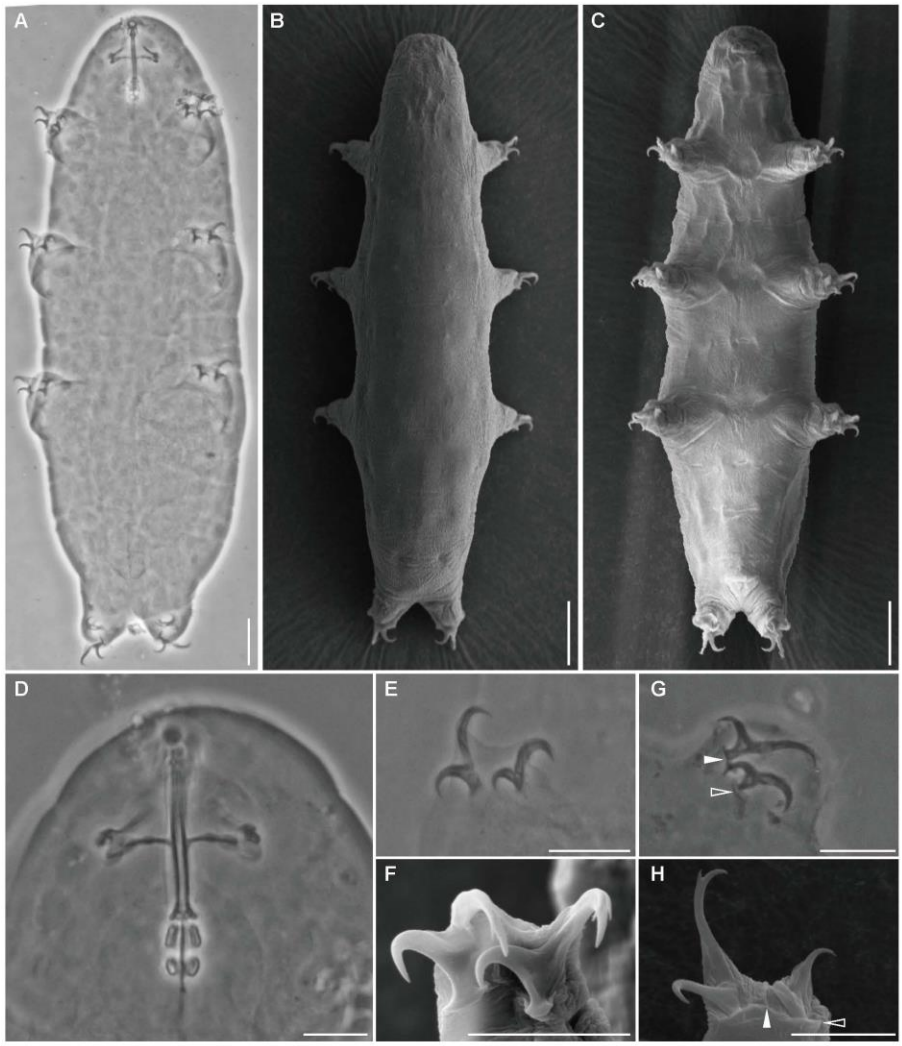
A
B
C
D
E
G
F
H

Fig. S1. Morphological analysis of *H. henanensis* sp. nov. (A) Adult habitus (ventral view, holotype, PCM). **(B)** Habitus in dorsal view (SEM). **(C)** Ventral view (paratype, SEM). **(D)** Buccal apparatus (holotype, PCM). **(E)** claws III (holotype, PCM). **(F)** claws III (holotype, SEM). **(G)** claws IV (holotype, PCM). **(H)** claws IV (paratype, SEM). The arrowhead indicates the longitudinal bar at the posterior claw base, and the empty arrowhead indicates the pseudolunula at the anterior claw base. Scale bars, 20 μm in (A) to (C), and 10 μm in (D) to (H).

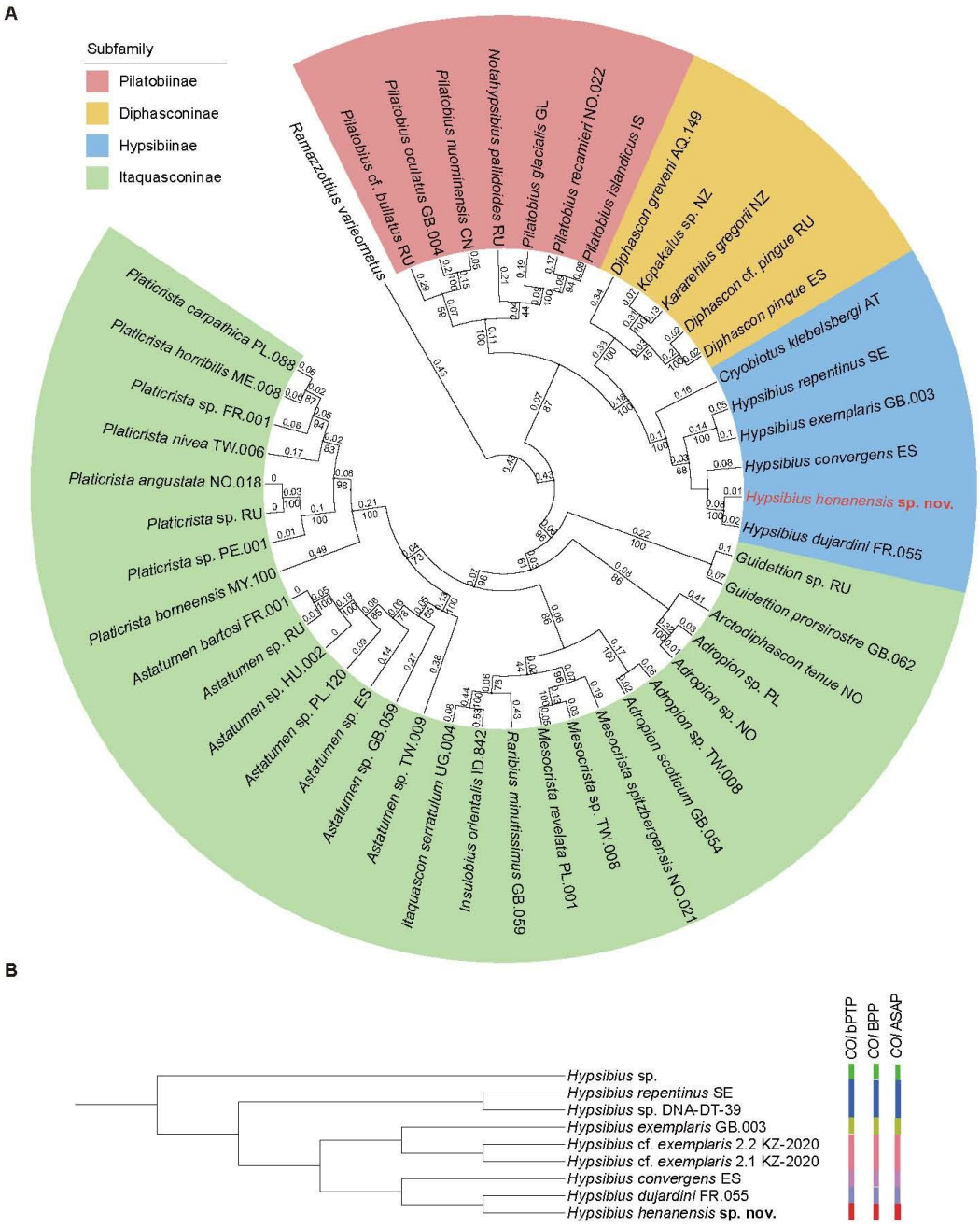
A
Subfamily
Pilatobiinae
Diphasconinae
Hypsibiinae
Itaquasconinae
Pilatobius glacialis GL
Pilatobius recamieri NO.022
Pilatobius islandicus IS
Notahypsibius pallidoides RU
Pilatobius nuominensis CN
Pilatobius oculatus GB.004
Pilatobius cf. bullatus RU
Ramazzottius varieornatus
Diphascon greveni AQ.149
Kopakalus sp. NZ
Kararehius gregorii NZ
Diphascon cf. pingue RU
Diphascon pingue ES
Cryobiotus klebelsbergi AT
Hypsibius repentinus SE
Hypsibius exemplaris GB.003
Hypsibius convergens ES
Hypsibius henanensis sp. nov.
Hypsibius dujardini FR.055
Guidettion sp. RU
Guidettion prorsirostre GB.062
Arctodiphascon tenue NO
Adropion sp. PL
Adropion sp. NO
Adropion sp. TW.008
Adropion scoticum GB.054
Mesocrista sp. TW.008
Mesocrista spitzbergensis NO.021
Mesocrista revelata PL.001
Raribius minutissimus GB.059
Insulobius orientalis ID.842
Itaquascon serratulum UG.004
Astatumen sp. TW.009
Astatumen sp. GB.059
Astatumen sp. ES
Astatumen sp. PL.120
Astatumen sp. HU.002
Astatumen sp. RU
Astatumen barfosi FR.001
Platicrista borneensis MY.100
Platicrista sp. PE.001
Platicrista sp. RU
Platicrista angustata NO.018
Platicrista nivea TW.006
Platicrista sp. FR.001
Platicrista horribilis ME.008
Platicrista carpathica PL.088
B
Hypsibius sp.
Hypsibius repentinus SE
Hypsibius sp. DNA-DT-39
Hypsibius exemplaris GB.003
Hypsibius cf. exemplaris 2.2 KZ-2020
Hypsibius cf. exemplaris 2.1 KZ-2020
Hypsibius convergens ES
Hypsibius dujardini FR.055
Hypsibius henanensis sp. nov.
COI bPTP
COI BPP
COI ASAP

c

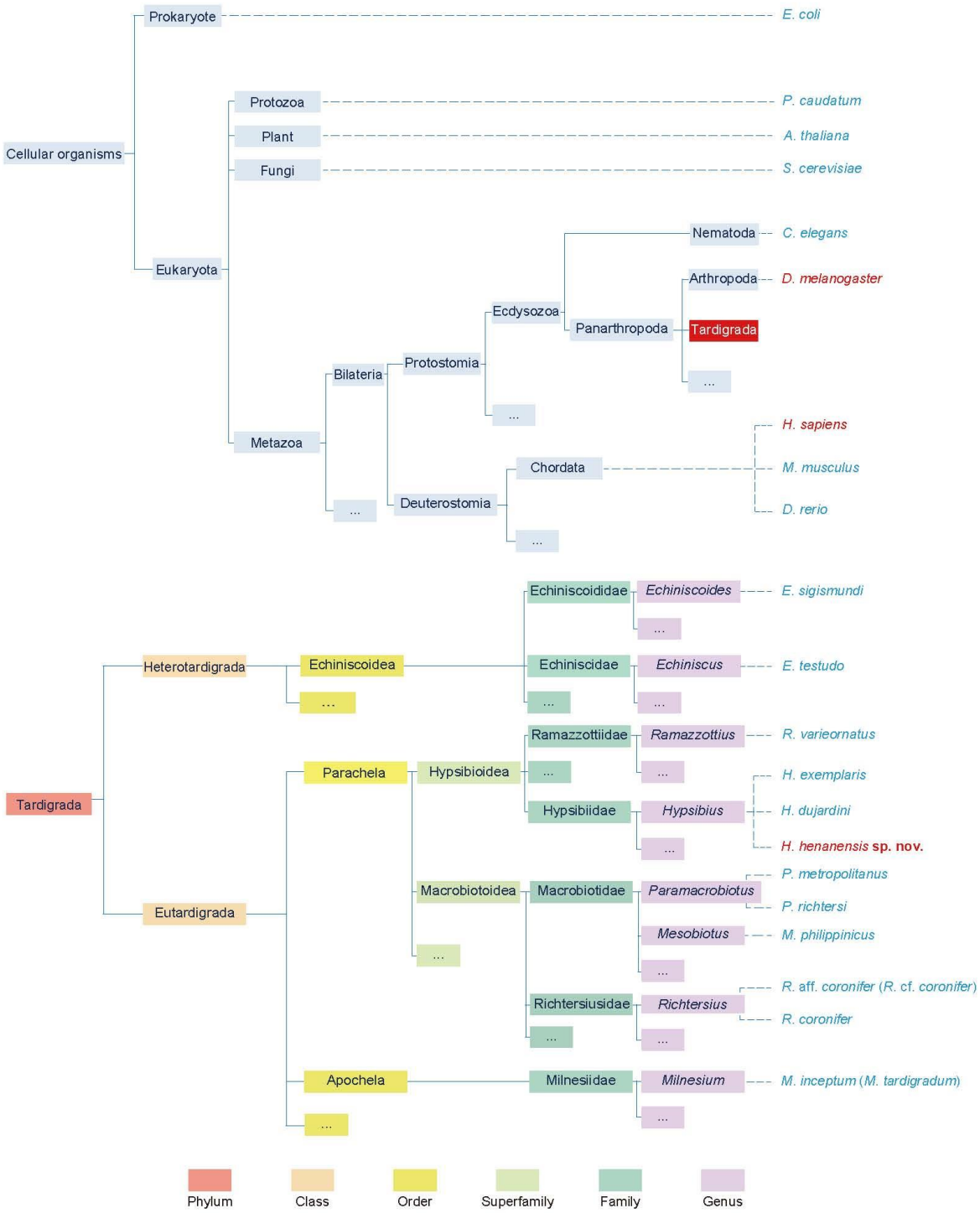
Prokaryote
E. coli
Protozoa
P. caudatum
Plant
A. thaliana
Cellular organisms
Fungi
S. cerevisiae
Nematoda
C. elegans
Eukaryota
Arthropoda
D. melanogaster
Ecdysozoa
Panarthropoda
Tardigrada
Bilateria
Protostomia
...
...
Metazoa
H. sapiens
Chordata
M. musculus
...
Deuterostomia
D. rerio
...
Echiniscoididae
Echiniscoides
E. sigismundi
...
Heterotardigrada
Echiniscoidea
Echiniscidae
Echiniscus
E. testudo
...
...
...
Ramazzottiidae
Ramazzottius
R. varieornatus
Parachela
Hypsibioidea
...
...
H. exemplaris
Tardigrada
Hypsibiidae
Hypsibius
H. dujardini
...
H. henanensis sp. nov.
P. metropolitanus
Macrobiotoidea
Macrobiotidae
Paramacrobiotus
P. richtersi
Eutardigrada
Mesobiotus
M. philippinicus
...
...
R. aff. coronifer (R. cf. coronifer)
Richtersiusidae
Richtersius
R. coronifer
...
...
Apochela
Milnesiidae
Milnesium
M. inceptum (M. tardigradum)
...
...
Phylum
Class
Order
Superfamily
Family
Genus

Fig. S2. Molecular taxonomy of *H. henanensis* sp. nov. (A) Phylogenetic analysis of *H. henanensis* **sp. nov.** and the other 45 known species in the family Hypsibiidae, with *Ramazzottius varieornatus* as an outgroup. Four DNA markers (18S rRNA, 28S rRNA, COI and ITS-2) sequences were concatenated and partitioned for the tree building using maximum likelihood method. **(B)** Species delimitation of *H. henanensis* **sp. nov.** Maximum likelihood phylogenetic reconstruction of the relationships between the specimens (*H. dujardini* morphogroup members and *Hypsibius convergens*), *Hypsibius* sp. is the outgroup. **(C)** Position of *H. henanensis* **sp. nov.** in the tree of life. The upper panel shows the position of the phylum Tardigrada in the evolutionary tree. The lower panel shows the tree of the phylum Tardigrada. Representative instance species are listed at the end of each branch. The full names of them (from top to bottom): *Escherichia coli*, *Paramoecium caudatum*, *Arabidopsis thaliana*, *Saccharomyces cerevisiae*, *Caenorhabditis elegans*, *Drosophila melanogaster*, *Homo sapiens*, *Mus musculus*, *Danio rerio*, *Echiniscoides sigismundi*, *Echiniscus testudo*, *Ramazzottius varieornatus*, *Hypsibius exemplaris*, *Hypsibius dujardini*, *Hypsibius henanensis* **sp. nov.**, *Paramacrobiotus metropolitanus*, *Paramacrobiotus richtersi*, *Mesobiotus philippinicus*, *Richtersius* aff. *coronifer* (previously misidentified as *Richtersius coronifer*) *(162), Richtersius coronifer*, *Milnesium inceptum* (previously misidentified as *Milnesium tardigradum*) (*163*).The most closed classic model organism *D. melanogaster* is labeled in red. To illustrate the relationship between tardigrades and humans, *H. sapiens* is also labeled in red. The grades are shown in different background colors.

A

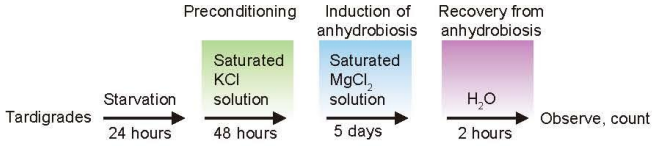

B

Group	1	2	3	4	Mean value	SD
Total	31	30	29	29		
Alive	27	27	25	23		
Survival rate (%)	87.10	90.00	86.21	79.31	85.65	4.53

C

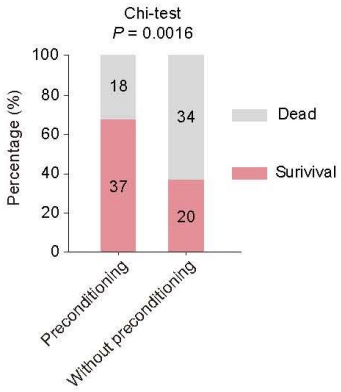

D

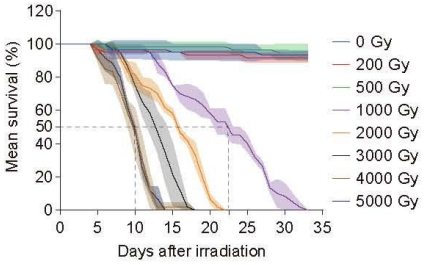

Fig. S3. Radiation and desiccation tolerance of *H. henanensis* sp. nov. (**A** and **B**) Desiccation tolerance of *H. henanensis* **sp. nov.** (A) Summary chart of the workflow for anhydrobiosis induction and recovery of *H. henanensis* **sp. nov.** (B) Survival rate analysis of *H. henanensis* **sp. nov.** after anhydrobiosis induction and recovery. Data are representative of four independent experiments. **(C)** Two groups of tardigrades, preconditioning (n = 55, exposed to saturated solution of KCl for 2 days and saturated solution of $MgCl_2$ for 5 days) and without-preconditioning (n = 54, only exposed to saturated solution of $MgCl_2$ for 7 days), were used to observe the effects of preconditioning on their survival. The Chi-square test was utilized for conducting differential statistical analysis. (**D**) Survival of adult *H. henanensis* **sp. nov.** after exposure to different doses of γ irradiation. The data are presented as mean ± SD from 3 repeats, each with 20 animals. The Jonckheere-Terpstra nonparametric test was used for the differential statistical analysis. The results of statistical analysis are in data S10.

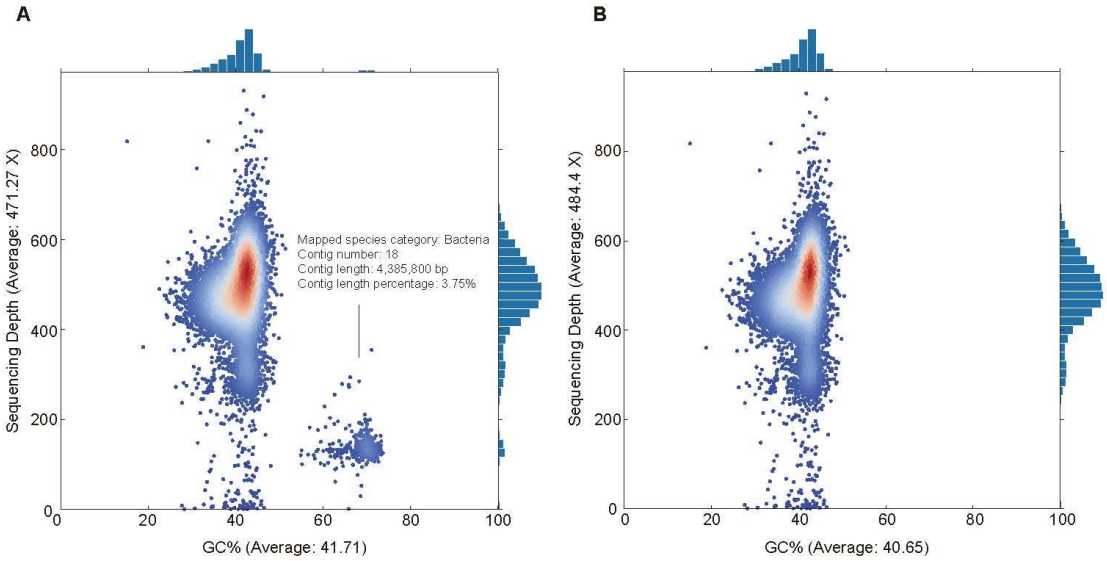
A
B
Sequencing Depth (Average: 471.27 X)
GC% (Average: 41.71)
Mapped species category: Bacteria
Contig number: 18
Contig length: 4,385,800 bp
Contig length percentage: 3.75%
Sequencing Depth (Average: 484.4 X)
GC% (Average: 40.65)
0
200
400
600
800
0
20
40
60
80
100

Fig. S4. GC-depth plot of the assembled genome and the potential contaminants. (**A**) The GC-depth plot before removing potential contaminants. The contig number and contig length of contigs matched with species from bacteria are presented. (**B**) The GC-depth plot after removing potential contaminants from bacteria.

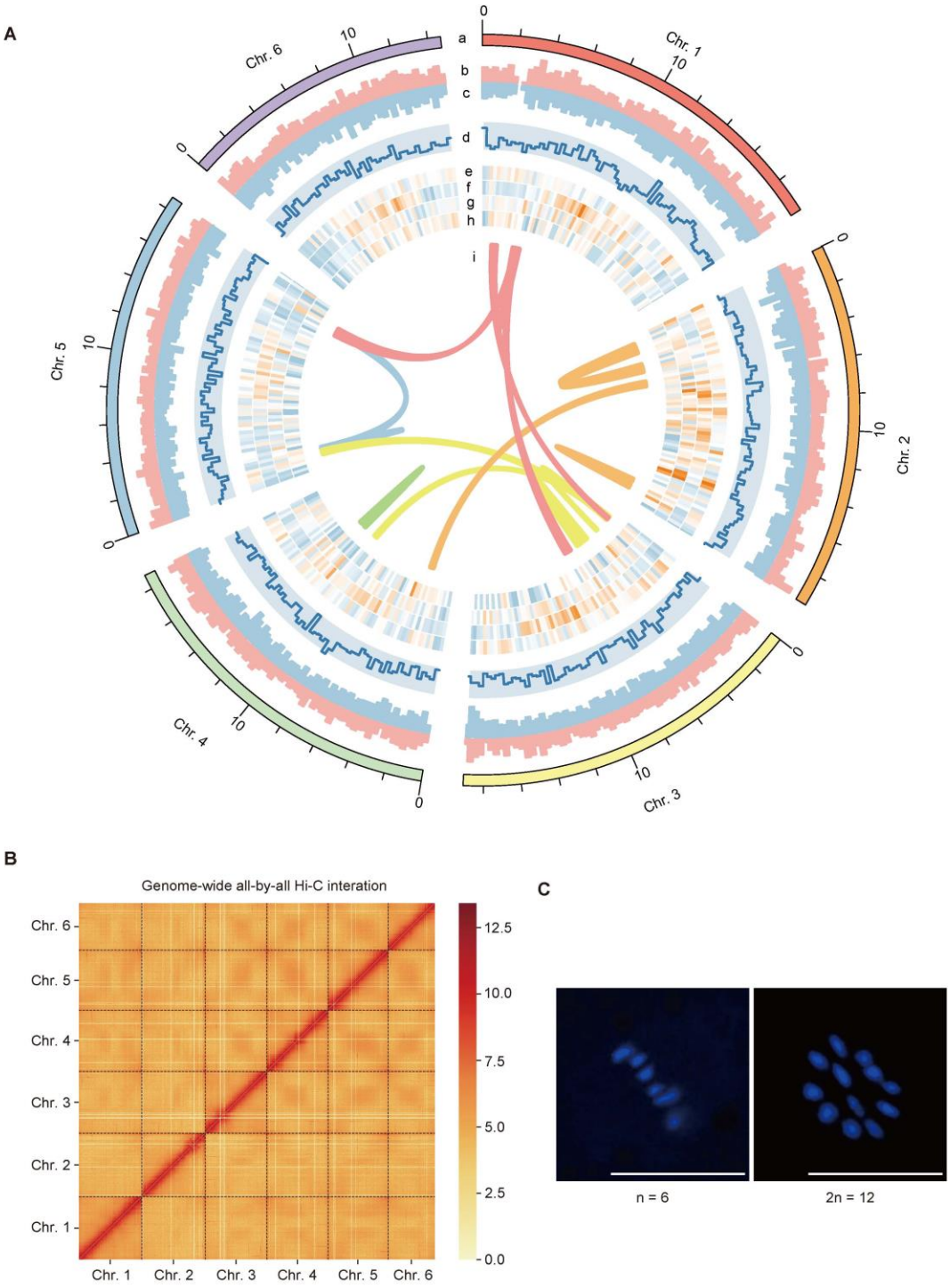
A
Chr. 1
Chr. 2
Chr. 3
Chr. 4
Chr. 5
Chr. 6
a
b
c
d
e
f
g
h
i
0
10
B
Genome-wide all-by-all Hi-C interation
Chr. 1
Chr. 2
Chr. 3
Chr. 4
Chr. 5
Chr. 6
12.5
10.0
7.5
5.0
2.5
0.0
C
n = 6
2n = 12

Fig. S5. Chromosome-level genome assembly and annotation. (**A**) The distribution of genes and transposable elements on different chromosomes of the genome of *H. henanensis* **sp. nov.** a, the 6 chromosomes. b & c, the density distribution of protein-coding genes in the genome (unit: 30,000 bp; b, the sense chain; c, the antisense chain). d, the distribution of simple sequence repeats (SSRs) in the genome. The heatmap color blocks show the distribution of transposable element in the genome, from e to h are LTR (long terminal repeats), MITE (miniature inverted-repeat transposable element)), LINE (long interspersed nuclear elements), and SINE (short interspersed nuclear elements), respectively. i, collinearity between different chromosomes. (**B**) The Hi-C heatmap indicates there are six pseudochromosomes in *H. henanensis* **sp. nov.** Red block represents a strong interaction between regions within/between the pseudochromosomes. (**C**) Karyotypes in haploid embryo (left) and diploid embryo (right) of *H. henanensis* **sp. nov.** stained by DAPI. Scale bars, 10 μm.

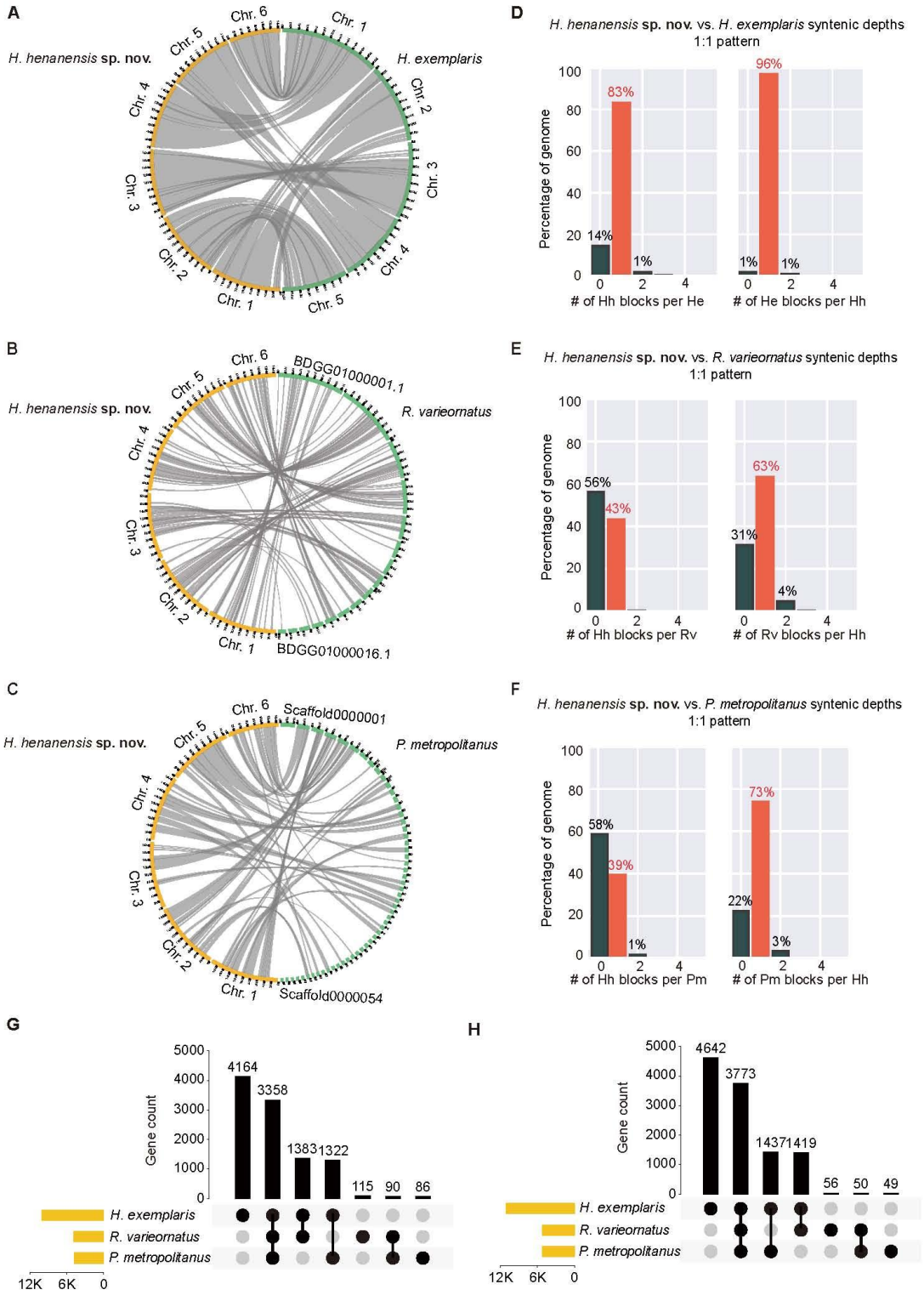
A
H. henanensis sp. nov.
H. exemplaris
Chr. 6
Chr. 1
Chr. 5
Chr. 4
Chr. 2
Chr. 3
B
H. henanensis sp. nov.
R. varieornatus
BDGG01000001.1
BDGG01000016.1
C
H. henanensis sp. nov.
P. metropolitanus
Scaffold0000001
Scaffold0000054
D
H. henanensis sp. nov. vs. H. exemplaris syntenic depths
1:1 pattern
Percentage of genome
# of Hh blocks per He
# of He blocks per Hh
14%
83%
1%
1%
96%
1%
E
H. henanensis sp. nov. vs. R. varieornatus syntenic depths
1:1 pattern
# of Hh blocks per Rv
# of Rv blocks per Hh
56%
43%
31%
63%
4%
F
H. henanensis sp. nov. vs. P. metropolitanus syntenic depths
1:1 pattern
# of Hh blocks per Pm
# of Pm blocks per Hh
58%
39%
1%
22%
73%
3%
G
Gene count
4164
3358
1383
1322
115
90
86
H. exemplaris
R. varieornatus
P. metropolitanus
12K
6K
0
H
Gene count
4642
3773
1437
1419
56
50
49
H. exemplaris
R. varieornatus
P. metropolitanus
12K
6K
0

Fig. S6. Genomic synteny between *H. henanensis* sp. nov. and the other three tardigrades with available genome sequence. (**A** to **C**) Circus diagram of synteny analysis between *H. henanensis* **sp. nov.** and *H. exemplaris* (A), *R. varieornatus* (B) and *P. metropolitanus* (C). Six yellow segments on the left half circle represent the six chromosomes of *H. henanensis* **sp. nov.** (Hh), and the green segments on the right half circle, correspond to each scaffold of the other three tardigrades. The inner gray line represents the synteny region. (**D** to **F**) The synteny patterns of all synteny blocks (with added anchor blocks). The red bars represent the proportion of 1:1 matches. (**G** and **H**) The Hh gene number in the synteny blocks (G for high-quality blocks, and H for the synteny pattern with added anchor points) between Hh and the other three tardigrades. The yellow and black bar charts represent the number of genes in synteny block. The black and gray circles indicate the presence and absence of synteny relationships, respectively. Abbreviations in the figure: Hh, *H. henanensis* **sp. nov.**; He, *H. exemplaris*; Rv, *R. varieornatus*; Pm, *P. metropolitanus*.

A

Experiment groups	0 Gy	200 Gy	2000 Gy	Total
Quantitative transcripts	12460	12224	12025	12629
Upregulated transcripts	~	240	1111	1140
Downregulated transcripts	~	131	1152	1183
Quantitative Protein IDs	2844	3162	3242	3366
Upregulated proteins	~	400	416	526
Downregulated proteins	~	44	25	64

B

Transcriptome

0 Gy_1	$< 1 \times 10^{-320}$	$< 1 \times 10^{-320}$
0.985	0 Gy_2	$< 1 \times 10^{-320}$
0.987	0.989	0 Gy_3

200 Gy_1	$< 1 \times 10^{-320}$	$< 1 \times 10^{-320}$
0.985	200 Gy_2	$< 1 \times 10^{-320}$
0.989	0.991	200 Gy_3

2000 Gy_1	$< 1 \times 10^{-320}$	$< 1 \times 10^{-320}$
0.989	2000 Gy_2	$< 1 \times 10^{-320}$
0.987	0.987	2000 Gy_3

C

Proteome

0 Gy_1	$< 1 \times 10^{-320}$	$< 1 \times 10^{-320}$
0.869	0 Gy_2	$< 1 \times 10^{-320}$
0.887	0.894	0 Gy_3

200 Gy_1	$< 1 \times 10^{-320}$	$< 1 \times 10^{-320}$
0.932	200 Gy_2	$< 1 \times 10^{-320}$
0.918	0.919	200 Gy_3

2000 Gy_1	$< 1 \times 10^{-320}$	$< 1 \times 10^{-320}$
0.903	2000 Gy_2	$< 1 \times 10^{-320}$
0.901	0.934	2000 Gy_3

D

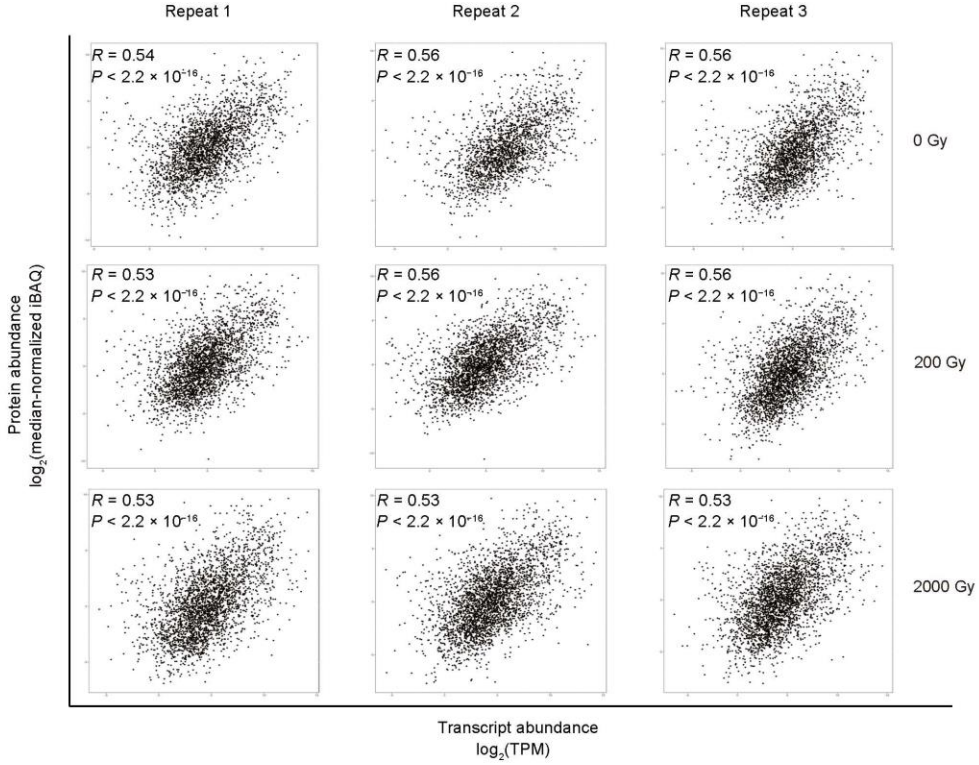

Fig. S7. Overview of multi-omics scheme of *H. henanensis* sp. nov. after irradiation and quality control of the data. (**A**) Summary of the identified and quantified transcripts, proteins, and differentially expressed genes (DEGs) at transcriptome and proteome levels. (**B** and **C**) The spearman correlation coefficient between the three replicates of the samples in three irradiation doses of transcriptome and proteome. The blue part in the table represents the *P* value. (**D**) The spearman correlation between the expression levels of transcripts and proteins under different irradiation doses. *R* and *P* represent the correlation coefficients and the *P* values, respectively.

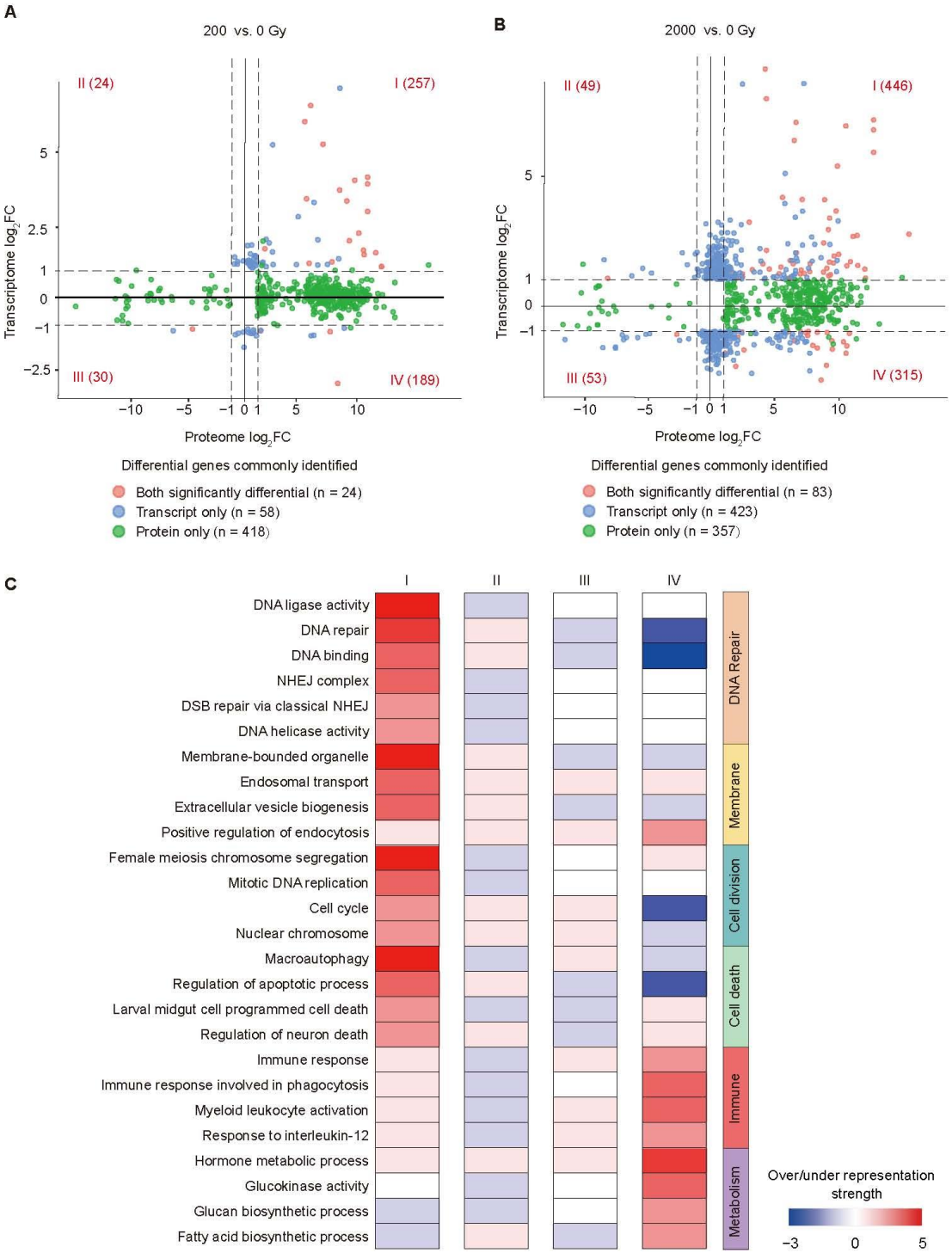
A
200 vs. 0 Gy
II (24)
I (257)
III (30)
IV (189)
Transcriptome log2FC
Proteome log2FC
Differential genes commonly identified
Both significantly differential (n = 24)
Transcript only (n = 58)
Protein only (n = 418)
B
2000 vs. 0 Gy
II (49)
I (446)
III (53)
IV (315)
Transcriptome log2FC
Proteome log2FC
Differential genes commonly identified
Both significantly differential (n = 83)
Transcript only (n = 423)
Protein only (n = 357)
C
I
II
III
IV
DNA ligase activity
DNA repair
DNA binding
NHEJ complex
DSB repair via classical NHEJ
DNA helicase activity
Membrane-bounded organelle
Endosomal transport
Extracellular vesicle biogenesis
Positive regulation of endocytosis
Female meiosis chromosome segregation
Mitotic DNA replication
Cell cycle
Nuclear chromosome
Macroautophagy
Regulation of apoptotic process
Larval midgut cell programmed cell death
Regulation of neuron death
Immune response
Immune response involved in phagocytosis
Myeloid leukocyte activation
Response to interleukin-12
Hormone metabolic process
Glucokinase activity
Glucan biosynthetic process
Fatty acid biosynthetic process
DNA Repair
Membrane
Cell division
Cell death
Immune
Metabolism
Over/under representation strength
−3
0
5

Fig. S8. Functional interpretation of the DEGs obtained from the combined analysis of transcriptome and proteome. (**A** and **B**) Filtrated 1,007 DEGs that were both identified in transcriptome and proteome after irradiation (A. 200 Gy, B. 2,000 Gy). It is divided into four quadrants based on the log_2FC (FC, fold change) value. Quadrants I and III include gene expression changes that are concordant at the transcript and protein level; whereas quadrants II and IV depict discordant changes. (**C**) Functional enrichment analysis of four quadrant differential genes both in (A) and (B).

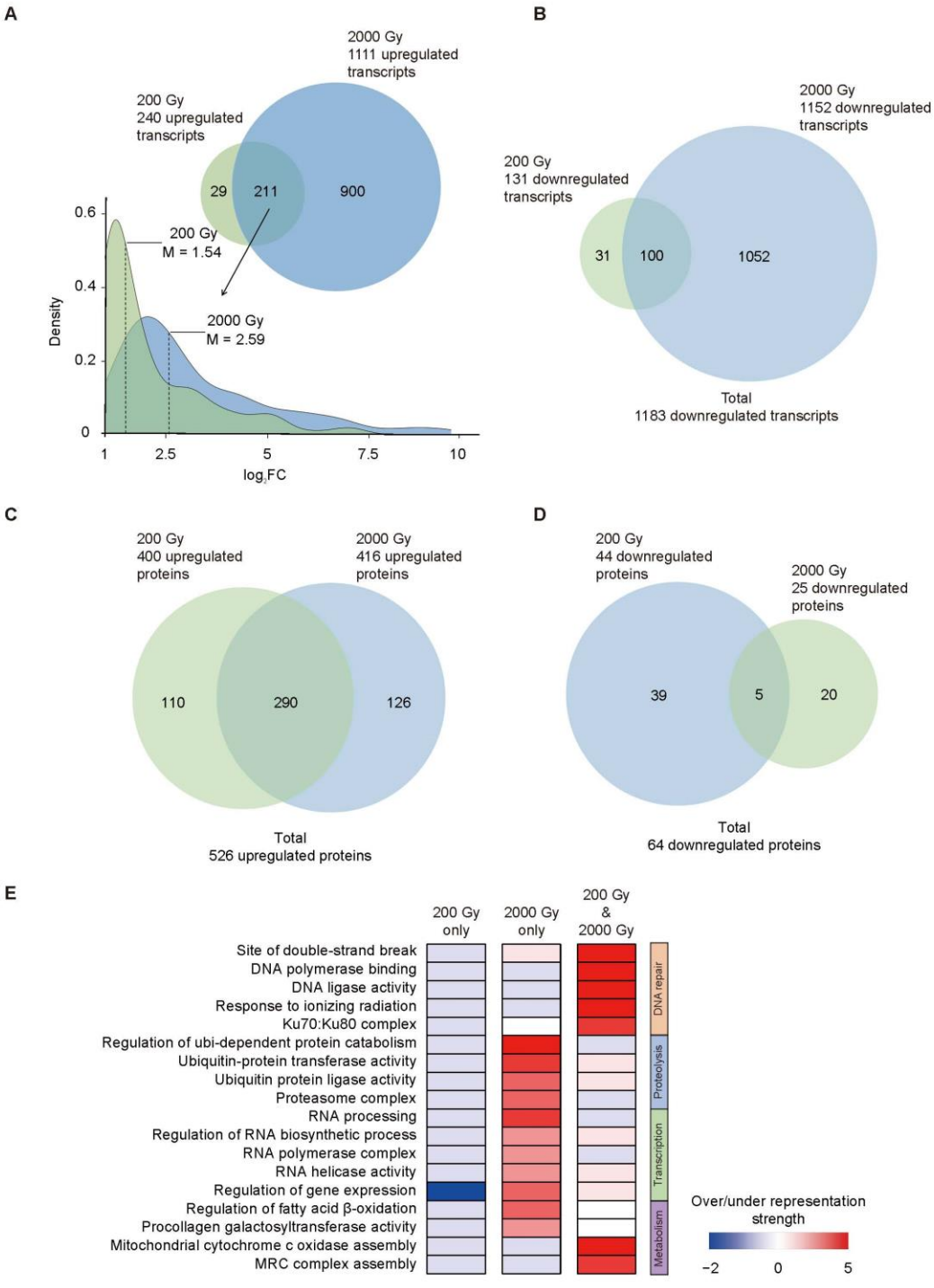
A
2000 Gy
1111 upregulated
transcripts
200 Gy
240 upregulated
transcripts
29
211
900
200 Gy
M = 1.54
2000 Gy
M = 2.59
Density
0.6
0.4
0.2
0
1
2.5
5
7.5
10
log2FC
B
2000 Gy
1152 downregulated
transcripts
200 Gy
131 downregulated
transcripts
31
100
1052
Total
1183 downregulated transcripts
C
200 Gy
400 upregulated
proteins
2000 Gy
416 upregulated
proteins
110
290
126
Total
526 upregulated proteins
D
200 Gy
44 downregulated
proteins
2000 Gy
25 downregulated
proteins
39
5
20
Total
64 downregulated proteins
E
200 Gy
only
2000 Gy
only
200 Gy
&
2000 Gy
Site of double-strand break
DNA polymerase binding
DNA ligase activity
Response to ionizing radiation
Ku70:Ku80 complex
Regulation of ubi-dependent protein catabolism
Ubiquitin-protein transferase activity
Ubiquitin protein ligase activity
Proteasome complex
RNA processing
Regulation of RNA biosynthetic process
RNA polymerase complex
RNA helicase activity
Regulation of gene expression
Regulation of fatty acid β-oxidation
Procollagen galactosyltransferase activity
Mitochondrial cytochrome c oxidase assembly
MRC complex assembly
DNA repair
Proteolysis
Transcription
Metabolism
Over/under representation
strength
−2
0
5

Fig. S9. Comparative analysis of DEGs at different irradiation doses. (**A**) The Venn diagram shows the number of upregulated transcripts at doses of 200 and 2,000 Gy, while the density plot shows the distribution of changes in upregulated transcripts at different radiation doses. (**B**) Venn diagram of the number of downregulated transcripts at doses of 200 and 2,000 Gy. (**C** and **D**) Venn diagram of the number of upregulated (C) or downregulated (D) proteins at doses of 200 and 2,000 Gy. (**E**) Functional enrichment analysis of upregulated transcripts at different doses. The three columns represent "upregulated only at 200 Gy irradiation", "upregulated only at 2,000 Gy irradiation", and "upregulated at both 200 Gy and 2,000 Gy irradiation" respectively. The over/under-representation strengths are represented by the graded values of −/+ log(P) (for detailed information, please refer to Materials and Methods section) and displayed in a gradient color from red (over-representation) to dark blue (under-representation).

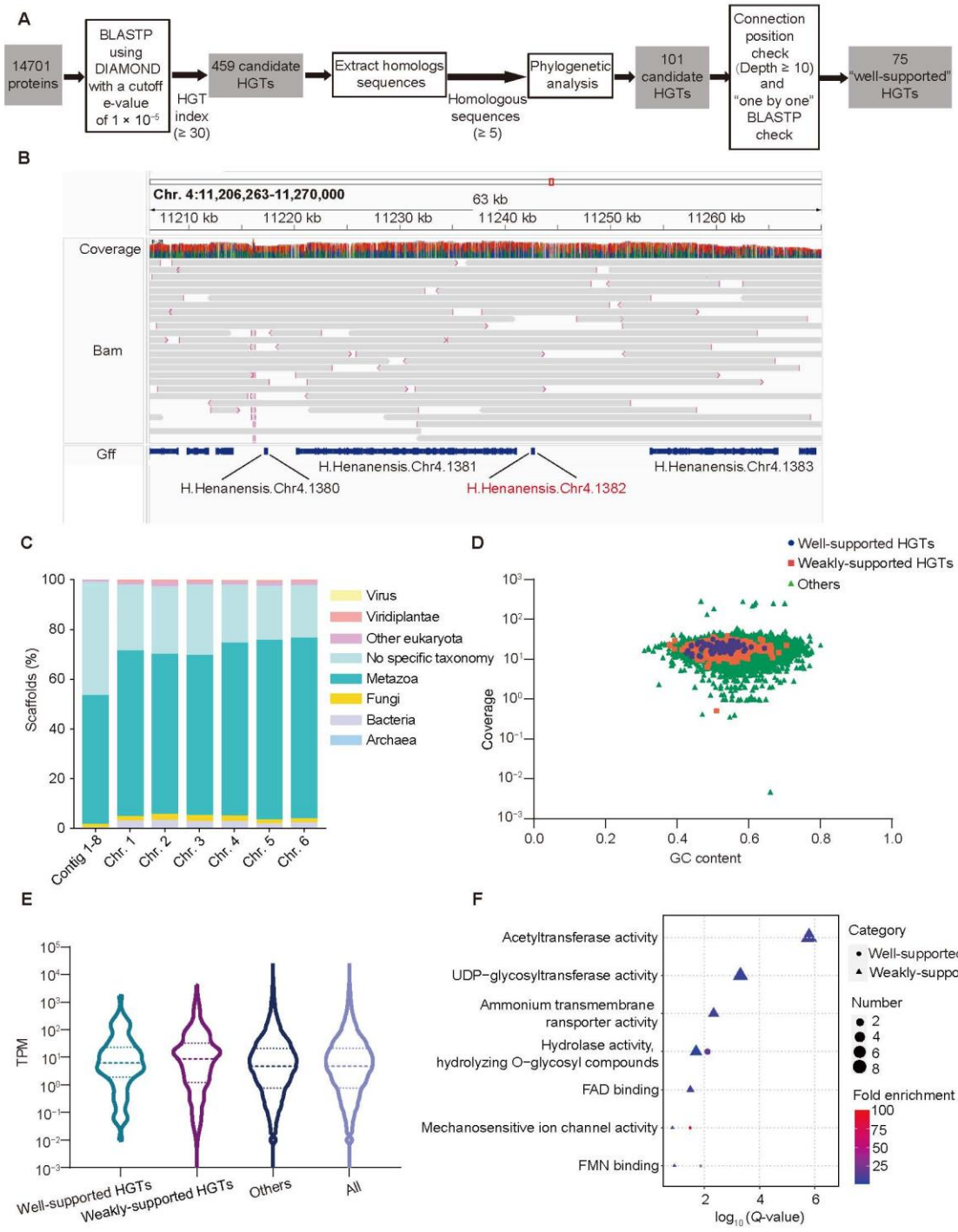
A
14701 proteins
BLASTP using DIAMOND with a cutoff e-value of 1 × 10⁻⁵
HGT index (≥ 30)
459 candidate HGTs
Extract homologs sequences
Homologous sequences (≥ 5)
Phylogenetic analysis
101 candidate HGTs
Connection position check (Depth ≥ 10) and "one by one" BLASTP check
75 "well-supported" HGTs
B
Chr. 4:11,206,263-11,270,000
63 kb
11210 kb
11220 kb
11230 kb
11240 kb
11250 kb
11260 kb
Coverage
Bam
Gff
H.Henanensis.Chr4.1380
H.Henanensis.Chr4.1381
H.Henanensis.Chr4.1382
H.Henanensis.Chr4.1383
C
Scaffolds (%)
Virus
Viridiplantae
Other eukaryota
No specific taxonomy
Metazoa
Fungi
Bacteria
Archaea
Contig 1-8
Chr. 1
Chr. 2
Chr. 3
Chr. 4
Chr. 5
Chr. 6
D
Well-supported HGTs
Weakly-supported HGTs
Others
Coverage
GC content
E
TPM
Well-supported HGTs
Weakly-supported HGTs
Others
All
F
Acetyltransferase activity
UDP−glycosyltransferase activity
Ammonium transmembrane ransporter activity
Hydrolase activity, hydrolyzing O−glycosyl compounds
FAD binding
Mechanosensitive ion channel activity
FMN binding
log10(Q-value)
Category
Well-supported
Weakly-supported
Number
Fold enrichment

Fig. S10. Identifying HGT candidates and Gene ontology (GO) term enrichment analysis. (**A**) The workflow used for the identification of "well-supported" HGT genes. (**B**) Representative results (DOPA dioxygenase) for connection positions check of HGT candidates. Bacterially derived DOPA dioxygenase was marked as "H.Henanensis.Chr4.1382", and neighboring genes were metazoan origin, and the connection positions of three genes can be spanned smoothly by a same Nanopore read. Connection positions check was visualized in IGV software. (**C**) Stacked histogram showing all scaffolds distribution in different kingdoms. (**D)** Distribution of genes (weakly-supported and well-supported HGT candidates, and all other genes) based on GC content and coverage with Nanopore genomic reads (20 ×). (**E**) Expression level of weakly-supported and well-supported HGT candidates, all other genes, and all genes in *H. henanensis* **sp. nov.** assembly. TPM, transcripts per million. (**F**) Gene ontology (GO) term enrichment analysis of well-supported and weakly-supported genes in *H. henanensis* **sp. nov.** Well-supported HGTs and weakly-supported HGTs were represented as different shapes.

A

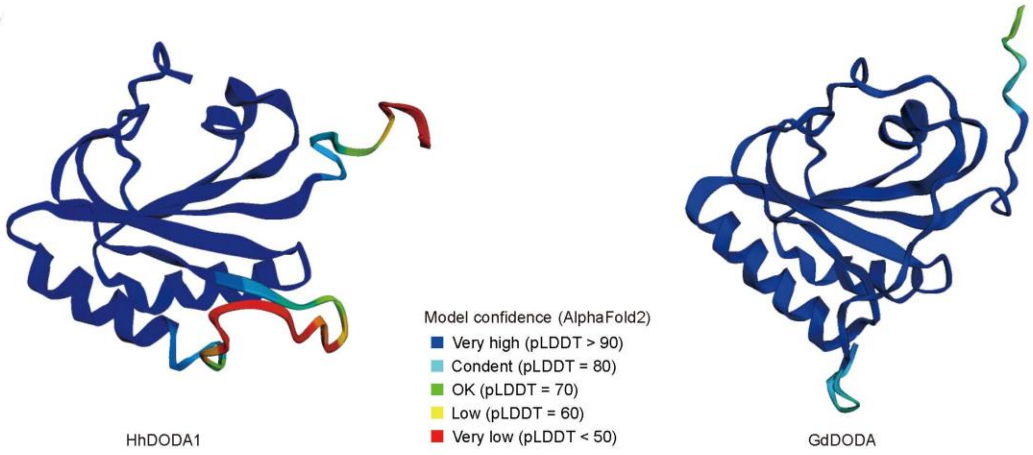

HhDODA1

GdDODA

B

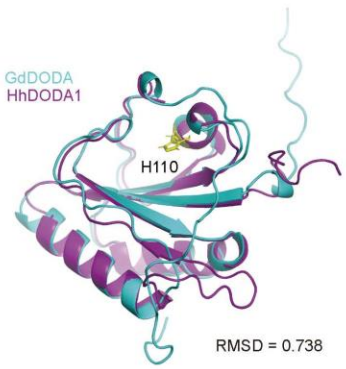

Fig. S11. Structure and model for DODA. (**A**) Structure models of HhDODA1 or GdDODA predicted by AlphaFold2. Colours ranging from blue to orange depict the per-residue measure of local confidence (pLDDT) for the model. (**B**) Structural model for HhDODA1 (purple) superimposed on GdDODA (cyan). Yellow portions of the proteins indicate histidine 110 of HhDODA1, corresponding to predicted strictly conserved histidine 101 of GdDODA. Root Mean Square Deviation (RMSD) value is shown.

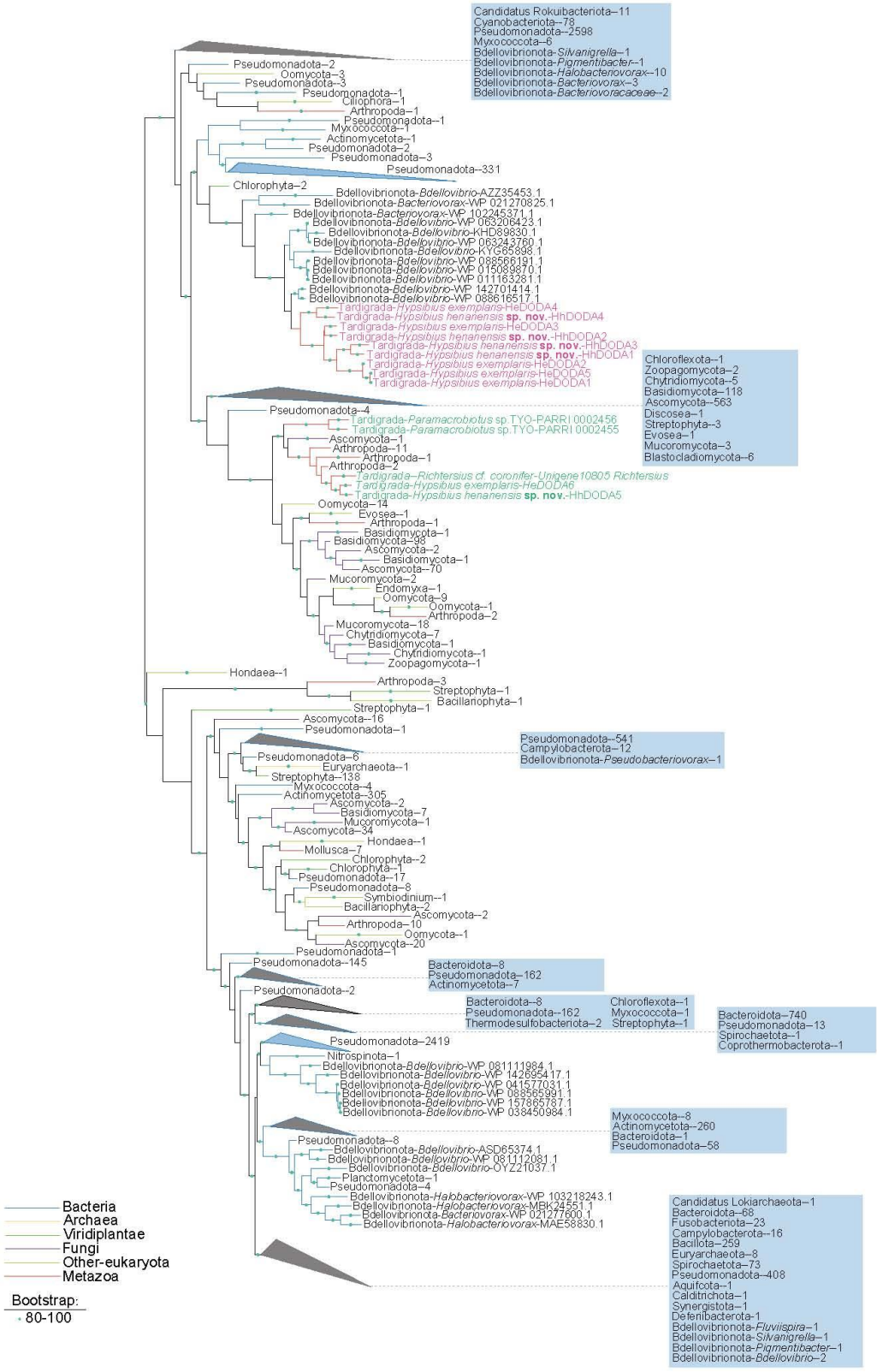
Candidatus Rokuibacteriota–11
Cyanobacteriota–78
Pseudomonadota–2598
Myxococcota–6
Bdellovibrionota-Silvanigrella–1
Bdellovibrionota-Pigmentibacter–1
Bdellovibrionota-Halobacteriovorax–10
Bdellovibrionota-Bacteriovorax–3
Bdellovibrionota-Bacteriovoracaceae–2
Pseudomonadota–2
Oomycota–3
Pseudomonadota–3
Pseudomonadota–1
Ciliophora–1
Arthropoda–1
Pseudomonadota–1
Myxococcota–1
Actinomycetota–1
Pseudomonadota–2
Pseudomonadota–3
Pseudomonadota–331
Chlorophyta–2
Bdellovibrionota-Bdellovibrio-AZZ35453.1
Bdellovibrionota-Bacteriovorax-WP 021270825.1
Bdellovibrionota-Bacteriovorax-WP 102245371.1
Bdellovibrionota-Bdellovibrio-WP 063206423.1
Bdellovibrionota-Bdellovibrio-KHD89830.1
Bdellovibrionota-Bdellovibrio-WP 063243760.1
Bdellovibrionota-Bdellovibrio-KYG85898.1
Bdellovibrionota-Bdellovibrio-WP 088566191.1
Bdellovibrionota-Bdellovibrio-WP 015089870.1
Bdellovibrionota-Bdellovibrio-WP 011163281.1
Bdellovibrionota-Bdellovibrio-WP 142701414.1
Bdellovibrionota-Bdellovibrio-WP 088616517.1
Tardigrada-Hypsibius exemplaris-HeDODA4
Tardigrada-Hypsibius henanensis sp. nov.-HhDODA4
Tardigrada-Hypsibius exemplaris-HeDODA3
Tardigrada-Hypsibius henanensis sp. nov.-HhDODA2
Tardigrada-Hypsibius henanensis sp. nov.-HhDODA3
Tardigrada-Hypsibius henanensis sp. nov.-HhDODA1
Tardigrada-Hypsibius exemplaris-HeDODA2
Tardigrada-Hypsibius exemplaris-HeDODA5
Tardigrada-Hypsibius exemplaris-HeDODA1
Chloroflexota–1
Zoopagomycota–2
Chytridiomycota–5
Basidiomycota–118
Ascomycota–563
Discosea–1
Streptophyta–3
Evosea–1
Mucoromycota–3
Blastocladiomycota–6
Pseudomonadota–4
Tardigrada-Paramacrobiotus sp.TYO-PARRI 0002456
Tardigrada-Paramacrobiotus sp.TYO-PARRI 0002455
Ascomycota–1
Arthropoda–11
Arthropoda–1
Arthropoda–2
Tardigrada–Richtersius cf. coronifer-Unigene10805 Richtersius
Tardigrada-Hypsibius exemplaris-HeDODA6
Tardigrada-Hypsibius henanensis sp. nov.-HhDODA5
Oomycota–14
Evosea–1
Arthropoda–1
Basidiomycota–1
Basidiomycota–98
Ascomycota–2
Basidiomycota–1
Ascomycota–70
Mucoromycota–2
Endomyxa–1
Oomycota–9
Oomycota–1
Arthropoda–2
Mucoromycota–18
Chytridiomycota–7
Basidiomycota–1
Chytridiomycota–1
Zoopagomycota–1
Hondaea–1
Arthropoda–3
Streptophyta–1
Bacillariophyta–1
Streptophyta–1
Ascomycota–16
Pseudomonadota–1
Pseudomonadota–541
Campylobacterota–12
Bdellovibrionota-Pseudobacteriovorax–1
Pseudomonadota–6
Euryarchaeota–1
Streptophyta–138
Myxococcota–4
Actinomycetota–305
Ascomycota–2
Basidiomycota–7
Mucoromycota–1
Ascomycota–34
Hondaea–1
Mollusca–7
Chlorophyta–2
Chlorophyta–1
Pseudomonadota–17
Pseudomonadota–8
Symbiodinium–1
Bacillariophyta–2
Ascomycota–2
Arthropoda–10
Oomycota–1
Ascomycota–20
Pseudomonadota–1
Pseudomonadota–145
Bacteroidota–8
Pseudomonadota–162
Actinomycetota–7
Pseudomonadota–2
Bacteroidota–8
Pseudomonadota–162
Thermodesulfobacteriota–2
Chloroflexota–1
Myxococcota–1
Streptophyta–1
Bacteroidota–740
Pseudomonadota–13
Spirochaetota–1
Coprothermobacterota–1
Pseudomonadota–2419
Nitrospinota–1
Bdellovibrionota-Bdellovibrio-WP 081111984.1
Bdellovibrionota-Bdellovibrio-WP 142695417.1
Bdellovibrionota-Bdellovibrio-WP 041577031.1
Bdellovibrionota-Bdellovibrio-WP 088565991.1
Bdellovibrionota-Bdellovibrio-WP 157865787.1
Bdellovibrionota-Bdellovibrio-WP 038450984.1
Myxococcota–8
Actinomycetota–260
Bacteroidota–1
Pseudomonadota–58
Pseudomonadota–8
Bdellovibrionota-Bdellovibrio-ASD65374.1
Bdellovibrionota-Bdellovibrio-WP 081112081.1
Bdellovibrionota-Bdellovibrio-OYZ21037.1
Planctomycetota–1
Pseudomonadota–4
Bdellovibrionota-Halobacteriovorax-WP 103218243.1
Bdellovibrionota-Halobacteriovorax-MBK24551.1
Bdellovibrionota-Bacteriovorax-WP 021277600.1
Bdellovibrionota-Halobacteriovorax-MAE58830.1
Candidatus Lokiarchaeota–1
Bacteroidota–68
Fusobacteriota–23
Campylobacterota–16
Bacillota–259
Euryarchaeota–8
Spirochaetota–73
Pseudomonadota–408
Aquifcota–1
Calditrichota–1
Synergistota–1
Defenibacterota–1
Bdellovibrionota-Fluviispira–1
Bdellovibrionota-Silvanigrella–1
Bdellovibrionota-Pigmentibacter–1
Bdellovibrionota-Bdellovibrio–2
Bacteria
Archaea
Viridiplantae
Fungi
Other-eukaryota
Metazoa
Bootstrap:
80-100

Fig. S12. Maximum likelihood phylogenetic analysis of DOPA dioxygenase. Homologous sequences of HhDODAs, DODAs that in Betalain-producing plants and *E. coli*, Lepidopteran insects and their homologous sequences were used for maximum likelihood tree construction with FastTree. The tree was midpoint rooted using the ape and phangorn R packages and visualized in iTOL (https://itol.embl.de/). Green dots were used when the relevant node was supported with 80% or more bootstrap support value. The triangle shape represents the collapsed subtree containing at least three phyla, and the phylum occupying more than 90% sequences in the subtree is shown. The values after the phylum names are the numbers of sequences included in the tree. For accession numbers and the raw tree file, see data S10. The species and gene names marked with red color represent homologous genes of *HhDODA1-4* in tardigrades and the green ones represent homologous genes of *HhDODA5* in tardigrades.

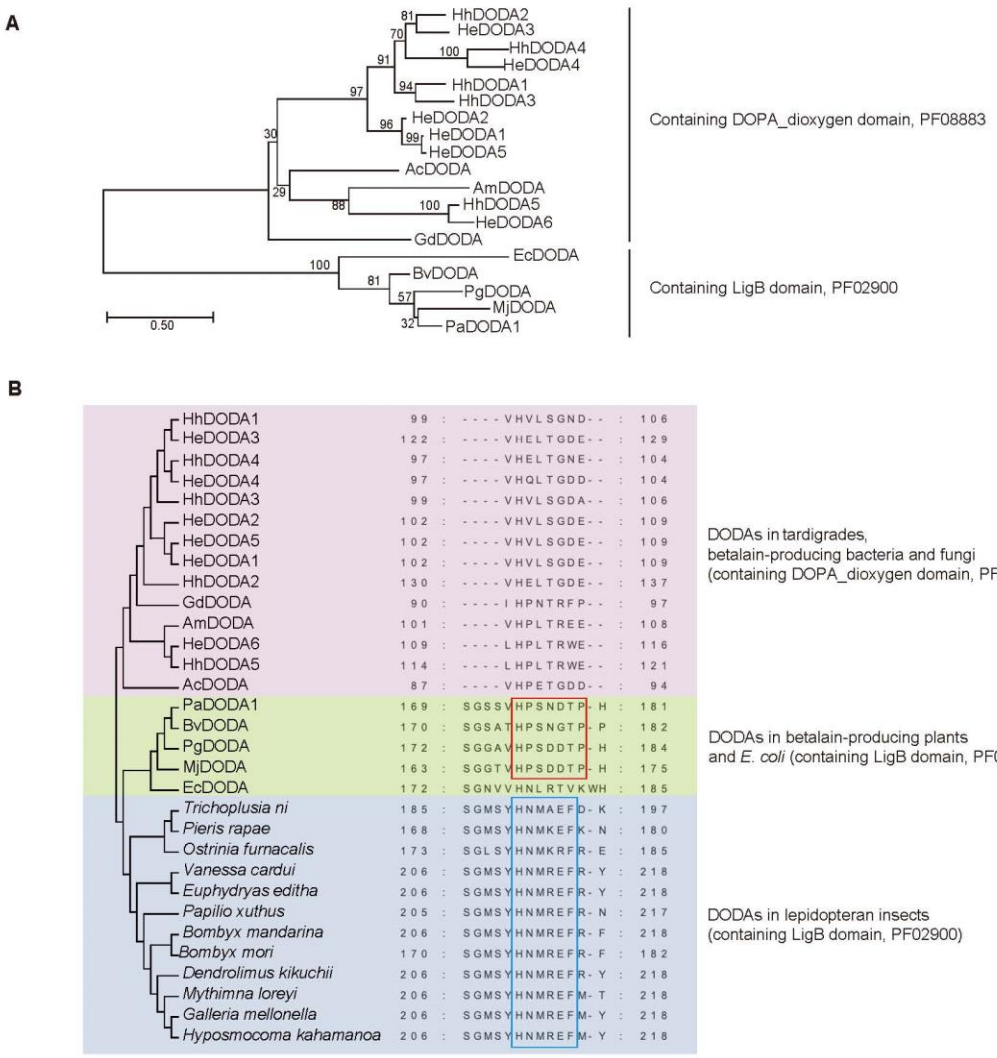
A
HhDODA2
HeDODA3
HhDODA4
HeDODA4
HhDODA1
HhDODA3
HeDODA2
HeDODA1
HeDODA5
AcDODA
AmDODA
HhDODA5
HeDODA6
GdDODA
EcDODA
BvDODA
PgDODA
MjDODA
PaDODA1
0.50
Containing DOPA_dioxygen domain, PF08883
Containing LigB domain, PF02900
B
HhDODA1 99 : ----VHVLSGND-- : 106
HeDODA3 122 : ----VHELTGDE-- : 129
HhDODA4 97 : ----VHELTGNE-- : 104
HeDODA4 97 : ----VHQLTGDD-- : 104
HhDODA3 99 : ----VHVLSGDA-- : 106
HeDODA2 102 : ----VHVLSGDE-- : 109
HeDODA5 102 : ----VHVLSGDE-- : 109
HeDODA1 102 : ----VHVLSGDE-- : 109
HhDODA2 130 : ----VHELTGDE-- : 137
GdDODA 90 : ----IHPNTRFP-- : 97
AmDODA 101 : ----VHPLTREE-- : 108
HeDODA6 109 : ----LHPLTRWE-- : 116
HhDODA5 114 : ----LHPLTRWE-- : 121
AcDODA 87 : ----VHPETGDD-- : 94
PaDODA1 169 : SGSSVHPSNDTP-H : 181
BvDODA 170 : SGSATHPSNGTP-P : 182
PgDODA 172 : SGGAVHPSDDTP-H : 184
MjDODA 163 : SGGTVHPSDDTP-H : 175
EcDODA 172 : SGNVVHNLRTVKWH : 185
Trichoplusia ni 185 : SGMSYHNMAEFD-K : 197
Pieris rapae 168 : SGMSYHNMKEFK-N : 180
Ostrinia furnacalis 173 : SGLSYHNMKRFR-E : 185
Vanessa cardui 206 : SGMSYHNMREFR-Y : 218
Euphydryas editha 206 : SGMSYHNMREFR-Y : 218
Papilio xuthus 205 : SGMSYHNMREFR-N : 217
Bombyx mandarina 206 : SGMSYHNMREFR-F : 218
Bombyx mori 170 : SGMSYHNMREFR-F : 182
Dendrolimus kikuchii 206 : SGMSYHNMREFR-Y : 218
Mythimna loreyi 206 : SGMSYHNMREFM-T : 218
Galleria mellonella 206 : SGMSYHNMREFM-Y : 218
Hyposmocoma kahamanoa 206 : SGMSYHNMREFM-Y : 218
DODAs in tardigrades, betalain-producing bacteria and fungi (containing DOPA_dioxygen domain, PF08883)
DODAs in betalain-producing plants and E. coli (containing LigB domain, PF02900)
DODAs in lepidopteran insects (containing LigB domain, PF02900)
C
Chr. 4
0 Mb
2 Mb
4 Mb
6 Mb
8 Mb
10 Mb
12 Mb
14 Mb
16 Mb
18 Mb
20 Mb
DODA5 (H.Henanensis.Chr4.493)
DODA2 (H.Henanensis.Chr4.1376)
DODA3 (H.Henanensis.Chr4.1380)
DODA1 (H.Henanensis.Chr4.1382)
DODA4 (H.Henanensis.Chr4.1389)

Fig. S13. Phylogenetic analysis of tardigrade and the other known DODAs. (**A**) Phylogenetic analysis of DOPA 4,5-dioxygenases from bacteria (*Gluconacetobacter diazotrophicus* -GdDODA, *Anabaena cylindrica* -AcDODA, *Escherichia coli* -EcDODA), fungi (*Amanita muscaria* -AmDODA), plants (*Mirabilis jalapa* -MjDODA, *Beta vulgaris* -BvDODA, *Portulaca grandiflora* -PgDODA, and *Phytolacca americana* -PaDODA1) and tardigrades. HeDODAs were putative DODAs from *H. exemplaris*. HhDODAs were putative DODAs from *H. henanensis* **sp. nov.** Multiple-sequence alignment was performed using MEGA-X software (v10.2.2) (Align by MUSCLE). The evolutionary history was inferred using the Neighbor-Joining method and Jones-Taylor-Thornton (JTT) mode. The UniProt accession numbers were as follows: GdDODA (A9H2M2), EcDODA (P24197), AmDODA (P87064), MjDODA (B6F0W8), BvDODA (Q70FG7), PgDODA (Q7XA48), and PaDODA1 (C4TGA5). The NCBI Reference Sequence ID for AcDODA is WP_015213489.1. For HeDODAs and HhDODAs gene IDs or accession numbers, see table S8. Bootstrap values are shown near nodes. The scale bar represents the branch length. (**B**) Phylogenetic analysis of DOPA dioxygenases. The H-P-(S/A/L)-(N/D)-X-T-P (where X stands for any amino acid) motif in betalain-producing plants are marked with red box. The conserved HNMREF motif in DODAs of lepidoptera are marked with blue box. The NCBI Reference Sequence ID were as follows: *Trichoplusia_ni* (XP_026725509.1), *Pieris_rapae* (XP_022125669.1), *Ostrinia_furnacalis* (XP_028166524.1), *Vanessa_cardui* (XP_046975244.1), *Papilio xuthus* (XP_013174413.1), *Bombyx mandarina* (XP_028030843.1), *Bombyx_mori* (XP_012546100.2), *Galleria_mellonella* (XP_026749362.1), and *Hyposmocoma_kahamanoa* (XP_026318512.1). The GenBank accession numbers were as follows: *Euphydryas editha* (CAH2101406.1), *Dendrolimus kikuchii* (KAJ0169833.1), *Mythimna loreyi* (KAJ8705797.1). Other DODA accession numbers or gene IDs are the same as in (A). (**C)** The genetic map of *DODA* genes from *H. henanensis* **sp. nov.** generated by MG2C (http://mg2c.iask.in/mg2c_v2.1/) (*164*).

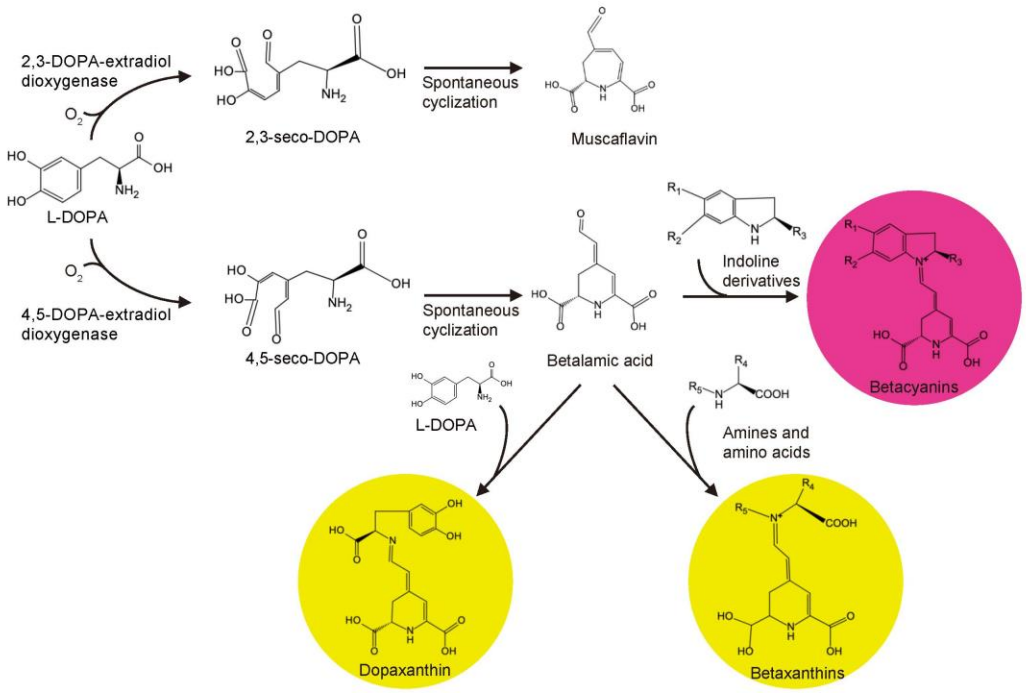
2,3-DOPA-extradiol dioxygenase
O2
L-DOPA
2,3-seco-DOPA
Spontaneous cyclization
Muscaflavin
4,5-DOPA-extradiol dioxygenase
4,5-seco-DOPA
Betalamic acid
Indoline derivatives
Betacyanins
L-DOPA
Amines and amino acids
Dopaxanthin
Betaxanthins

Fig. S14. Key steps in the biosynthesis of betalamic acid and betalains. DOPA dioxygenase (DODA) enzymes catalyze the cleavage of L-DOPA between C2 and C3, yielding 2,3-seco-DOPA, or between C4 and C5, yielding 4,5-seco-DOPA. Both compounds are intermediates which, by spontaneous cyclization, give rise to muscaflavin and betalamic acid respectively. Betalamic acid carries out spontaneous condensation reactions with amino acids or amines, producing betaxanthins which have a yellow coloration, or with indoline derivatives, producing violet betacyanins. R1 and R2 can be hydroxyl groups with or without sugar derivatives. R3 can be a carboxylic acid group. R4 can be side-chains of amino acids. This figure was adapted from Guerrero-Rubio, M. A (*141*, *159*).

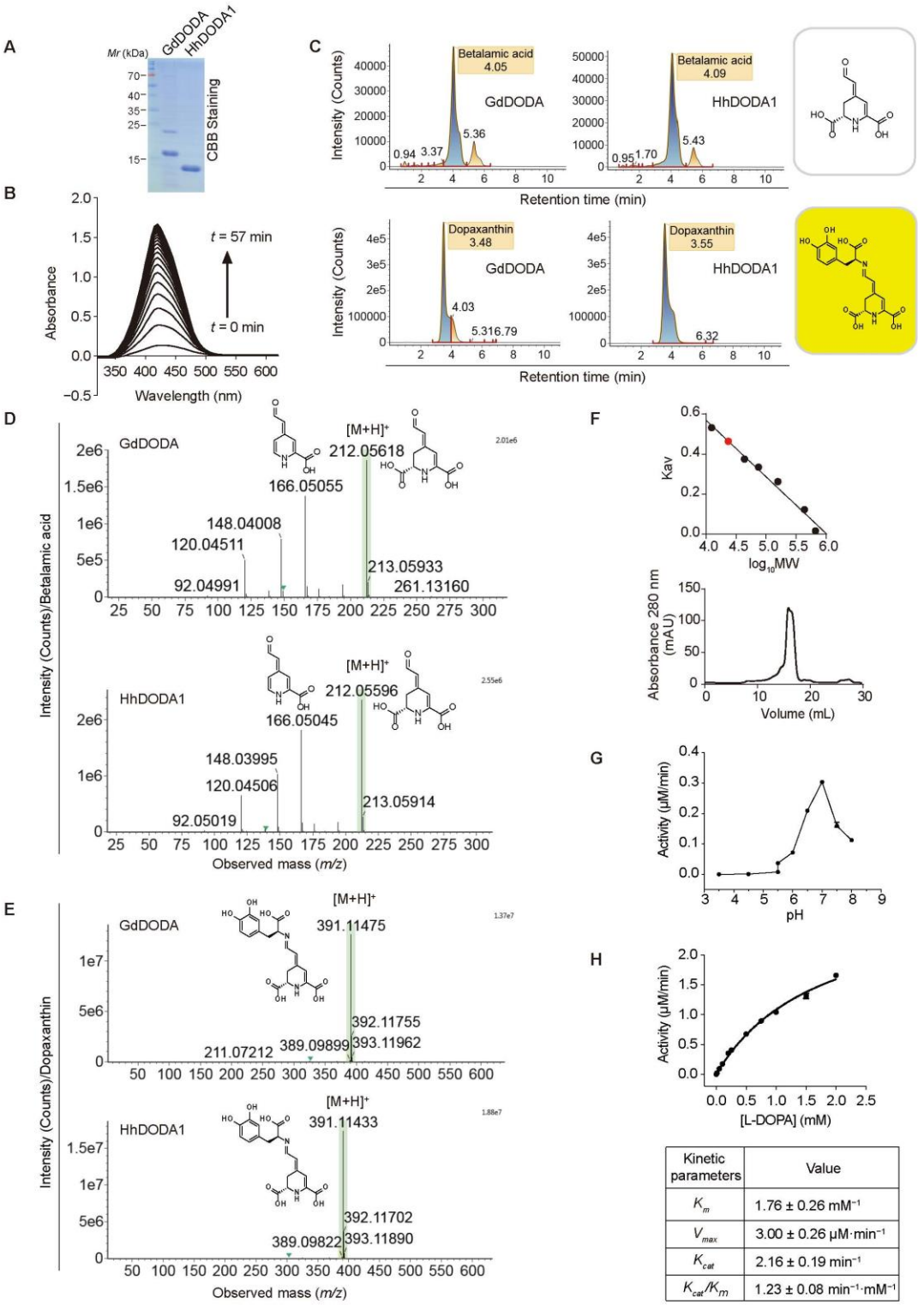

Kinetic parameters	Value
K_m	1.76 ± 0.26 mM^{-1}
V_{max}	3.00 ± 0.26 μM·min^{-1}
K_{cat}	2.16 ± 0.19 min^{-1}
K_{cat}/K_m	1.23 ± 0.08 min^{-1}·mM^{-1}

Fig. S15. Identification and characteristion of DOPA 4,5-dioxygenase from *H. henanensis* sp. nov. (**A**) The recombinant His-tagged GdDODA and HhDODA1 proteins were resolved on SDS-PAGE and stained with Coomassie brilliant blue (CBB). (**B**) Spectral evolution of the transformation of L-DOPA (2.5 mM) by the addition of HhDODA1 to the reaction medium. Measurements were performed at 25℃. Spectra were recorded at 3 min intervals for 57 min. (**C**) Extracted ion chromatograms (EICs) for betalamic acid or dopaxanthin monitored by UPLC-IMS QTOF from the samples in Fig. 2B. (**D**) Mass spectrum of the betalamic acid at a retention time of ~4.1 min in (C). MS-MS fragmentation spectra of betalamic acid is the same as previously reported (*45*). (**E**) Mass spectrum of the dopaxanthin at a retention time of ~3.5 min in (C). (**F**) Analysis of HhDODA1 proteins freed from GST-fusion by gel filtration chromatography. (The upper panel) Calibration curve and molecular mass determination. (The lower panel) The profile shows a single peak corresponding to a homodimeric form. Kav, distribution coefficient; MW, molecular weight. (**G**) Effect of pH on dioxygenase activity. Reactions were performed with 0.25 mM L-DOPA in 50 mM sodium acetate buffer for pH values ranging from 3.5 to 5.5 and in 50 mM sodium phosphate for pH values ranging from 5.5 to 8.0. (**H**) Enzyme activity dependence on L-DOPA concentration measured in 50 mM sodium phosphate buffer, pH 7.0. Kinetic parameters of HhDODA1 were shown in the lower panel.

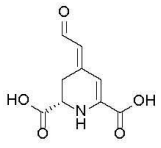

Betalamic acid

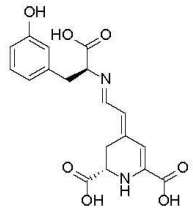

Dopaxanthin

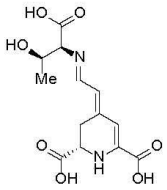

Threonine-betaxanthin

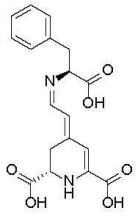

Phenylalanine-betaxanthin

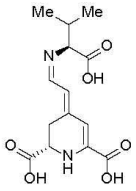

Valine-betaxanthin

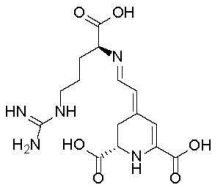

Arginine-betaxanthin

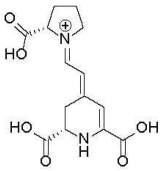

Proline-betaxanthin

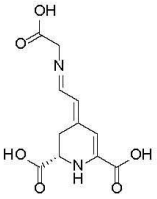

Glycine-betaxanthin

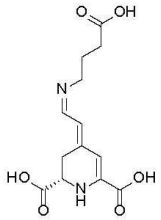

Gamma-aminobutyric acid-betaxanthin

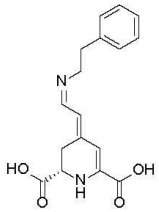

Phenethylamine-betaxanthin

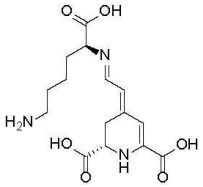

Lysine-betaxanthin

	Name	Trivialname / Synonyms	Chemical formula	Retention time (min)	*m/z* [M+H]$^+$	MS/MS
1	Betalamic acid		$C_9H_9NO_5$	4.24	212	166.1, 148.1
2	Dopaxanthin		$C_{18}H_{18}N_2O_8$	3.62	391	345.2, 301.1
3	Threonine-betaxanthin		$C_{13}H_{16}N_2O_7$	1.67	313	118.1, 119.1, 120.1, 179.2
4	Phenylalanine-betaxanthin		$C_{18}H_{18}N_2O_6$	5.55	359	313.2, 223.2
5	Valine-betaxanthin		$C_{14}H_{18}N_2O_6$	4.18	311	265.1, 219.2
6	Arginine-betaxanthin		$C_{15}H_{21}N_5O_6$	1.38	368	324.2, 236.3
7	Proline-betaxanthin	Indicaxanthin	$C_{14}H_{16}N_2O_6$	3.08	309	263.1, 217.2
8	Glycine-betaxanthin	Portulacaxanthin III	$C_{11}H_{12}N_2O_6$	1.48	269	223.2, 177.2
9	Gamma-aminobutyric acid-betaxanthin		$C_{13}H_{16}N_2O_6$	2.95	297	251.2, 187.2
10	Phethylamine-betaxanthin		$C_{17}H_{18}N_2O_4$	6.35	315	271.2, 105.1
11	Lysine-betaxanthin		$C_{15}H_{21}N_3O_6$	1.15+1.45	340	106.1, 296.3, 252.3

Fig. S16. Structures and their exact mass spectrometry information of betalain standards used in this study.

A

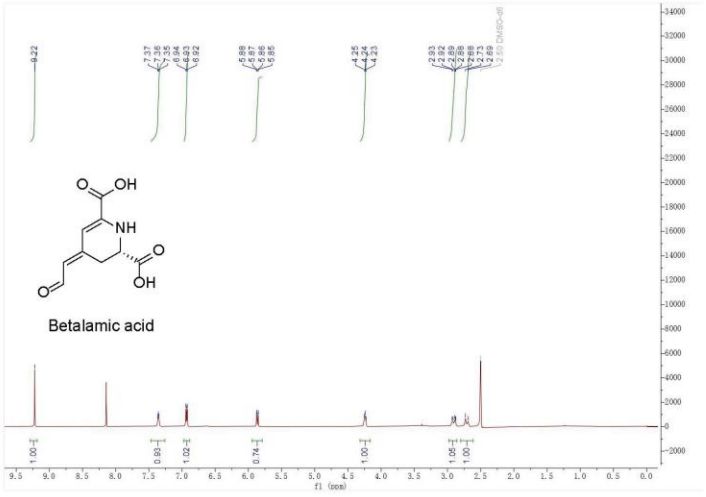
Betalamic acid

B

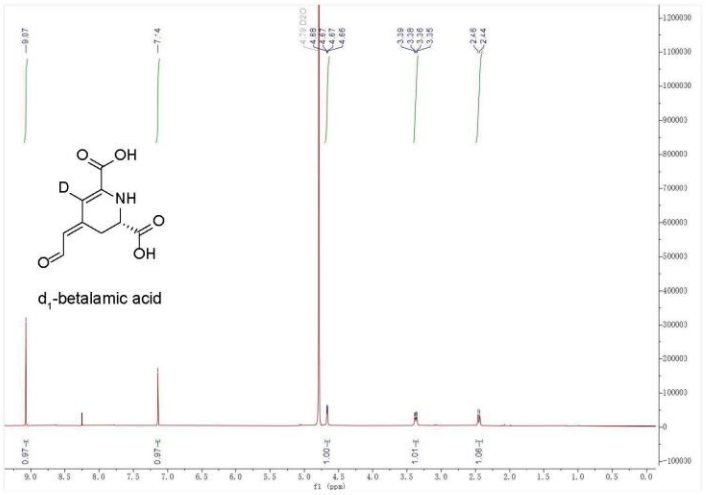
d1-betalamic acid

C

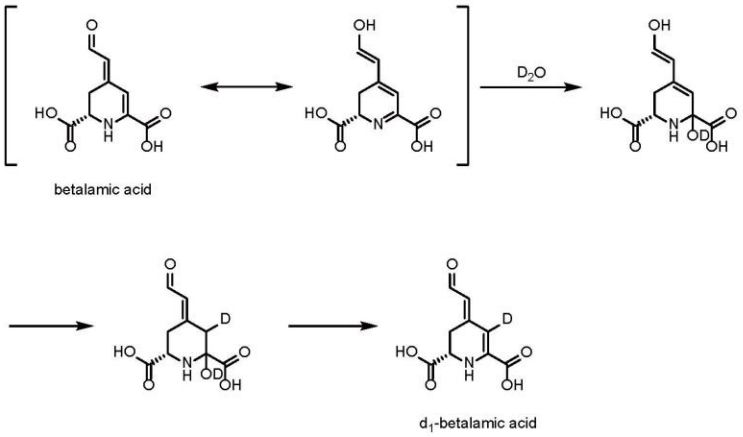
D2O
betalamic acid
d1-betalamic acid

D

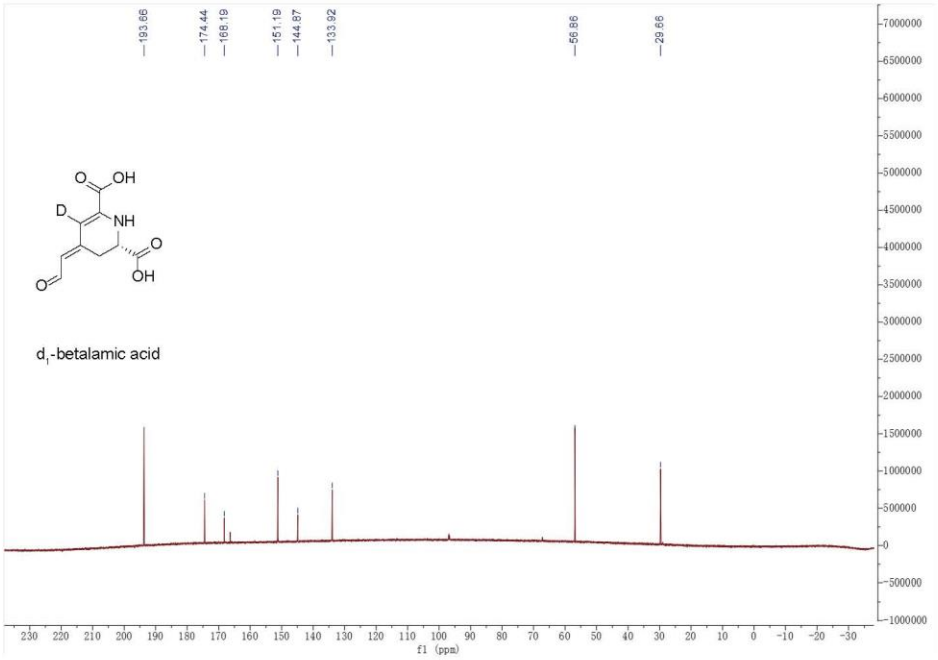
193.66
174.44
168.19
151.19
144.87
133.92
56.86
29.66
O
OH
D
NH
O
O
OH
d1-betalamic acid
f1 (ppm)

E

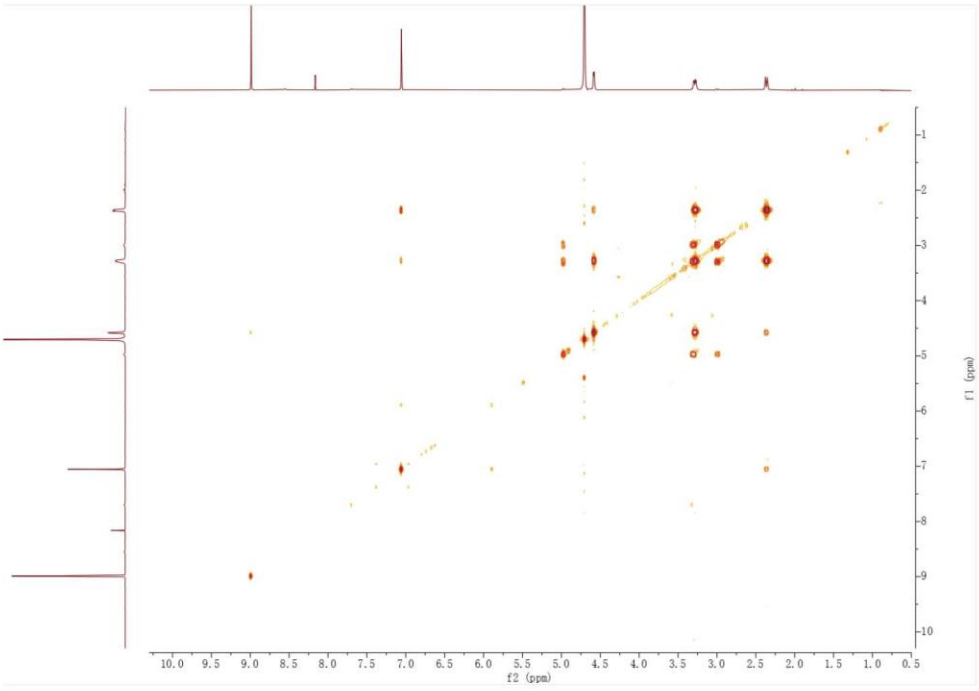
f2 (ppm)
f1 (ppm)

F

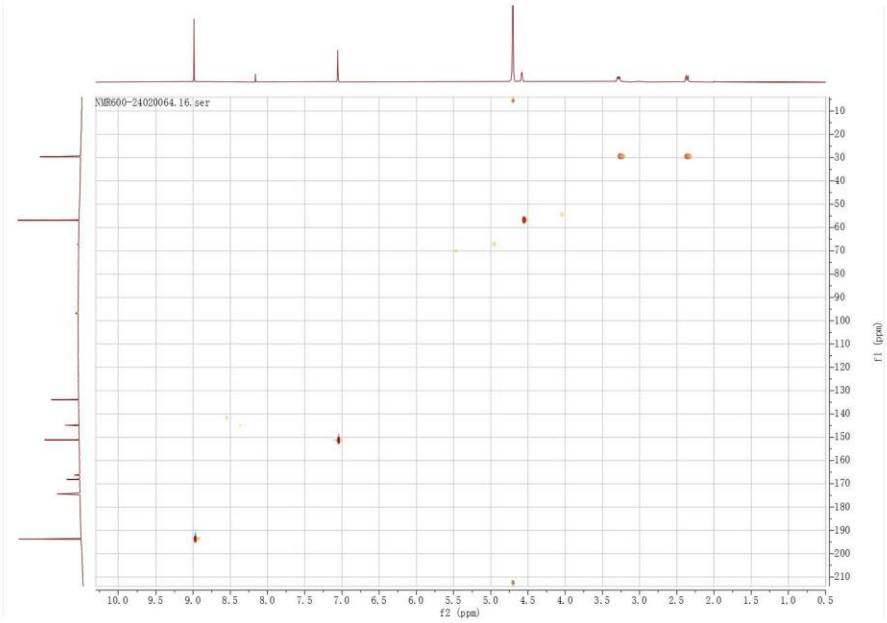
NMR600-24020064.16.ser
f2 (ppm)
f1 (ppm)

G

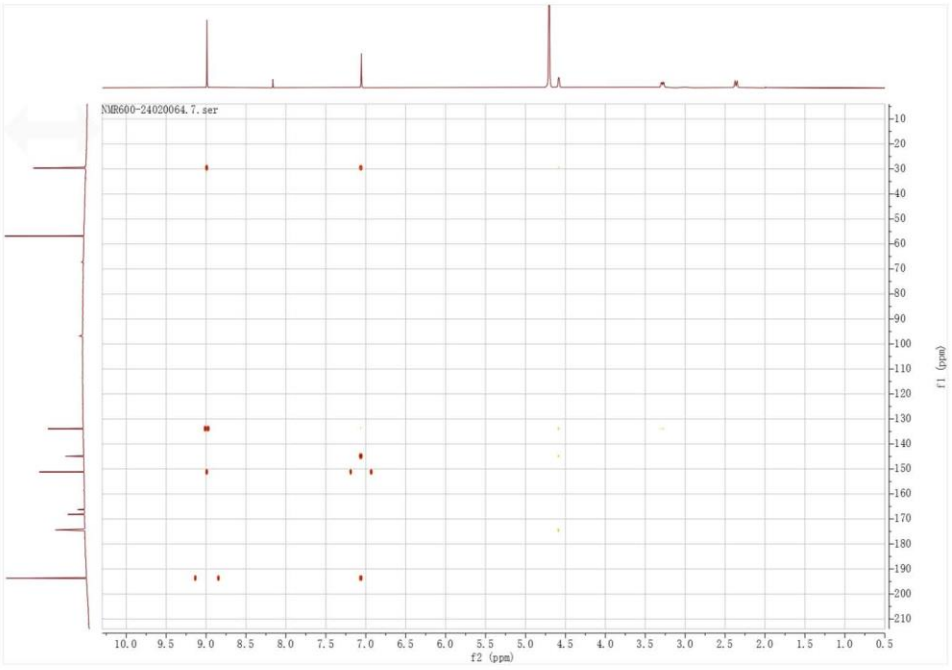
NMR600-24020064.7.ser
f2 (ppm)
f1 (ppm)

H

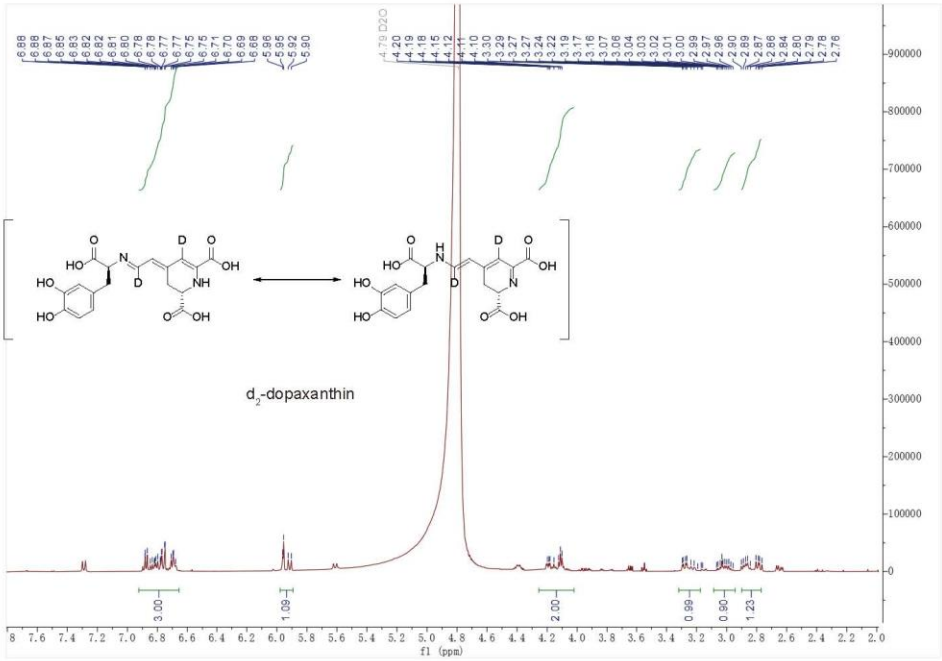

I

Name	Chemical formula	Parent Ion	MRM transition	Declustering Potential (volts)	Entrance Potential (volts)	Colision Potenial (volts)	Collision Cell Exit Potential (volts)
Betalamic acid	$C_9H_9NO_5$	$[M+H]^+$	212.0 > 166.1, 212.0 > 148.1	100, 100	10, 10	15, 22	15, 15
Dopaxanthin	$C_{18}H_{18}N_2O_8$	$[M+H]^+$	391.0 > 345.2, 391.0 > 301.1	100, 100	10, 10	35, 33	15, 15

J

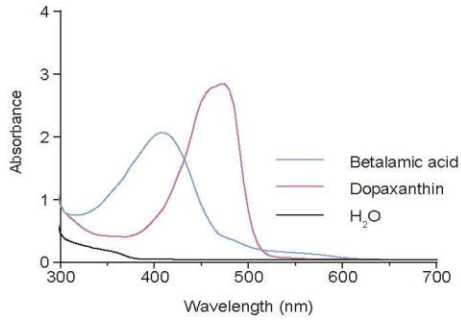

Fig. S17. NMR spectrum, MRM detection methods, and absorbance spectra of betalamic acid and dopaxanthin. (**A**) ^{1}H NMR spectrum of betalamic acid. ^{1}H NMR (400 MHz, DMSO-d_6) δ 9.22 (s, 1H), 8.14 (s, 1H), 7.36 (t, *J* = 3.9 Hz, 1H), 7.05-6.69 (m, 1H), 5.86 (dd, *J* = 8.4, 2.0 Hz, 1H), 4.25 (d, *J* = 5.6 Hz, 1H), 2.90 (dd, *J* = 15.8, 6.3 Hz, 1H), 2.71 (d, *J* = 15.6 Hz, 1H). (**B**) ^{1}H NMR of d1-betalamic acid. ^{1}H NMR (600 MHz, Deuterium Oxide) δ 9.07 (s, 1H), 7.14 (s, 1H), 4.67 (dd, *J* = 6.1, 2.1 Hz, 1H), 3.37 (dd, *J* = 15.2, 6.0 Hz, 1H), 2.45 (d, *J* = 15.3 Hz, 1H). (**C**) Mechanism of hydrogen-deuterium exchange. (**D**) ^{13}C NMR of d_1-betalamic acid. ^{13}C NMR (151 MHz, Deuterium Oxide) δ 193.66, 174.44, 168.19, 166.31, 151.19, 144.87, 133.92, 56.86, 29.66. (**E**) COSEY of d_1-betalamic acid. (**F**) HSQC of d_1-betalamic acid. (**G**) HMBC of d_1-betalamic acid. (**H**) ^{1}H NMR spectrum of dopaxanthin. Dopaxanthin undergoes hydrogen-deuterium exchange in deuterated water, so we only provide deuterated NMR of dopaxanthin. This compound had poor solvency or decomposed in other solvents, so no other non-deuterated dopaxanthin NMR was obtained. ^{1}H NMR (600 MHz, Deuterium Oxide) δ 6.97-6.46 (m, 3H), 6.01-5.77 (m, 1H), 4.11 (d, J = 6.5 Hz, 2H), 3.33-3.14 (m, 0H), 3.08-2.95 (m, 1H), 2.83 (ddd, J = 46.9, 15.5, 9.4 Hz, 1H). (**I**) MRM detection methods of betalamic acid and dopaxanthin. (**J**) Absorbance spectra of betalamic acid and dopaxanthin standards.

A

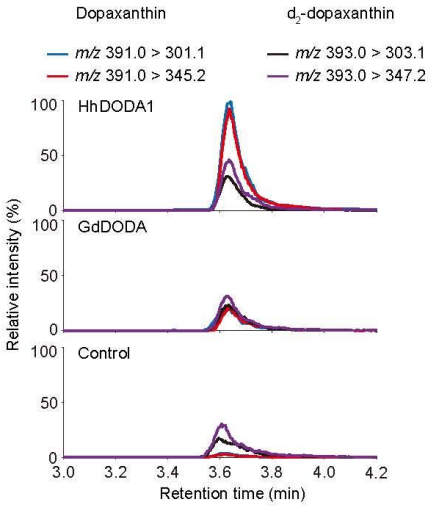

B

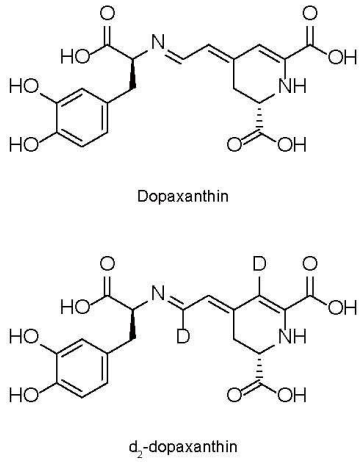

C

Name	Parent Ion	MRM transition	Declustering Potential (volts)	Entrance Potential (volts)	Colision Potenial (volts)	Collision Cell Exit Potential (volts)
Dopaxanthin	$[M+H]^+$	391.0 > 345.2, 391.0 > 301.1	100, 100	10, 10	35, 33	15, 15
d_2-dopaxanthin	$[M+H]^+$	393.0 > 347.2, 393.0 > 303.1	100, 100	10, 10	30, 30	15, 15

Fig. S18. Identification of dopaxanthin biosynthesis by d_2-dopaxanthin. (**A**) Representative MRM-LC/MS/MS chromatograms of dopaxanthin, $[M+H]^+$ *m/z* 391.0 > 301.1, *m/z* 391.0 > 345.2, and d_2-dopaxanthin, $[M+H]^+$ *m/z* 391.0 > 303.1, *m/z* 391.0 > 347.2, from the samples of HhDODA1 or GdDODA proteins supplemented with L-DOPA. d_2-dopaxanthin undergoes hydrogen-deuterium exchange in water, so the little amount of dopaxanthin detected in control samples were the result of hydrogen-deuterium exchange from d_2-dopaxanthin when the d_2-dopaxanthin standard were mixed with samples in water before mass spectrometry analysis. (**B**) Structures of dopaxanthin and d_2-dopaxanthin. (**C**) MRM detection methods of dopaxanthin and d_2-dopaxanthin.

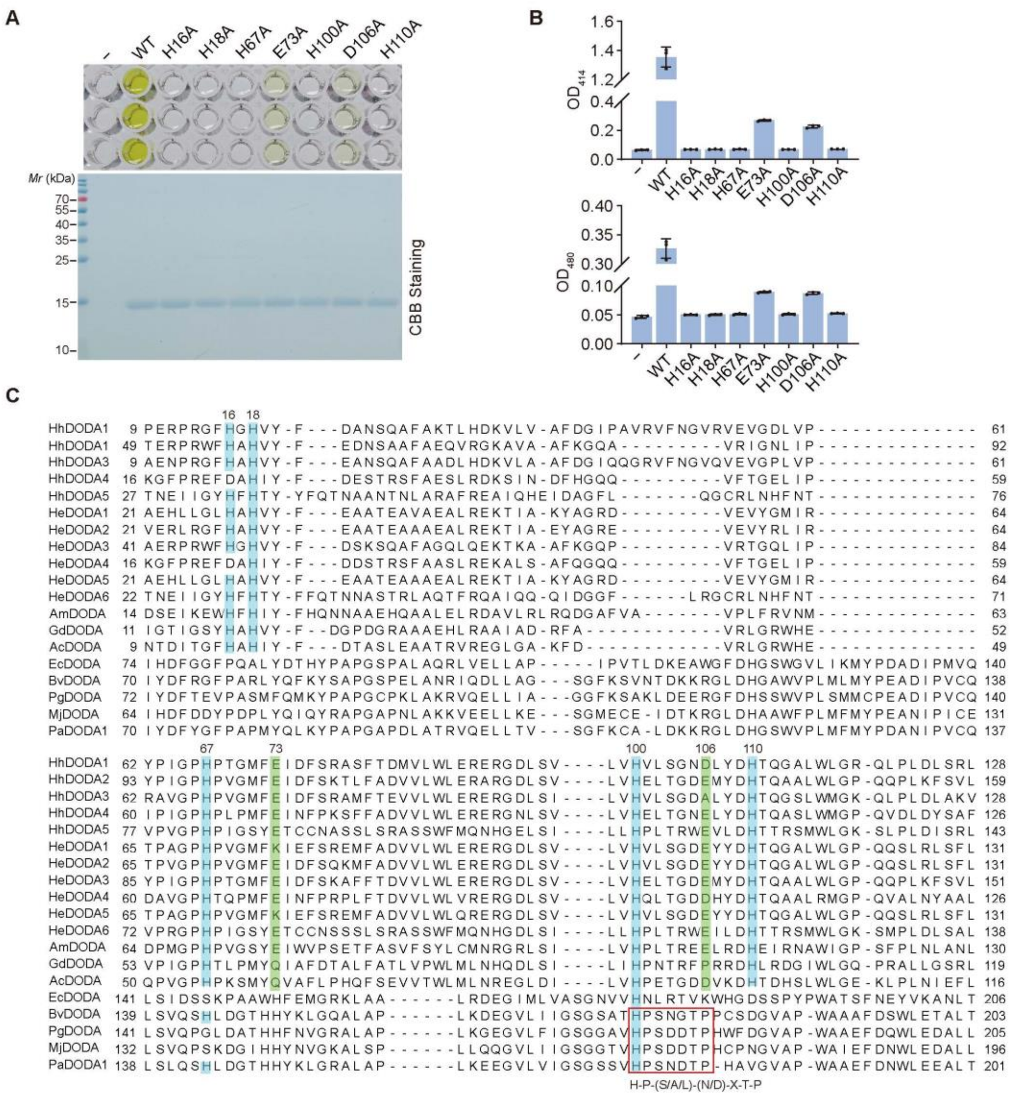
A
– WT H16A H18A H67A E73A H100A D106A H110A
Mr (kDa)
70
55
40
35
25
15
10
CBB Staining
B
OD414
1.6
1.4
1.2
0.4
0.2
0.0
– WT H16A H18A H67A E73A H100A D106A H110A
OD480
0.40
0.35
0.30
0.10
0.05
0.00
– WT H16A H18A H67A E73A H100A D106A H110A
C
16 18
HhDODA1 9 PERPRGFHGHVY-F---DANSQAFAKTLHDKVLV-AFDGIPAVRVFNGVRVEVGDLVP-------------- 61
HhDODA1 49 TERPRWFHAHVY-F---EDNSAAFAEQVRGKAVA-AFKGQA----------VRIGNLIP-------------- 92
HhDODA3 9 AENPRGFHAHVY-F---EANSQAFAADLHDKVLA-AFDGIQQGRVFNGVQVEVGPLVP-------------- 61
HhDODA4 16 KGFPREFDAHIY-F---DESTRSFAESLRDKSIN-DFHGQQ----------VFTGELIP-------------- 59
HhDODA5 27 TNEIIGYHFHTY-YFQTNAANTNLARAFREAIQHEIDAGFL-------QGCRLNHFNT-------------- 76
HeDODA1 21 AEHLLGLHAHVY-F---EAATEAVAEALREKTIA-KYAGRD----------VEVYGMIR-------------- 64
HeDODA2 21 VERLRGFHAHVY-F---EAATEAAAEALREKTIA-EYAGRE----------VEVYRLIR-------------- 64
HeDODA3 41 AERPRWFHGHVY-F---DSKSQAFAGQLQEKTKA-AFKGQP----------VRTGQLIP-------------- 84
HeDODA4 16 KGFPREFDAHIY-F---DDSTRSFAASLREKALS-AFQGQQ----------VFTGELIP-------------- 59
HeDODA5 21 AEHLLGLHAHVY-F---EAATEAAAEALREKTIA-KYAGRD----------VEVYGMIR-------------- 64
HeDODA6 22 TNEIIGYHFHTY-FFQTNNASTRLAQTFRQAIQQ-QIDGGF------LRGCRLNHFNT-------------- 71
AmDODA 14 DSEIKEWHFHIY-FHQNNAAEHQAALELRDAVLRLRQDGAFVA-------VPLFRVNM-------------- 63
GdDODA 11 IGTIGSYHAHVY-F--DGPDGRAAAEHLRAAIAD-RFA------------VRLGRWHE-------------- 52
AcDODA 9 NTDITGFHAHIY-F---DTASLEAATRVREGLGA-KFD------------VRLGRWHE-------------- 49
EcDODA 74 IHDFGGFPQALYDTHYPAPGSPALAQRLVELLAP-----IPVTLDKEAWGFDHGSWGVLIKMYPDADIPMVQ 140
BvDODA 70 IYDFRGFPARLYQFKYSAPGSPELANRIQDLLAG---SGFKSVNTDKKRGLDHGAWVPLMLMYPEADIPVCQ 138
PgDODA 72 IYDFTEVPASMFQMKYPAPGCPKLAKRVQELLIA---GGFKSAKLDEERGFDHSSWVPLSMMCPEADIPVCQ 140
MjDODA 64 IHDFDDYPDPLYQIQYRAPGAPNLAKKVEELLKE---SGMECE-IDTKRGLDHAAWFPLMFMYPEANIPICE 131
PaDODA1 70 IYDFYGFPAPMYQLKYPAPGAPDLATRVQELLTV---SGFKCA-LDKKRGLDHGSWVPLMFMYPDANIPVCQ 137
67 73 100 106 110
HhDODA1 62 YPIGPHPTGMFEIDFSRASFTDMVLWLERERGDLSV----LVHVLSGNDLYDHTQGALWLGR-QLPLDLSRL 128
HhDODA2 93 YPIGPHPVGMFEIDFSKTLFADVVLWLERARGDLSV----LVHELTGDEMYDHTQAALWLGP-QQPLKFSVL 159
HhDODA3 62 RAVGPHPVGMFEIDFSRAMFTEVVLWLERERGDLSI----LVHVLSGDALYDHTQGSLWMGK-QLPLDLAKV 128
HhDODA4 60 IPIGPHPLPMFEINFPKSFFADVVLWLERERGNLSV----LVHELTGNELYDHTQASLWMGP-QVDLDYSAF 126
HhDODA5 77 VPVGPHPIGSYETCCNASSLSRASSWFMQNHGELSI----LLHPLTRWEVLDHTTRSMWLGK-SLPLDISRL 143
HeDODA1 65 TPAGPHPVGMFKIEFSREMFADVVLWLERERGDLSV----LVHVLSGDEYYDHTQGALWLGP-QQSLRLSFL 131
HeDODA2 65 TPVGPHPVGMFEIDFSQKMFADVVLWLERERGDLSV----LVHVLSGDEYYDHTQGALWLGP-QQSLRLSFL 131
HeDODA3 85 YPIGPHPTGMFEIDFSKAFFTDVVLWLERERGDLSV----LVHELTGDEMYDHTQAALWLGP-QQPLKFSVL 151
HeDODA4 60 DAVGPHTQPMFEINFPRPLFTDVVLWLVRERGDLSV----LVHQLTGDDHYDHTQAALRMGP-QVALNYAAL 126
HeDODA5 65 TPAGPHPVGMFKIEFSREMFADVVLWLQRERGDLSV----LVHVLSGDEYYDHTQGALWLGP-QQSLRLSFL 131
HeDODA6 72 VPRGPHPIGSYETCCNSSSLSRASSWFMQNHGDLSI----LLHPLTRWEILDHTTRSMWLGK-SMPLDLSAL 138
AmDODA 64 DPMGPHPVGSYEIWVPSETFASVFSYLCMNRGRLSI----LVHPLTREELRDHEIRNAWIGP-SFPLNLANL 130
GdDODA 53 VPIGPHTLPMYQIAFDTALFATLVPWLMLNHQDLSI----LIHPNTRFPRRDHLRDGIWLGQ-PRALLGSRL 119
AcDODA 50 QPVGPHPKSMYQVAFLPHQFSEVVTWLMLNREGLDI----LVHPETGDDVKDHTDHSLWLGE-KLPLNIEFL 116
EcDODA 141 LSIDSSKPAAWHFEMGRKLAA------LRDEGIMLVASGNVVHNLRTVKWHGDSSPYPWATSFNEYVKANLT 206
BvDODA 139 LSVQSHLDGTHHYKLGQALAP------LKDEGVLIIGSGSATHPSNGTPPCSDGVAP-WAAAFDSWLETALT 203
PgDODA 141 LSVQPGLDATHHFNVGRALAP------LKGEGVLFIGSGGAVHPSDDTPHWFDGVAP-WAAEFDQWLEDALL 205
MjDODA 132 LSVQPSKDGIHHYNVGKALSP------LLQQGVLIIGSGGTVHPSDDTPHCPNGVAP-WAIEFDNWLEDALL 196
PaDODA1 138 LSLQSHLDGTHHYKLGRALAP------LKEEGVLVIGSGSSVHPSNDTP-HAVGVAP-WAAEFDNWLEEALT 201
H-P-(S/A/L)-(N/D)-X-T-P

Fig. S19. Active sites identification of DOPA 4,5-dioxygenase from *H. henanensis* sp. nov. (**A** and **B**) Enzymatic assay in HhDODA1-WT and mutant proteins supplemented with L-DOPA. Meanwhile the HhDODA1 proteins were resolved on SDS-PAGE and stained with CBB (A). Spectrophotometric detection of betalamic acid (OD_{414}) and dopaxanthin (OD_{480}) in samples (B). (**C**) Sequence alignment of HhDODAs and HeDODAs with DODA proteins from other betalain-producing species. The highly conserved and moderately conserved active sites are marked with wathet and green, respectively. The H-P-(S/A/L)-(N/D)-X-T-P motif in betalain-producing plants are marked with red box. The numbers indicate the amino acid residues in HhDODA1. The accession numbers of these sequences are listed in the caption of fig. S13.

A

```
HsTH   317 QLRPVAGLLSARDFLASLAFRVFQCTQYIRHASSPMHSPEPDCCHELLGHVPMLADRTFAQFSQDIGLASLGASD 391
MmTH   287 QLRPVAGLLSARDFLASLAFRVFQCTQYIRHASSPMHSPEPDCCHELLGHVPMLADRTFAQFSQDIGLASLGASD 361
DmTH   365 SLRPAAGLLTARDFLASLAFRIFQSTQYVRHVNSPYHTPEPDSIHELLGHMPLLADPSFAQFSQEIGLASLGASD 439
CeTH   303 ELRPCSGLLSARDFLASLAFRVFQTTTYLRHHKSPHHSPEPDLIHELLGHVPMFSDPLLAQMSQDIGLMSLGASD 377
HeTH   314 ILRPAAGLLTARDFLASLAFRVFQCTQYIRHASKPQHSPEPDCVHELLGHVPLLADPAFAQLSQEIGLASIGASD 388
HhTH1  312 VLRPAAGLLSARDFLASLAFRVFQCTQYIRHASKPQHSPEPDCVHELLGHVPLLADPGFAQLSQEIGLASLGASD 386
HhTH2  275 ILRPAAGLLSARDFLASLAFRVFQCTQYVRHPSKPQHSPEPDCVHELLGHVPLLADPKFAEFSQEIGLASLGVSE 349

HsTH   392 EEIEKLSTLYWFTVEFGLCKQNGEVKAYGAGLLSSYGELLHCLSEEPEIRAF-DPEAAAVQPYQDQTYQSVYFVS 465
MmTH   362 EEIEKLSTVYWFTVEFGLCKQNGELKAYGAGLLSSYGELLHSLSEEPEVRAF-DPDTAAVQPYQDQTYQPVYFVS 435
DmTH   440 EEIEKLSTVYWFTVEFGLCKEHGQIKAYGAGLLSSYGELLHAISDKCEHRAF-EPASTAVQ YQDQEYQPIYYVA 513
CeTH   378 EHIEKLSTVYWFIVEFGLCKEDGKLKAIGAGLLSAYGELMHACSDAPEHKDF-DPAVTAVQKYEDDDYQPLYFVA 451
HeTH   389 DDITKLATLYWFTVEFGLCKENDMIKAYGAGLLSSFGELQHALSDVPERRKF-DPYVTAIQPYQDQTYQDVYFVA 462
HhTH1  387 DDITKLSTLYWFTVEFGLCKENESVRAYGAGLLSSFGELQHALSDVPDRRKF-DPHVTAVQPYQDQTYQDVYFVA 460
HhTH2  350 DDITKLSTLYWFTVEFGLCKENESVRAYGGGLLSSFGELPHALSDVPDRRELPDPHFIAVQTYQDQTYQDAYFVA 424
```

B

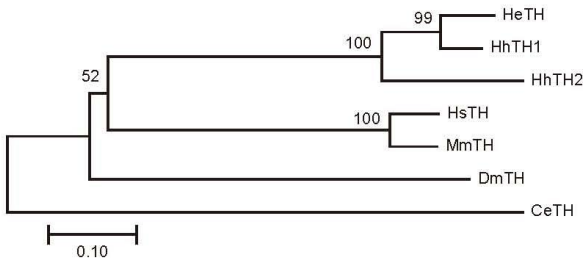

Fig. S20. Sequence analysis of tyrosine hydroxylases. (**A**) Sequence alignment of tyrosine hydroxylases (THs) from *Homo sapiens* (Hs), *Mus musculus* (Mm), *Drosophila melanogaster* (Dm), *Caenorhabditis elegans* (Ce), *H. exemplaris* (He), and *H. henanensis* **sp. nov.** (Hh). The active sites (*165*) are marked with red color. For accession numbers, see table S8. (**B**) Phylogenetic analysis of tyrosine hydroxylases (THs). Multiple-sequence alignment was performed using MEGA-X software (Align by MUSCLE). The evolutionary history was inferred by using the Neighbor-Joining method and Jones-Taylor-Thornton (JTT) mode. Bootstrap values are shown near nodes. The scale bar represents the branch length.

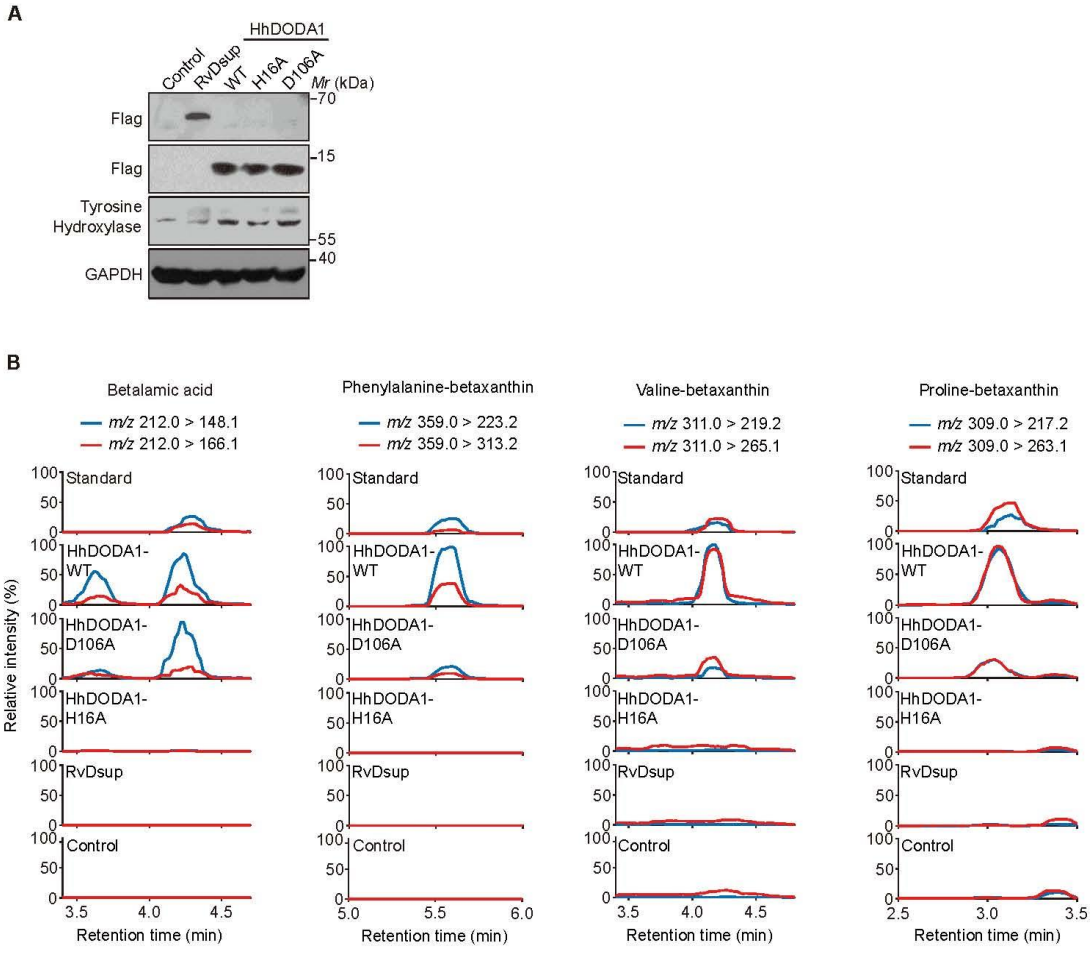
A
HhDODA1
Control
RvDsup
WT
H16A
D106A
Mr (kDa)
70
Flag
15
Flag
Tyrosine Hydroxylase
55
40
GAPDH
B
Betalamic acid
m/z 212.0 > 148.1
m/z 212.0 > 166.1
Phenylalanine-betaxanthin
m/z 359.0 > 223.2
m/z 359.0 > 313.2
Valine-betaxanthin
m/z 311.0 > 219.2
m/z 311.0 > 265.1
Proline-betaxanthin
m/z 309.0 > 217.2
m/z 309.0 > 263.1
Standard
HhDODA1-WT
HhDODA1-D106A
HhDODA1-H16A
RvDsup
Control
Relative intensity (%)
Retention time (min)

Fig. S21. Establishment of the betalains biosynthetic pathway in human cells. (**A**) Western blotting analysis of the expression of the indicated proteins in HeLa cells. (**B**) Representative MRM-LC/MS/MS chromatograms of betalamic acid, $[M+H]^+$ *m/z* 212.0 > 148.1, *m/z* 212.0 > 166.1, phenylalanine-betaxanthin, $[M+H]^+$ *m/z* 359.0 > 223.2, *m/z* 359.0 > 313.2, valine-betaxanthin, $[M+H]^+$ *m/z* 311.0 > 219.2, *m/z* 311.0 > 265.1, and proline-betaxanthin, $[M+H]^+$ *m/z* 309.0 > 217.2, *m/z* 309.0 > 263.1, in the extracts of HeLa cells expressing the indicated proteins. The detailed MRM transitions for 11 compounds are listed in table S11.

A

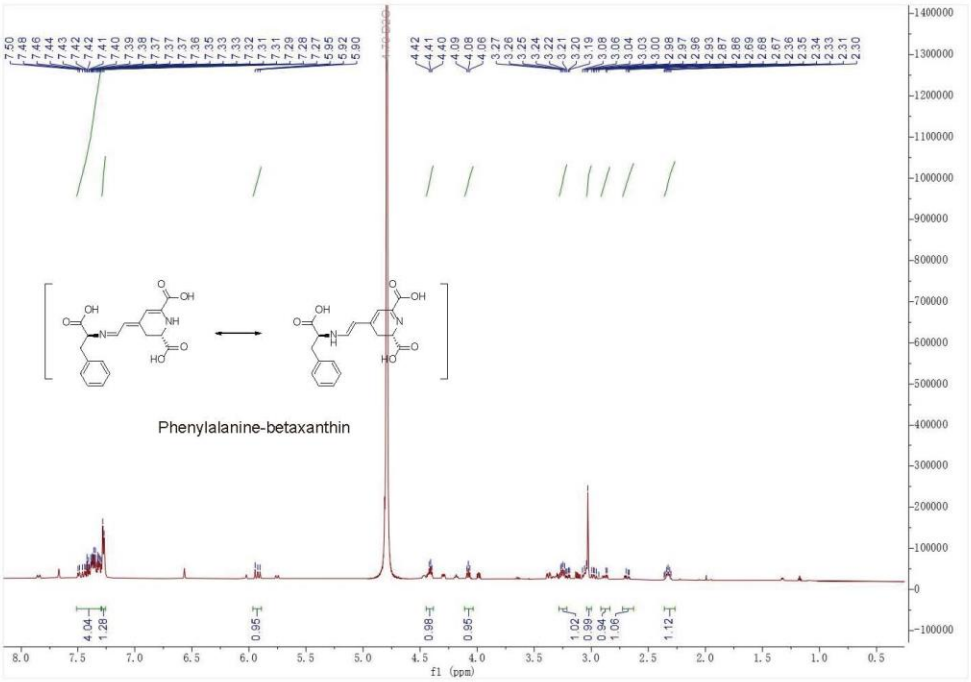
Phenylalanine-betaxanthin
f1 (ppm)

B

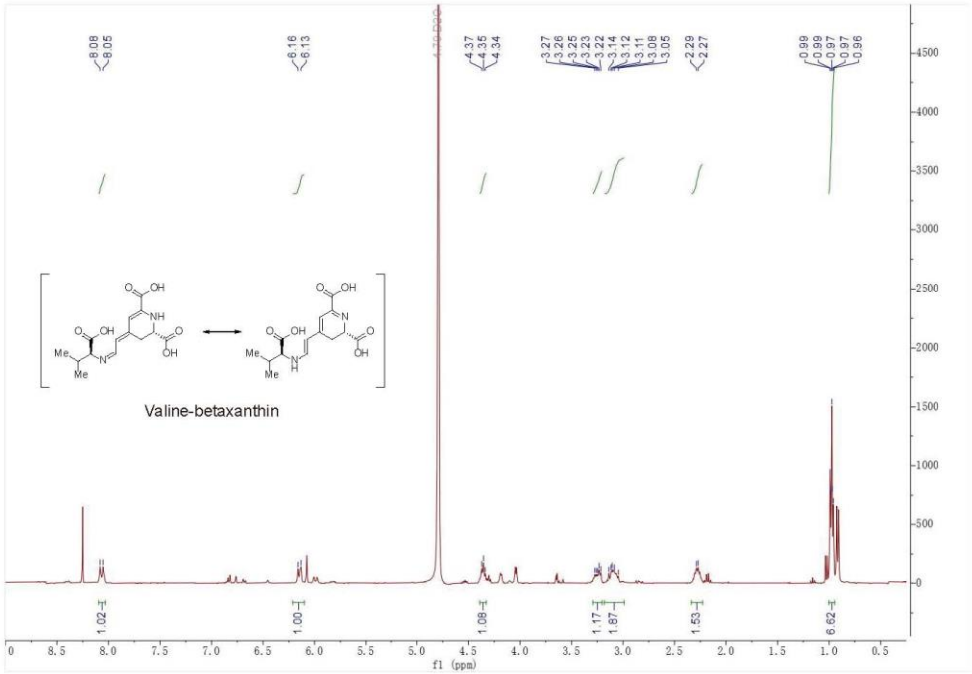
Valine-betaxanthin
f1 (ppm)

C

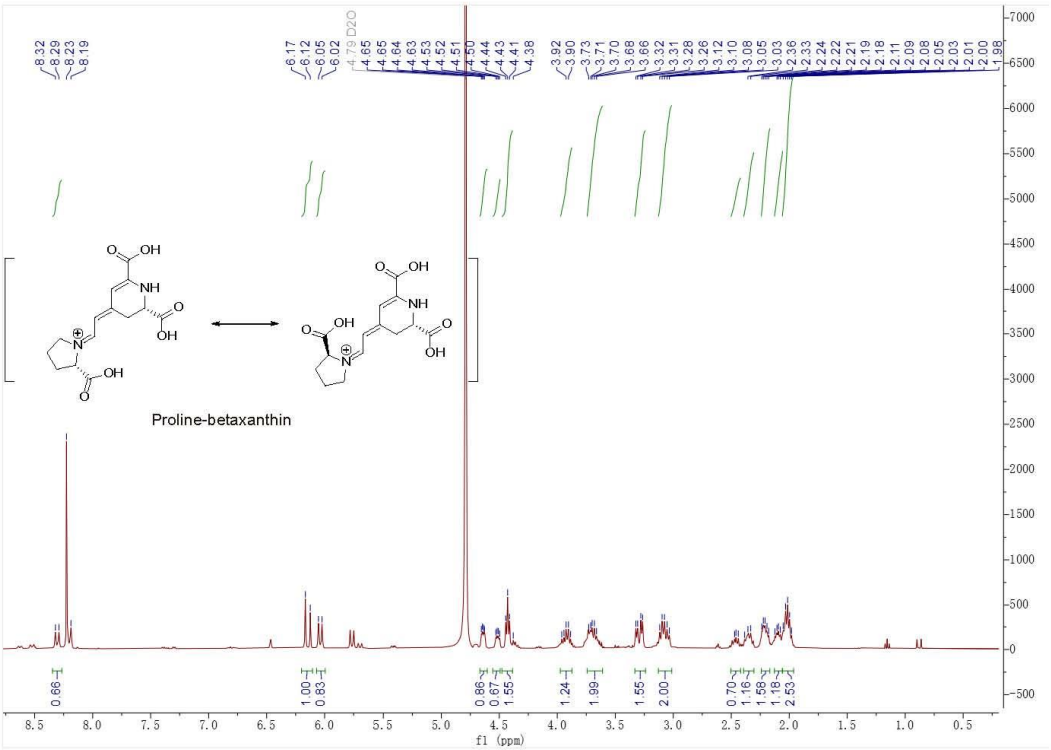

Fig. S22. NMR spectrum of phenylalanine-betaxanthin, valine-betaxanthin, and proline-betaxanthin standards. (**A**) ^{1}H NMR spectrum of phenylalanine-betaxanthin. ^{1}H NMR (600 MHz, Deuterium Oxide) δ 7.45-7.05 (m, 5H), 5.88-5.77 (m, 1H), 4.33 (q, *J* = 7.1 Hz, 1H), 3.99 (t, *J* = 7.6 Hz, 1H), 3.29 (dd, *J* = 13.9, 4.3 Hz, 1H), 3.22-3.10 (m, 1H), 2.94 (s, 1H), 2.79 (dd, *J* = 17.0, 7.9 Hz, 1H), 2.24 (t, *J* = 7.9 Hz, 1H). (**B**) ^{1}H NMR spectrum of valine-betaxanthin. ^{1}H NMR (400 MHz, Deuterium Oxide) δ 8.07 (d, *J* = 11.9 Hz, 1H), 6.15 (d, *J* = 11.3 Hz, 1H), 4.33 (dt, *J* = 20.2, 6.8 Hz, 1H), 3.24 (dd, *J* = 17.0, 6.3 Hz, 1H), 3.16-3.01 (m, 2H), 2.31-2.23 (m, 1H), 1.06-0.94 (m, 6H). (**C**) ^{1}H NMR spectrum of proline-betaxanthin. ^{1}H NMR (400 MHz, Deuterium Oxide) δ 8.31 (d, *J* = 12.3 Hz, 1H), 6.14 (d, *J* = 17.1 Hz, 1H), 6.02 (d, J = 12.2Hz, 1H), 4.65-4.59 (m, 1H), 4.43 (t, *J* = 6.6 Hz, 1H), 3.69 (td, *J* = 13.2, 12.7, 6.5 Hz, 2H), 3.09 (dq, *J* = 16.7, 7.6 Hz, 2H), 2.38-2.27 (m, 1H), 2.14-2.07 (m, 1H), 2.05-1.90 (m, 2H).

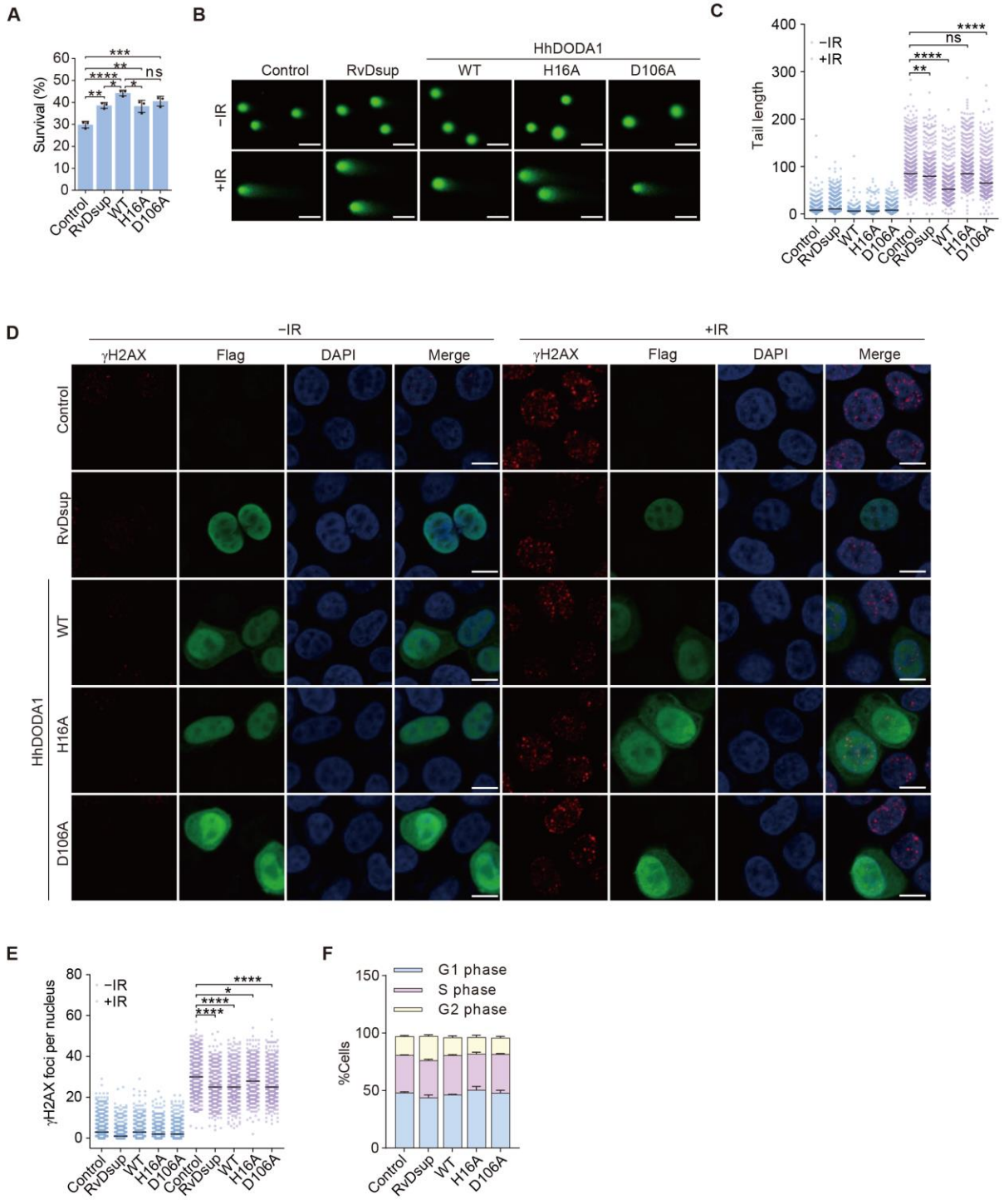
A
Survival (%)
Control
RvDsup
WT
H16A
D106A
B
HhDODA1
−IR
+IR
C
Tail length
−IR
+IR
ns
D
−IR
+IR
γH2AX
Flag
DAPI
Merge
HhDODA1
E
γH2AX foci per nucleus
F
G1 phase
S phase
G2 phase
%Cells

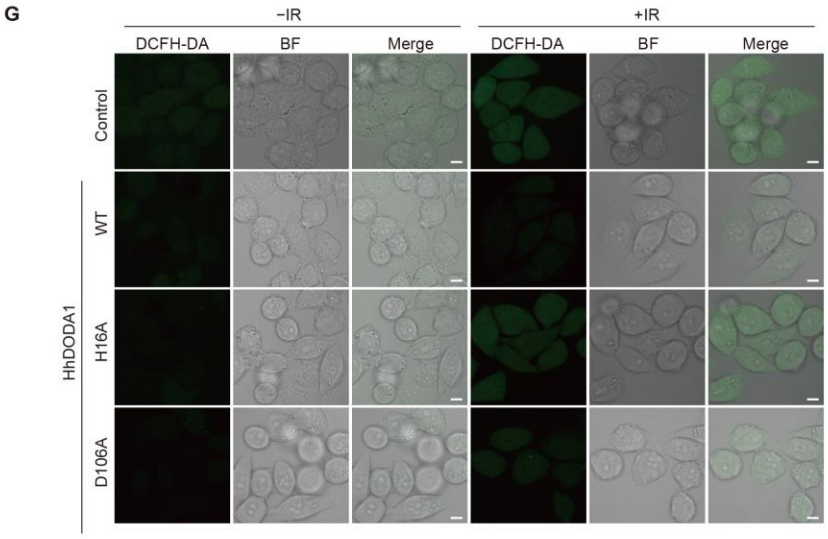
G
−IR
+IR
DCFH-DA
BF
Merge
DCFH-DA
BF
Merge
Control
HhDODA1
WT
H16A
D106A

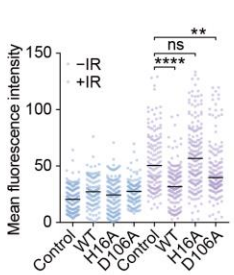
H
Mean fluorescence intensity
150
100
50
0
−IR
+IR
ns
****
**
Control
WT
H16A
D106A
Control
WT
H16A
D106A

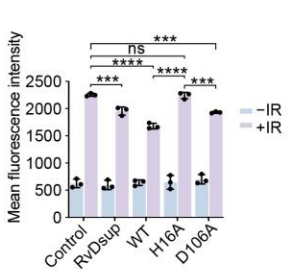
I
Mean fluorescence intensity
2500
2000
1500
1000
500
0
***
ns
****
****
***
***
−IR
+IR
Control
RvDsup
WT
H16A
D106A

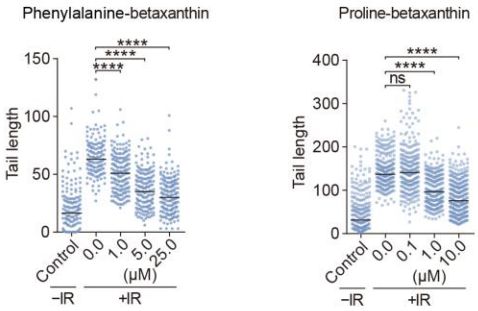
J
Phenylalanine-betaxanthin
Tail length
150
100
50
0
****
****
****
Control
0.0
1.0
5.0
25.0
(μM)
−IR
+IR
Proline-betaxanthin
Tail length
400
300
200
100
0
****
****
ns
Control
0.0
0.1
1.0
10.0
(μM)
−IR
+IR

Fig. S23. Reduced DNA damage in HhDODA1-expressing cells after radiation. (**A**) HeLa cells stably expressing indicated proteins were treated with or without 3 Gy IR and the cell survival rates were counted by colony formation assay. (**B** and **C**) The effects of HhDODA1 on DNA damage of HeLa cells under non-irradiation or 10 Gy X-ray irradiation condition in alkaline comet assays. DNA fragmentation was assessed by the tail length. At least 300 cells were analyzed for each condition. Representative images are shown (B). Scale bars, 50 μm. Quantitative results are shown (C). (**D** and **E**) Analysis of γH2AX foci number of HeLa cells expressing HhDODA1-WT or its mutants under non-irradiation or 2 Gy X-ray irradiation conditions. RvDsup was used as a positive control. At least 295 cells were analyzed for each condition. Representative images are shown for each condition (D). Scale bars, 10 μm. Quantitative results are shown (E)**. (F)** FACS analysis of the cell cycle distribution of HeLa cells expressing HhDODA1-WT or its mutants. (**G** and **H**) HeLa cells stably expressing HhDODA1-WT or its mutants were treated with or without 10 Gy X-ray irradiation and then stained with 2,7-dichlorodihydrofluorescein diacetate (DCFH-DA, in green). At least 100 cells were analyzed for each condition. Representative images are shown (G). BF, bright field. Scale bars, 10 μm. Quantitative results are shown (H). **(I)** FACS analysis of the mean fluorescence intensities of the chloromethyl derivative of H2DCFDA (CM-H2DCFDA) in HeLa cells stably expressing indicated proteins and treated with or without IR. (**J**) The effects of different dose of phenylalanine-betaxanthin and proline-betaxanthin on protection of DNA damage in HeLa cells under non-irradiation or 10 Gy X-ray irradiation condition in alkaline comet assays. DNA fragmentation was assessed by the tail length. At least 188 cells were analyzed for each condition. The data are presented as mean ± SD [n = 3 in (A), (F), and (I)]. The median values are shown as a black bar in (C), (E), (H), and (J). The unit of tail length is μm. One-way ANOVA with Tukey's post-hoc test for (A) and (I). Kruskal-Wallis test followed by Dunn's test for (C), (E), (H), and (J). $P > 0.05$, not significant (ns); * $P < 0.05$; ** $P < 0.01$; *** $P < 0.001$; **** $P < 0.0001$.

A

Compound	Formula	*m/z* (measured)	*m/z* (calculated)	Adducts	Retention time (min)	ppm
Valine-betaxanthin	$C_{14}H_{18}N_2O_6$	311.123	310.307	$[M+H]^+$	2.85	−1.44
Threonine-betaxanthin	$C_{13}H_{16}N_2O_7$	295.094	312.279	$[M+H-H_2O]^+$	6.04	4.01
Phenethylamine-betaxanthin	$C_{17}H_{18}N_2O_4$	353.090	314.341	$[M+K]^+$	12.45	1.64
Glutamine-betaxanthin	$C_{14}H_{17}N_3O_7$	378.071	339.305	$[M+K]^+$	0.78	2.22

B

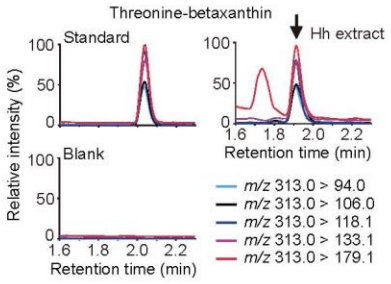

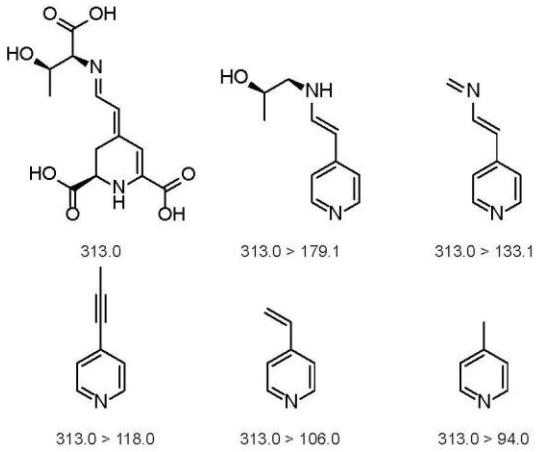

C

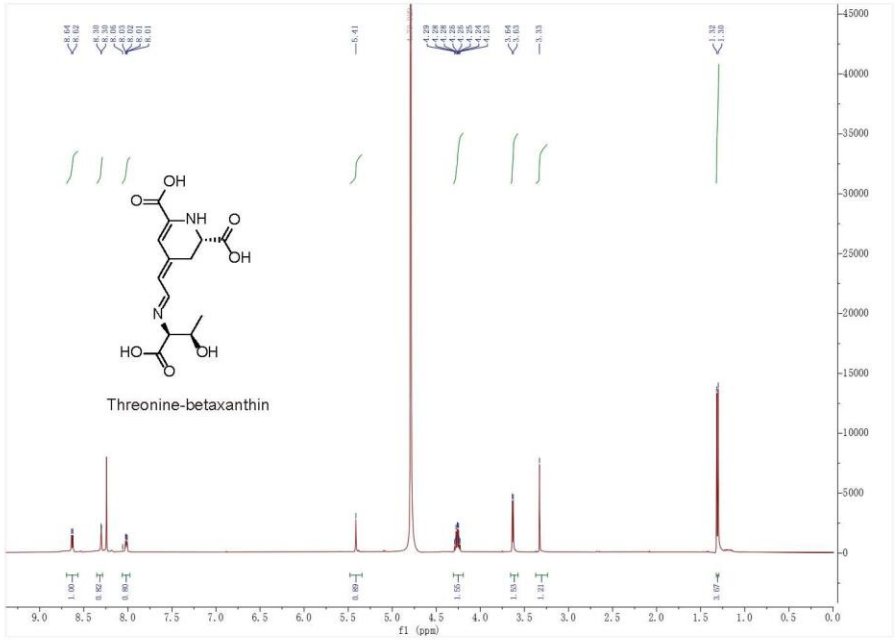

Fig. S24. Identification of betalains in *H. henanensis* sp. nov. (**A**) Untargeted mass spectrometry analysis of betalains from the extracts of *H. henanensis* **sp. nov.** by UPLC-IMS QTOF analysis. (**B**) Targeted mass spectrometry analysis of the extract of *H. henanensis* **sp. nov.** by MRM-LC-MS/MS. Representative MRM-LC/MS/MS chromatograms of threonine-betaxanthin from threonine-betaxanthin standard, the extracts of *H. henanensis* **sp. nov.**, and the blank were shown. The black arrow indicates the peak of threonine-betaxanthin identified in the Hh extract. The corresponding structures of the daughter ions were shown. The detailed MRM methods are listed in table S12. (**C**) ^{1}H NMR of threonine-betaxanthin. ^{1}H NMR (400 MHz, Deuterium Oxide) δ 8.63 (d, *J* = 6.0 Hz, 1H), 8.30 (d, *J* = 1.8 Hz, 1H), 8.02 (dd, *J* = 6.0, 1.8 Hz, 1H), 5.41 (s, 1H), 4.37-4.17 (m, 2H), 3.63 (d, *J* = 4.7 Hz, 2H), 3.33 (s, 1H), 1.31 (d, *J* = 6.6 Hz, 3H).

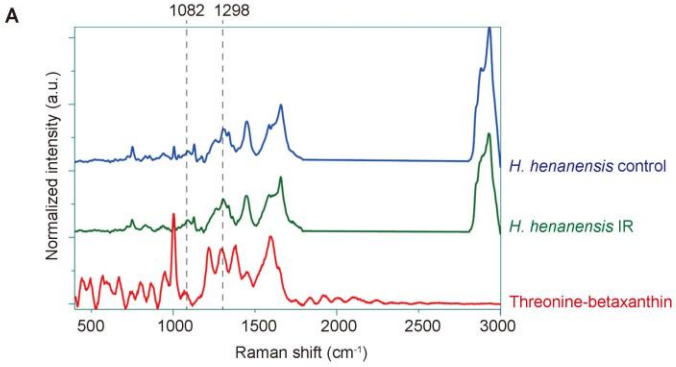
A
1082
1298
Normalized intensity (a.u.)
H. henanensis control
H. henanensis IR
Threonine-betaxanthin
500
1000
1500
2000
2500
3000
Raman shift (cm-1)

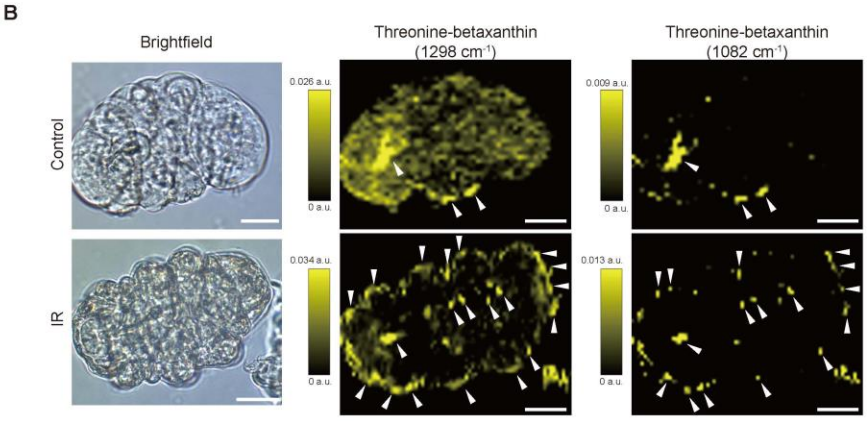
B
Brightfield
Threonine-betaxanthin (1298 cm-1)
Threonine-betaxanthin (1082 cm-1)
Control
IR
0.026 a.u.
0 a.u.
0.009 a.u.
0 a.u.
0.034 a.u.
0 a.u.
0.013 a.u.
0 a.u.

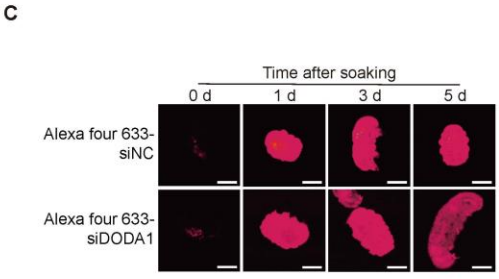
C
Time after soaking
0 d
1 d
3 d
5 d
Alexa four 633-siNC
Alexa four 633-siDODA1

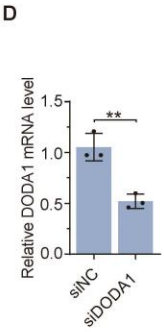
D
Relative DODA1 mRNA level
1.5
1.0
0.5
0.0
**
siNC
siDODA1

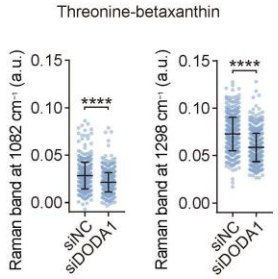
E
Threonine-betaxanthin
Raman band at 1082 cm-1 (a.u.)
0.15
0.10
0.05
0.00
****
siNC
siDODA1
Raman band at 1298 cm-1 (a.u.)
0.15
0.10
0.05
0.00
****
siNC
siDODA1

Fig. S25. Raman spectroscopy analysis betalains in *H. henanensis* sp. nov. (**A**) Spectra corresponding to the threonine-betaxanthin standards and the mean spectra of control or IR treated (2 days after 500 Gy IR treatment) tardigrades were displayed with different colors. 381 single spectra in 9 specimens without IR and 354 single spectra in 14 specimens with 500 Gy IR were analyzed. The annotated peak (1082 cm^{-1} and 1298 cm^{-1}) used for semi-quantification analysis are indicated by dotted lines. a.u., arbitrary units. (**B**) Confocal Raman spectroscopic imaging was used to image tardigrades 2 days after 500 Gy IR. Brightfield microscopic images of a representative single tardigrade from each group and their Raman images colored by their band intensities of threonine-betaxanthin at 1298 cm^{-1} and 1082 cm^{-1} were shown. The maximum values of normalized intensity were marked in the corresponding bars. Scale bars, 20 μm. Results are representative of three independent biological replicates. (**C**) The fluorescence images of *H. henanensis* **sp. nov.** soaked in Alexa Fluor 633-labled siRNA for the indicated days were captured using mixed lasers with four wavelengths: 405 nm, 488 nm, 561 nm, and 633 nm. Scale bars, 50 μm. (**D**) Quantitative RT-PCR analysis of DODA1 with control or DODA1 siRNA soaking tardigrades. The data are presented as mean ± SD **(**n = 3**)**. (**E**) Semi-quantification of threonine-betaxanthin by the indicated Raman bands. 444 single spectra in 7 specimens with siNC soaking and 600 single spectra in 6 specimens with siDODA1 soaking (5 days) were analyzed. The data are presented as mean ± SD. Unpaired two-tailed *t*-tests for (D). Mann-Whitney U test for (E). ** $P < 0.01$; **** $P < 0.0001$.

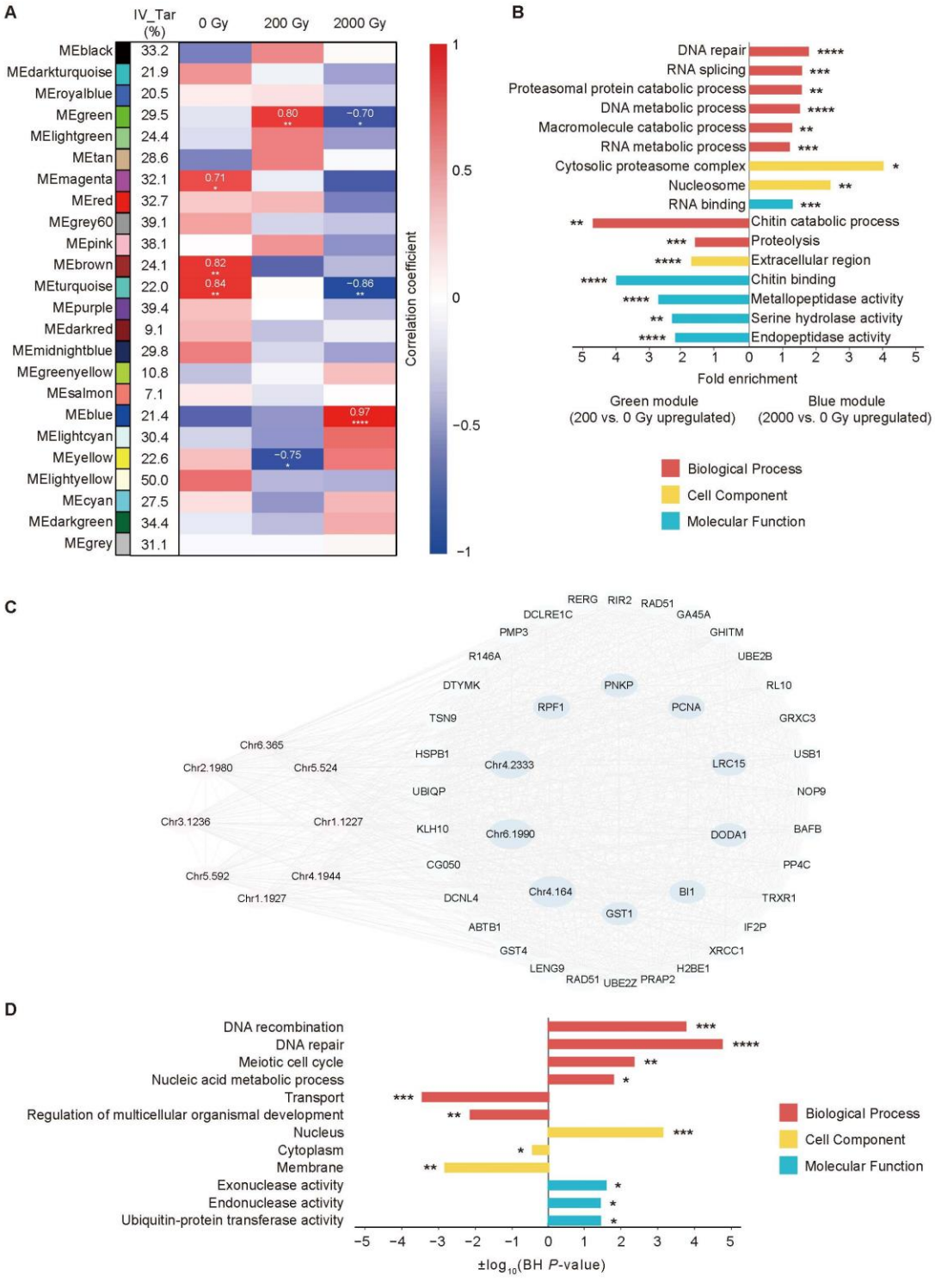
A
IV_Tar (%)
0 Gy
200 Gy
2000 Gy
MEblack 33.2
MEdarkturquoise 21.9
MEroyalblue 20.5
MEgreen 29.5
MElightgreen 24.4
MEtan 28.6
MEmagenta 32.1
MEred 32.7
MEgrey60 39.1
MEpink 38.1
MEbrown 24.1
MEturquoise 22.0
MEpurple 39.4
MEdarkred 9.1
MEmidnightblue 29.8
MEgreenyellow 10.8
MEsalmon 7.1
MEblue 21.4
MElightcyan 30.4
MEyellow 22.6
MElightyellow 50.0
MECyan 27.5
MEdarkgreen 34.4
MEgrey 31.1
0.80 **
−0.70 *
0.71 *
0.82 **
0.84 **
−0.86 **
0.97 ****
−0.75 *
Correlation coefficient
1
0.5
0
−0.5
−1
B
DNA repair ****
RNA splicing ***
Proteasomal protein catabolic process **
DNA metabolic process ****
Macromolecule catabolic process **
RNA metabolic process ***
Cytosolic proteasome complex *
Nucleosome **
RNA binding ***
Chitin catabolic process **
Proteolysis ***
Extracellular region ****
Chitin binding ****
Metallopeptidase activity ****
Serine hydrolase activity **
Endopeptidase activity ****
5 4 3 2 1 0 1 2 3 4 5
Fold enrichment
Green module (200 vs. 0 Gy upregulated)
Blue module (2000 vs. 0 Gy upregulated)
Biological Process
Cell Component
Molecular Function
C
RERG
RIR2
RAD51
DCLRE1C
GA45A
PMP3
GHITM
R146A
UBE2B
DTYMK
PNKP
RL10
RPF1
PCNA
TSN9
GRXC3
Chr6.365
HSPB1
USB1
Chr2.1980
Chr5.524
Chr4.2333
LRC15
UBIQP
NOP9
Chr3.1236
Chr1.1227
KLH10
Chr6.1990
DODA1
BAFB
CG050
PP4C
Chr5.592
Chr4.1944
Chr1.1927
DCNL4
Chr4.164
BI1
TRXR1
GST1
ABTB1
IF2P
GST4
XRCC1
LENG9
H2BE1
RAD51
UBE2Z
PRAP2
D
DNA recombination ***
DNA repair ****
Meiotic cell cycle **
Nucleic acid metabolic process *
Transport ***
Regulation of multicellular organismal development **
Nucleus ***
Cytoplasm *
Membrane **
Exonuclease activity *
Endonuclease activity *
Ubiquitin-protein transferase activity *
−5 −4 −3 −2 −1 0 1 2 3 4 5
±log10(BH P-value)
Biological Process
Cell Component
Molecular Function

Fig. S26. Weighted Gene Co-Expression Network Analysis (WGCNA) of tardigrades specific genes. (**A**) The expression patterns of each module under different doses irradiation. The heatmap shows the correlation coefficients. The significant correlations are shown and the FDR value is indicated as asterisks. The proportions of tardigrade-specific genes are shown after the color blocks. (**B**) GO annotation enrichment analysis of the blue module. (**C**) The top 50 genes with highest connectivity in the blue module. Light blue represents top 10 and lavender represents tardigrade-specific genes. (**D**) GO annotations enrichment analysis of the top 50 high-connected genes. * FDR < 0.05, ** FDR < 0.01, *** FDR < 0.001, **** FDR < 0.0001

A

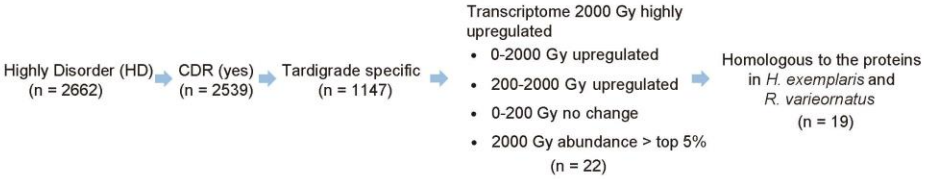

Gene ID	Disordered Regions			Nuclear localization	
	IUpred2	pONDR	PLAAC	cNLS Mapper	WoLF PSORT II
H.Henanensis.Chr4.1468（TRID1）	+	+	+	+	+
H.Henanensis.Chr1.1812	+	+			+
H.Henanensis.Chr1.1921	+	+	+		+
H.Henanensis.Chr2.1902	+	+	+		+
H.Henanensis.Chr3.614	+	+			
H.Henanensis.Chr3.1042	+	+		+	+
H.Henanensis.Chr3.2037	+	+		+	+
H.Henanensis.Chr3.2234	+	+	+		
H.Henanensis.Chr3.2253	+	+		+	+
H.Henanensis.Chr3.719	+	+	+		
H.Henanensis.Chr4.102	+	+			+
H.Henanensis.Chr4.288	+	+	+		
H.Henanensis.Chr4.297	+	+			+
H.Henanensis.Chr4.1171	+				
H.Henanensis.Chr4.1471	+	+			
H.Henanensis.Chr4.2375	+	+			+
H.Henanensis.Chr5.1316	+	+			+
H.Henanensis.Chr6.433	+	+			
H.Henanensis.Chr6.949	+	+	+		

B

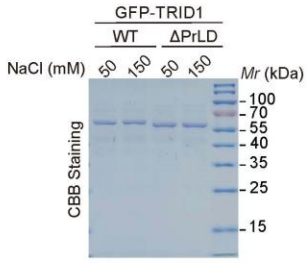

C

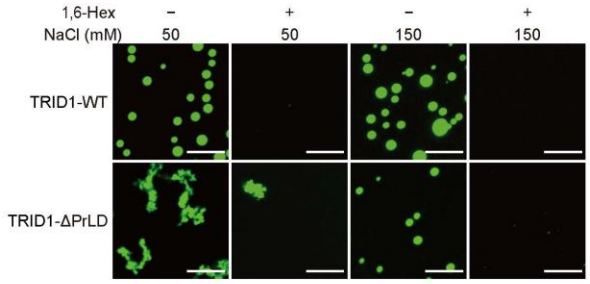

D

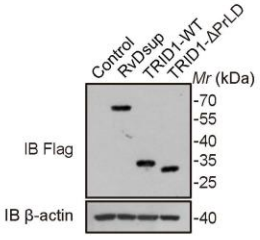

E

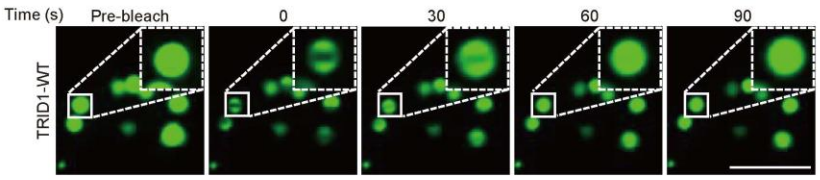

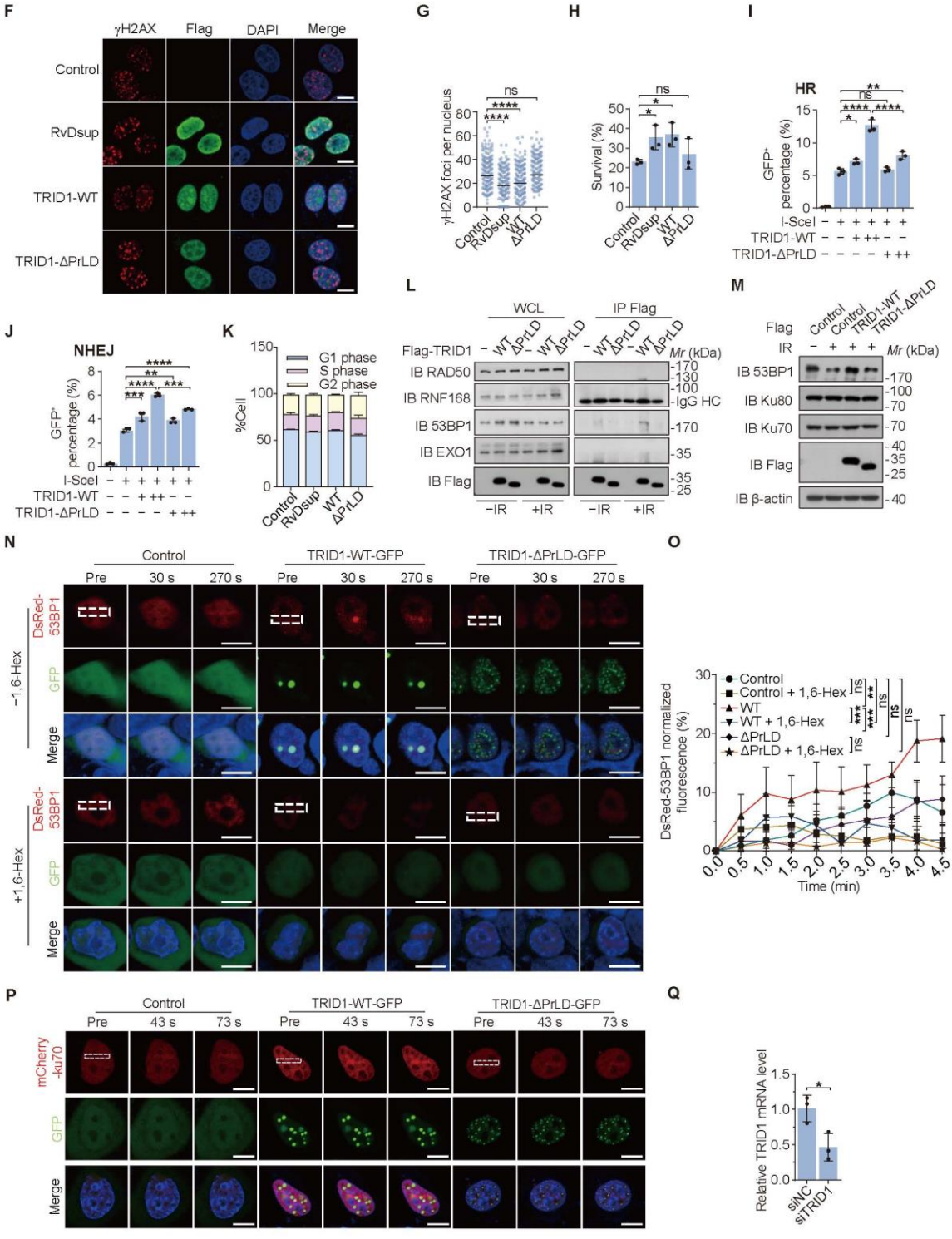
F
γH2AX
Flag
DAPI
Merge
Control
RvDsup
TRID1-WT
TRID1-ΔPrLD
G
γH2AX foci per nucleus
ns
****
****
Control
RvDsup
WT
ΔPrLD
H
Survival (%)
ns
*
*
I
HR
GFP+ percentage (%)
**
ns
****
****
*
I-SceI
TRID1-WT
TRID1-ΔPrLD
J
NHEJ
GFP+ percentage (%)
****
**
****
***
****
***
K
%Cell
G1 phase
S phase
G2 phase
L
WCL
IP Flag
Flag-TRID1
WT
ΔPrLD
Mr (kDa)
IB RAD50
IB RNF168
IB 53BP1
IB EXO1
IB Flag
IgG HC
−IR
+IR
M
Flag
IR
Mr (kDa)
IB 53BP1
IB Ku80
IB Ku70
IB Flag
IB β-actin
N
Control
TRID1-WT-GFP
TRID1-ΔPrLD-GFP
Pre
30 s
270 s
−1,6-Hex
+1,6-Hex
DsRed-53BP1
GFP
Merge
O
DsRed-53BP1 normalized fluorescence (%)
Control
Control + 1,6-Hex
WT
WT + 1,6-Hex
ΔPrLD
ΔPrLD + 1,6-Hex
ns
***
***
**
ns
ns
ns
Time (min)
P
Control
TRID1-WT-GFP
TRID1-ΔPrLD-GFP
Pre
43 s
73 s
mCherry-ku70
GFP
Merge
Q
Relative TRID1 mRNA level
*
siNC
siTRID1

Fig. S27. Reduced DNA damage in TRID1-expressing cells after radiation. (**A**) Summary chart of the workflow for the identification of upregulated, tardigrades specific, and intrinsically disordered proteins. CDR, consecutive disordered region (more than 30 amino acids). (**B**) The purified GFP-TRID1 proteins were resolved on SDS-PAGE and stained with CBB. (**C**) Phase separation of TRID1-WT (10 μM) and TRID1-ΔPrLD (10 μM) treated with or without 5% 1,6-Hexanediol for 10 min. Scale bars, 10 μm. (**D**) Western blotting analysis of the expression of indicated proteins in HeLa cells. (**E**) Photobleaching and recovery analysis of TRID1-WT droplet in HeLa cell. Magnified view (Dashed box) of TRID1-WT droplet is shown. Scale bar, 10 μm. (**F** and **G**) Analysis of γH2AX foci number of HeLa cells expressing TRID1-WT or its mutants under 2 Gy X-ray irradiation. RvDsup was used as a positive control. Representative images are shown for each condition. Scale bars, 10 μm. Quantitative results are shown in (G). The median values are shown as a black bar. At least 300 cells were analyzed for each condition. (**H**) Cells stably expressing indicated proteins were pretreated with or without 3 Gy X-ray irradiation and cell survival rates were counted by colony formation assay. RvDsup was used as a positive control. (**I** and **J**) HEK293T cells expressing indicated proteins were subject to experiments for HR or NHEJ efficiency analysis. (**K**) FACS analysis of the cell cycle distribution of HeLa cells expressing TRID1-WT or its mutants. (**L**) Immunoprecipitates of TRID1-WT and TRID1-ΔPrLD in HEK293T cells with or without 3 Gy X-ray irradiation and immunoblot with the indicated antibodies. (**M**) Immunoblot of 53BP1, Ku70 and Ku80 in HEK293T cells expressing indicated proteins with or without 3 Gy X-ray irradiation. (**N** and **O**) HEK293T cells expressing indicated proteins were subjected to laser microirradiation and analyzed for the accumulation of DsRed-53BP1 in DSB sites by fluorescent microscopy in the presence or absence of 5% 1,6-hexanediol (N). Dashed box indicated the area of laser microirradiation. Scale bars, 10 μm. The real-time recruitment of DsRed-53BP1 was analysed in (O). (**P**) HeLa cells expressing indicated proteins were subjected to laser microirradiation and analyzed for the accumulation of mCherry-Ku70 in DSB sites by fluorescent microscopy. Dashed box indicated the area of laser microirradiation. Scale bars, 10 μm. The real-time recruitment of mCherry-Ku70 was shown in Fig. 3M. (**Q**) Quantitative RT-PCR analysis of TRID1 in control and TRID1 siRNA soaking tardigrades. The data are presented as mean ± SD [n = 3 in (H), (I), (J), (K), and (Q)] or mean ± SEM [n = 10 in (O)]. One-way ANOVA with Dunnett's post-hoc test for (H), with Tukey's post-hoc test for (I), (J), and (O). Kruskal-Wallis test followed by Dunn's test for (G). Unpaired two-tailed t-tests for (Q). $P > 0.05$, not significant (ns); * $P < 0.05$; ** $P < 0.01$; *** $P < 0.001$; **** $P < 0.0001$.

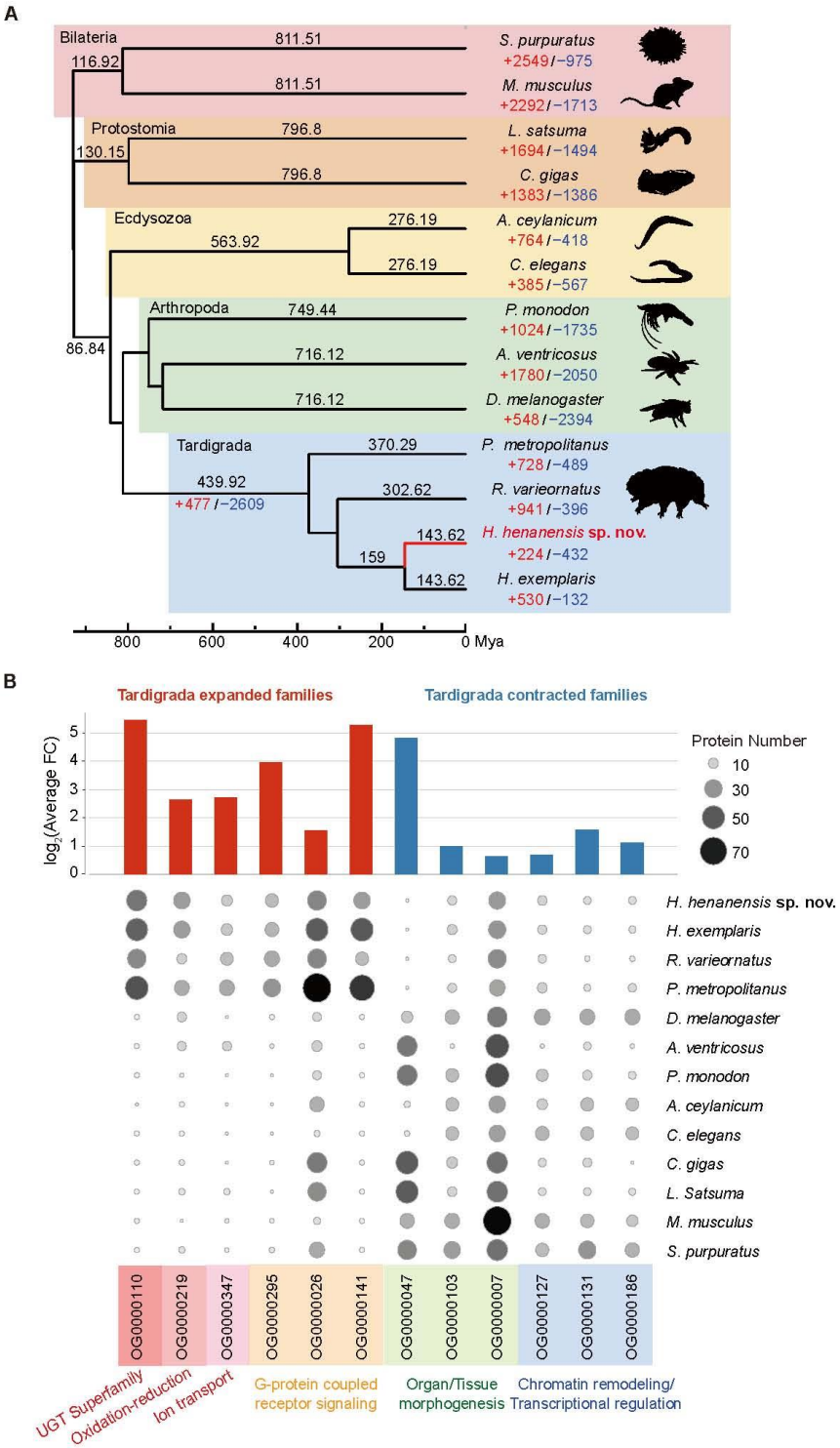
A
Bilateria
811.51
116.92
811.51
S. purpuratus
+2549 / −975
M. musculus
+2292 / −1713
Protostomia
796.8
130.15
796.8
L. satsuma
+1694 / −1494
C. gigas
+1383 / −1386
Ecdysozoa
276.19
563.92
276.19
A. ceylanicum
+764 / −418
C. elegans
+385 / −567
Arthropoda
749.44
86.84
716.12
716.12
P. monodon
+1024 / −1735
A. ventricosus
+1780 / −2050
D. melanogaster
+548 / −2394
Tardigrada
370.29
439.92
+477 / −2609
302.62
143.62
159
143.62
P. metropolitanus
+728 / −489
R. varieornatus
+941 / −396
H. henanensis sp. nov.
+224 / −432
H. exemplaris
+530 / −132
800
600
400
200
0 Mya
B
Tardigrada expanded families
Tardigrada contracted families
log2(Average FC)
0
1
2
3
4
5
Protein Number
10
30
50
70
H. henanensis sp. nov.
H. exemplaris
R. varieornatus
P. metropolitanus
D. melanogaster
A. ventricosus
P. monodon
A. ceylanicum
C. elegans
C. gigas
L. Satsuma
M. musculus
S. purpuratus
OG0000110
OG0000219
OG0000347
OG0000295
OG0000026
OG0000141
OG0000047
OG0000103
OG0000007
OG0000127
OG0000131
OG0000186
UGT Superfamily
Oxidation-reduction
Ion transport
G-protein coupled receptor signaling
Organ/Tissue morphogenesis
Chromatin remodeling/ Transcriptional regulation

Fig. S28. Expansion and contraction analysis of gene family. (**A**) Loss and gain of gene families mapped onto the phylogeny of 13 bilaterians (based on the CAFE results). Red and blue numbers indicate number of gene families with gained and lost on each branch, respectively. Divergence time estimates (mya, million years ago) between each node is shown as black numbers. (**B**) The representative function categories for the gene families significantly expanded/contracted in tardigrades. The size and color of the circle represent the number of proteins of the gene family in the species, and the histogram represents the fold change between the average number of proteins of the gene family in tardigrades and that of other species (red refers to 'tardigrades/other species', blue refers to 'other species/tardigrades').

A

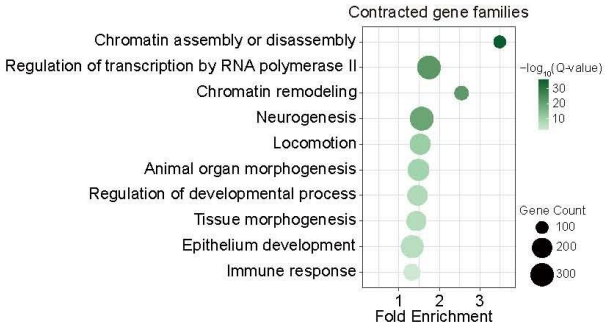
Contracted gene families
Chromatin assembly or disassembly
Regulation of transcription by RNA polymerase II
Chromatin remodeling
Neurogenesis
Locomotion
Animal organ morphogenesis
Regulation of developmental process
Tissue morphogenesis
Epithelium development
Immune response
−log10(Q-value)
30
20
10
Gene Count
100
200
300
1
2
3
Fold Enrichment

B

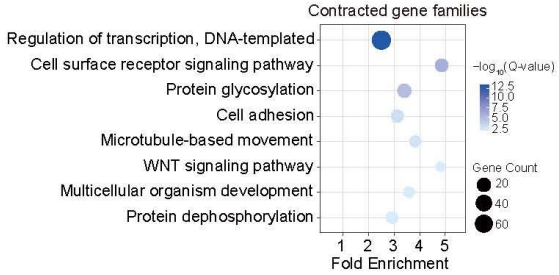
Contracted gene families
Regulation of transcription, DNA-templated
Cell surface receptor signaling pathway
Protein glycosylation
Cell adhesion
Microtubule-based movement
WNT signaling pathway
Multicellular organism development
Protein dephosphorylation
−log10(Q-value)
12.5
10.0
7.5
5.0
2.5
Gene Count
20
40
60
1
2
3
4
5
Fold Enrichment

C

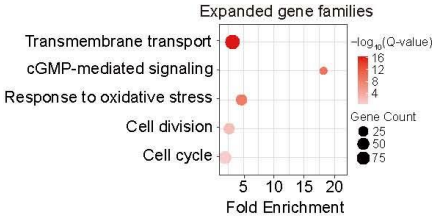
Expanded gene families
Transmembrane transport
cGMP-mediated signaling
Response to oxidative stress
Cell division
Cell cycle
−log10(Q-value)
16
12
8
4
Gene Count
25
50
75
5
10
15
20
Fold Enrichment

D

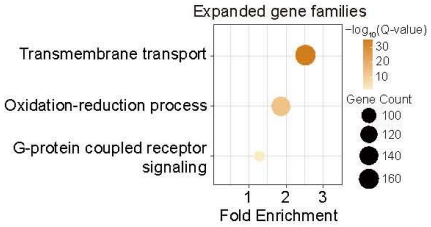
Expanded gene families
Transmembrane transport
Oxidation-reduction process
G-protein coupled receptor signaling
−log10(Q-value)
30
20
10
Gene Count
100
120
140
160
1
2
3
Fold Enrichment

Fig. S29. Functional enrichment analysis of the contracted (A and B) and expanded (C and D) gene families in tardigrades. The upper panels show the results based on the gene GO annotation of *D. melanogaster* and the lower are the results based on the gene GO annotation of *H. henanensis* **sp. nov.** inferred in this study.

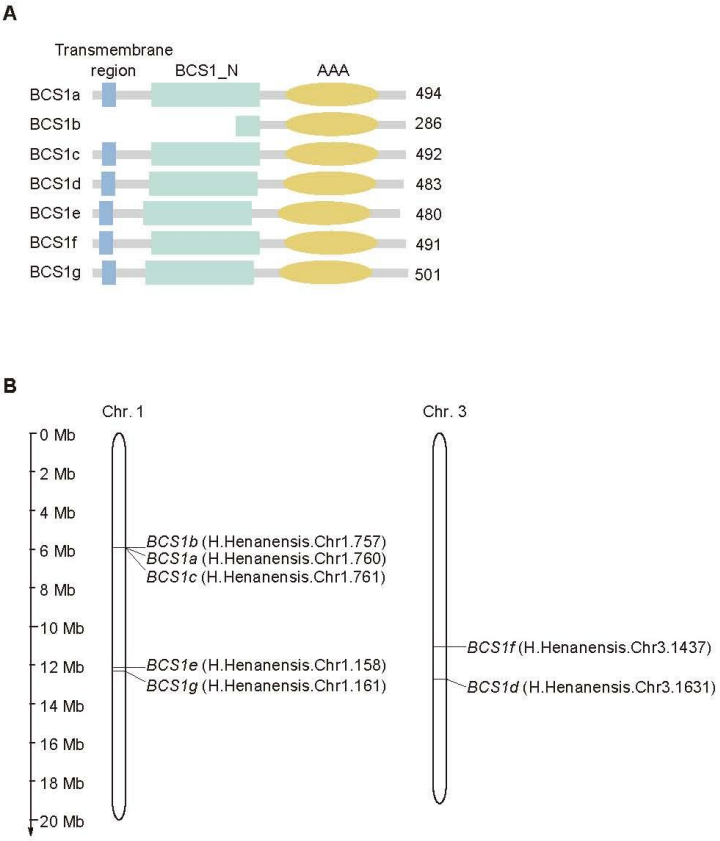
A
Transmembrane region
BCS1_N
AAA
BCS1a
BCS1b
BCS1c
BCS1d
BCS1e
BCS1f
BCS1g
494
286
492
483
480
491
501
B
Chr. 1
Chr. 3
0 Mb
2 Mb
4 Mb
6 Mb
8 Mb
10 Mb
12 Mb
14 Mb
16 Mb
18 Mb
20 Mb
BCS1b (H.Henanensis.Chr1.757)
BCS1a (H.Henanensis.Chr1.760)
BCS1c (H.Henanensis.Chr1.761)
BCS1e (H.Henanensis.Chr1.158)
BCS1g (H.Henanensis.Chr1.161)
BCS1f (H.Henanensis.Chr3.1437)
BCS1d (H.Henanensis.Chr3.1631)

Fig. S30. Schematic diagram of the BCS1 proteins and the genetic map of *BCS1* genes in *H. henanensis* sp. nov. (**A**) Schematic diagram of the BCS1 proteins in *H. henanensis* **sp. nov.** (**B**) The genetic map of *BCS1* genes from *H. henanensis* **sp. nov.** generated by MG2C.

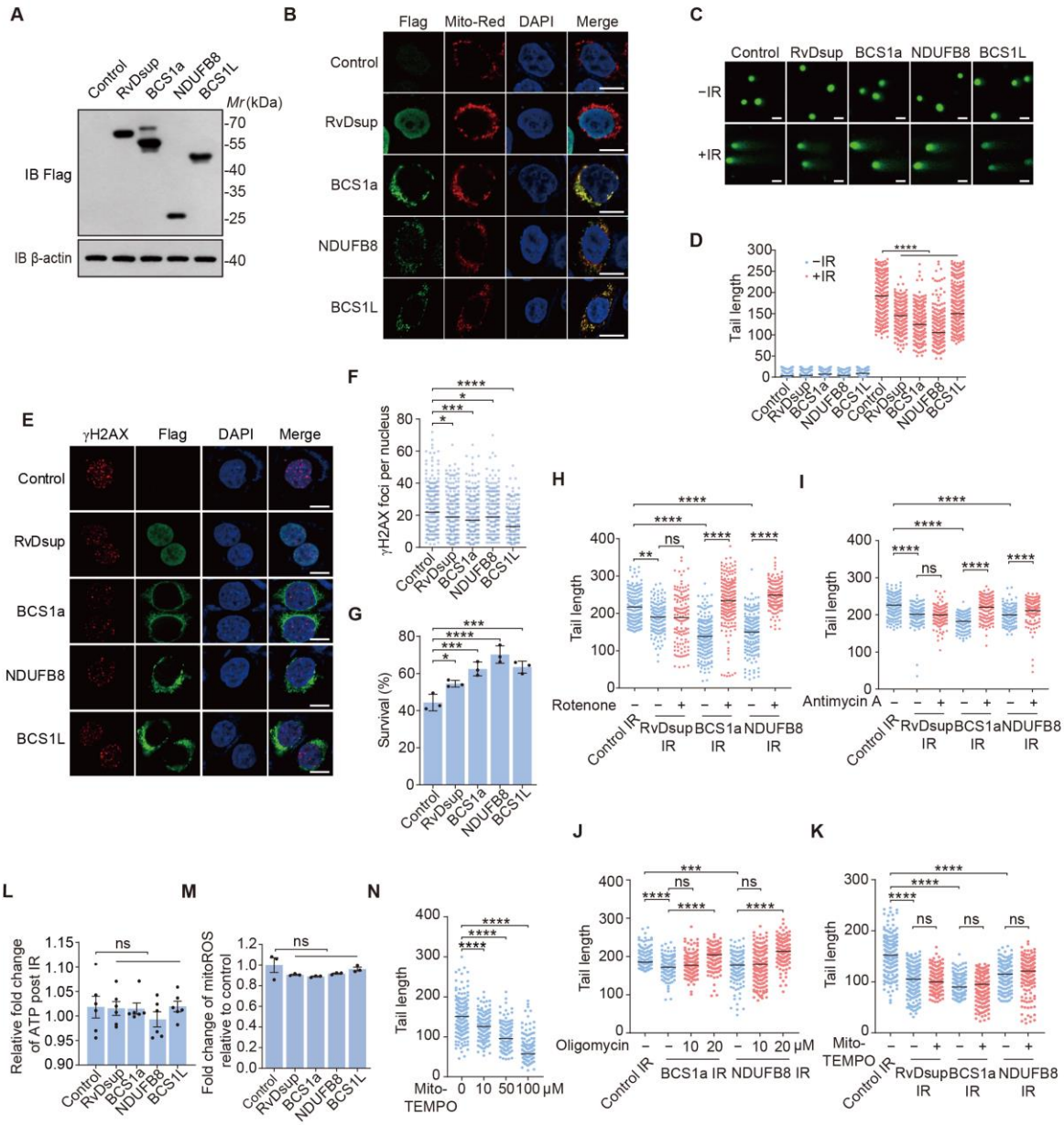
A
Control
RvDsup
BCS1a
NDUFB8
BCS1L
Mr(kDa)
-70
-55
-40
-35
-25
IB Flag
IB β-actin
-40
B
Flag
Mito-Red
DAPI
Merge
Control
RvDsup
BCS1a
NDUFB8
BCS1L
C
Control
RvDsup
BCS1a
NDUFB8
BCS1L
−IR
+IR
D
−IR
+IR
Tail length
E
γH2AX
Flag
DAPI
Merge
F
γH2AX foci per nucleus
G
Survival (%)
H
Tail length
Rotenone
Control IR
RvDsup IR
BCS1a IR
NDUFB8 IR
I
Tail length
Antimycin A
J
Tail length
Oligomycin
10
20
μM
K
Tail length
Mito-TEMPO
L
Relative fold change of ATP post IR
M
Fold change of mitoROS relative to control
N
Tail length
Mito-TEMPO
0
10
50
100
μM
ns

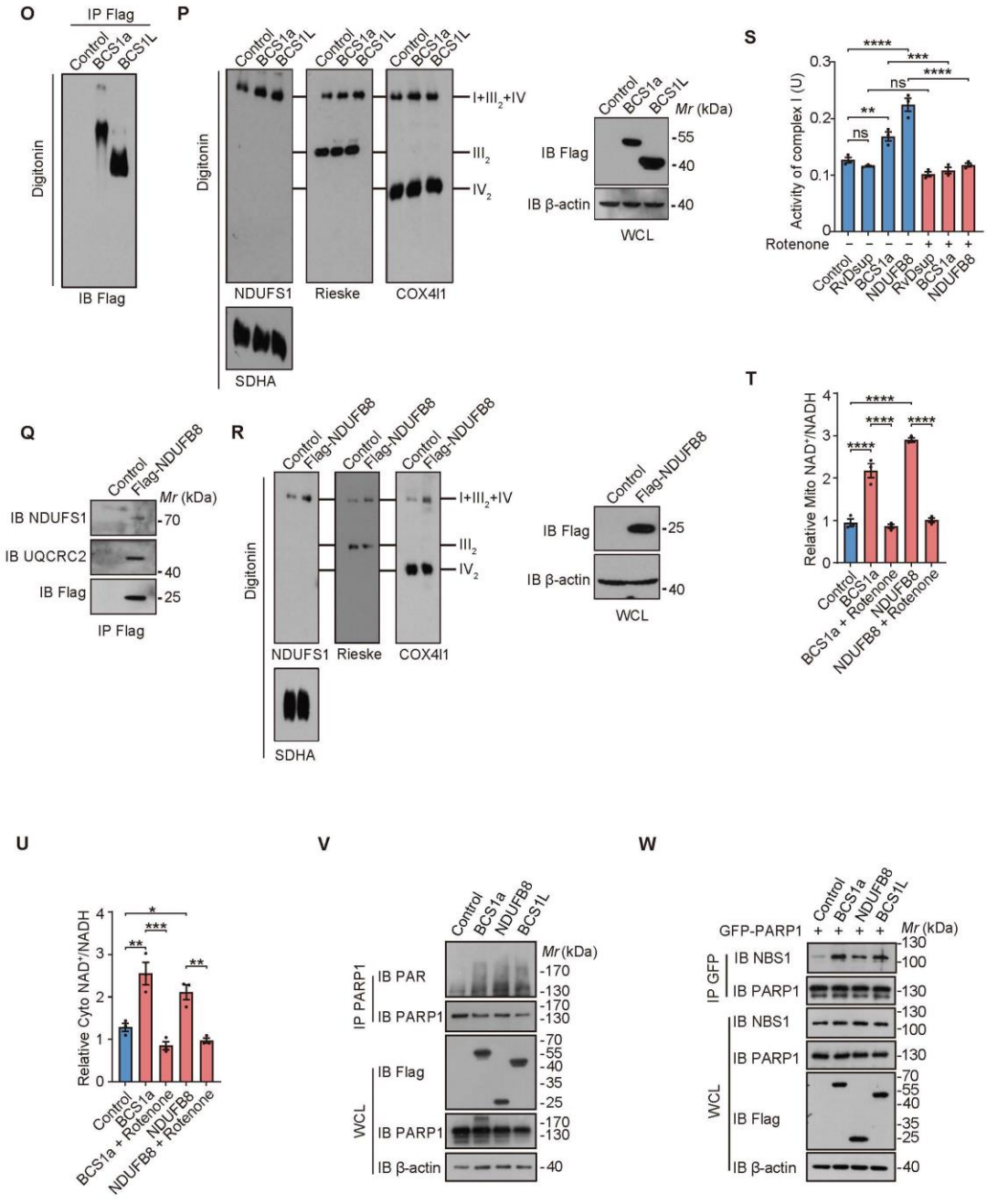
O
IP Flag
Control
BCS1a
BCS1L
Digitonin
IB Flag
P
Control
BCS1a
BCS1L
Digitonin
I+III2+IV
III2
IV2
NDUFS1
Rieske
COX4I1
SDHA
Mr (kDa)
IB Flag
IB β-actin
-55
-40
-40
WCL
S
Activity of complex I (U)
0.3
0.2
0.1
0
****
***
****
ns
**
ns
Rotenone
Control
RvDsup
BCS1a
NDUFB8
RvDsup
BCS1a
NDUFB8
Q
Control
Flag-NDUFB8
Mr (kDa)
IB NDUFS1
IB UQCRC2
IB Flag
-70
-40
-25
IP Flag
R
Control
Flag-NDUFB8
Digitonin
I+III2+IV
III2
IV2
NDUFS1
Rieske
COX4I1
SDHA
IB Flag
IB β-actin
-25
-40
WCL
T
Relative Mito NAD+/NADH
4
3
2
1
0
****
****
****
****
Control
BCS1a
BCS1a + Rotenone
NDUFB8
NDUFB8 + Rotenone
U
Relative Cyto NAD+/NADH
4
3
2
1
0
*
***
**
**
Control
BCS1a
BCS1a + Rotenone
NDUFB8
NDUFB8 + Rotenone
V
Control
BCS1a
NDUFB8
BCS1L
Mr (kDa)
IP PARP1
IB PAR
IB PARP1
-170
-130
-170
-130
WCL
IB Flag
IB PARP1
IB β-actin
-70
-55
-40
-35
-25
-170
-130
-40
W
GFP-PARP1
+ + + +
Control
BCS1a
NDUFB8
BCS1L
Mr (kDa)
IP GFP
IB NBS1
IB PARP1
-130
-100
-130
WCL
IB NBS1
IB PARP1
IB Flag
IB β-actin
-130
-100
-130
-70
-55
-40
-35
-25
-40

Fig. S31. Radioprotective effects of BCS1a and NDUFB8. (**A**) Immunoblot of the expression of RvDsup, BCS1a, NDUFB8 and BCS1L proteins in HeLa cells. (**B**) Analysis of subcellular localization of BCS1a, NDUFB8 and BCS1L proteins by immunofluorescent assays. Mito-red was used as a mitochondria marker. (**C** and **D**) DNA fragmentation was assessed by the tail length under non-irradiation or 10 Gy X-ray irradiation. Representative images were shown in (C). Scale bars, 50 μm. At least 250 cells were analyzed for each condition. (**E** and **F**) Analysis of γH2AX foci number of cells under 2 Gy X-ray irradiation. The representative images are shown in (E). Scale bars, 10 μm. At least 280 cells were analyzed for each condition. (**G**) HeLa cells stably expressing indicated proteins were treated with or without 3 Gy X-ray irradiation and cell survival rates were counted by colony formation assay. RvDsup was used as a positive control. **(H)** DNA fragmentations of HeLa cells stably expressing indicated proteins were assessed by the tail length under 10 Gy X-ray irradiation with or without 10 μM rotenone pretreatment for 6 hours. The median values are shown as a black bar. At least 150 cells were analyzed for each condition. RvDsup was used as a positive control. **(I)** DNA fragmentations of HeLa cells stably expressing indicated proteins were assessed by the tail length under 10 Gy X-ray irradiation with or without 10 μM antimycin A pretreatment for 2 hours. The median values are shown as a black bar. At least 150 cells were analyzed for each condition. RvDsup was used as a positive control. (**J**) DNA fragmentations of HeLa cells stably expressing indicated proteins were assessed by the tail length under 10 Gy X-ray irradiation with 10 μM oligomycin pretreatment for 0, 1, and 2 hours. At least 120 cells were analyzed for each condition. (**K**) DNA fragmentations of HeLa cells stably expressing indicated proteins were assessed by the tail length under 10 Gy X-ray irradiation with or without 10 μM mitoTEMPO pretreatment for 2 hours. At least 150 cells were analyzed for each condition. (**L**) HeLa cells stably expressing indicated proteins were treated with or without 3 Gy X-ray irradiation and harvested for ATP analysis 24 hours post irradiation. (**M**) HeLa cells stably expressing indicated proteins were harvested for mitochondria ROS analysis. (**N**) DNA fragmentations of HeLa cells stably expressing indicated proteins were assessed by the tail length under 10 Gy X-ray irradiation with different concentrations of mitoTEMPO pretreatment for 2 hours. At least 150 cells were analyzed for each condition. (**O**) Immunoaffinity purification, blue native PAGE (BN-PAGE) and immunodetection of the indicated proteins by using digitonin-solubilized mitochondria from cells expressing the indicated proteins. (**P**) Immunodetection of the indicated proteins representing CI, CIII, and CIV, after blue native PAGE (BN-PAGE) of digitonin-solubilized mitochondria. CII (anti-SDHA) as a loading control. The expression of BCS1a and BCS1L were verified by SDS-PAGE with the whole cell lysate. (**Q**) Immunoaffinity purification, SDS-PAGE and immunodetection of the indicated proteins by using digitonin-solubilized mitochondria from cells expressing the indicated proteins. (**R**) Immunodetection of the indicated proteins representing CI, CIII, and CIV, after BN-PAGE of digitonin-solubilized mitochondria. CII (anti-SDHA) as a loading control. The expression of NDUFB8 was verified by SDS-PAGE with the whole cell lysate. **(S)** HeLa cells stably expressing indicated proteins were harvested for mitochondria complex I activity analysis. **(T** and **U)** HEK293T cells transfected with indicated proteins were harvested for mitochondrial (U) and cytosol (V) NAD^+ /NADH analysis by using SoNar probes. (**V**) Immunoprecipitates of PARP1 in HEK293T cells with 10 Gy X-ray irradiation and immunoblot with anti-PAR antibody. (**W**) Immunoprecipitates of GFP-PARP1 in HEK293T cells post 2 Gy X-ray irradiation for 0.5 hour and immunoblot with the anti-NBS1 antibody. The data are presented as mean ± SD [n = 3 in (G) and (S)] or mean ± SEM [n = 3 in (M)，(T), and (U) or n = 6 in (L)]. The median values are shown as a black bar in (D), (F), (H), (I), (J), (K), and (N). The unit of tail length is μm. One-way ANOVA with Dunnett's post-hoc test

for (G), (L) and (M). Kruskal-Wallis test followed by Dunn's test for (D), (F), (H), (I), (J), (K), and (N). One-way ANOVA with Tukey's post-hoc test for (S), (T), and (U). $P > 0.05$, not significant (ns); * $P < 0.05$; ** $P < 0.01$; *** $P < 0.001$; **** $P < 0.0001$.

Fig. 4I

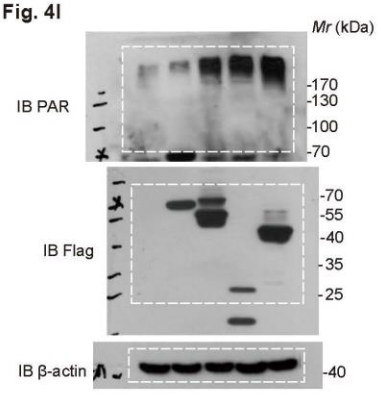

Fig. S21A

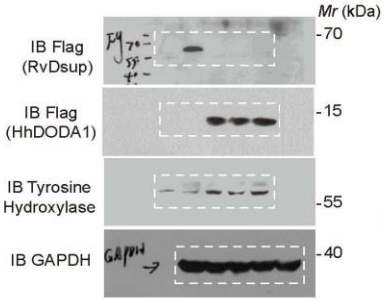

Fig. S27D

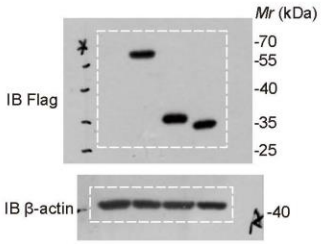

Fig. S27L

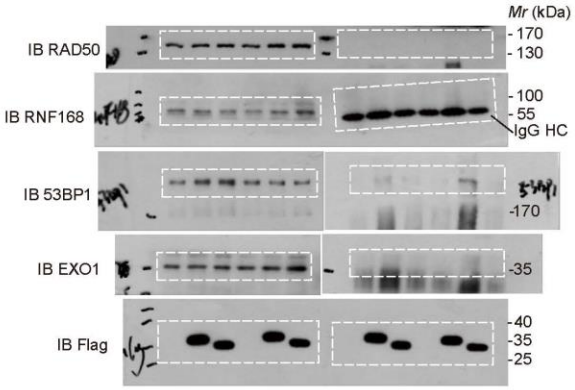

Fig. S27M

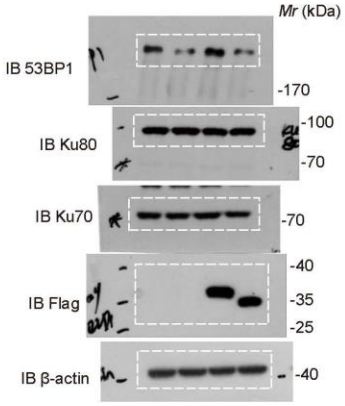

Fig. S31A

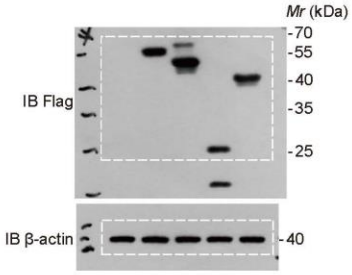

Fig. S31O

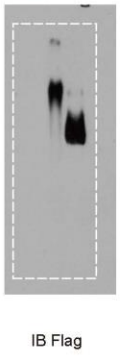

Fig. S31P

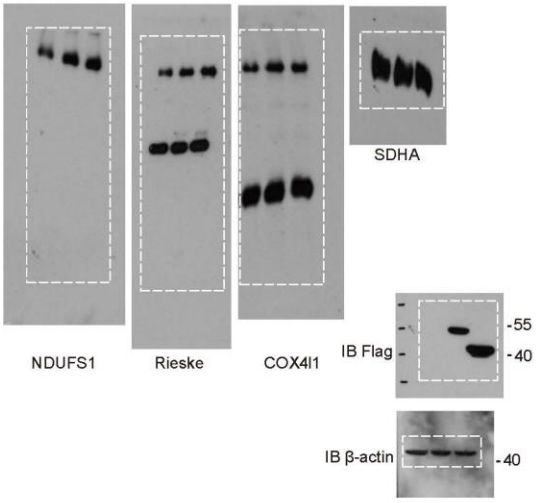

Fig. S31Q

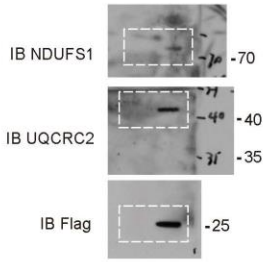

Fig. S31R

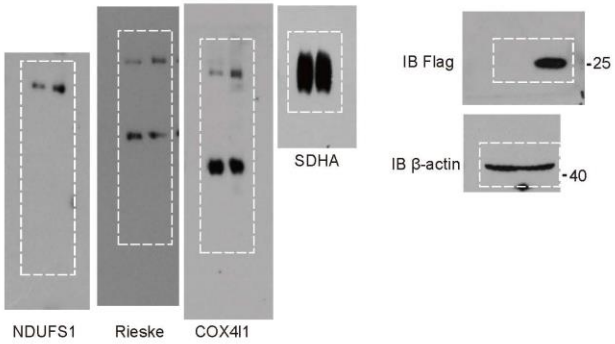

Fig. S31V

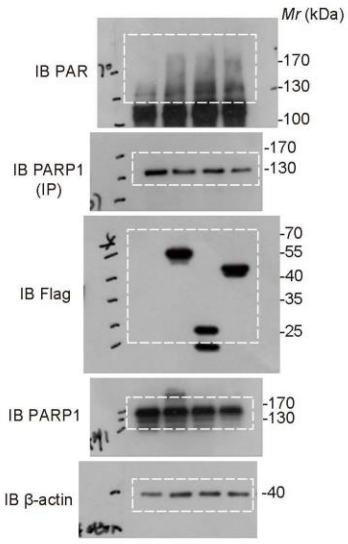

Fig. S31W

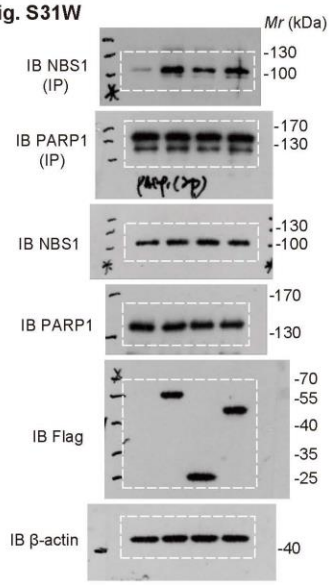

Fig. S32. Uncropped blots related to Fig. 4J, fig. S21A, fig. S27D, fig. S27L, fig. S27M, fig. S31A, fig. S31, O-R, fig. S31V and fig. S31W.

Table S1. Summary of morphological data for *H. henanensis* sp. nov. Measurements are given in µm. N, number of specimens/structures measured. SD, standard deviation. *pt* index is percentage ratio between the length of a structure and the length of the buccal tube.

Character	N	Holotype		Range		Mean ± SD	
		µm	*pt*	µm	*pt*	µm	*pt*
Body length	20	305.2	*1261*	198 – 327	*1067 – 1288*	278 ± 38	*1237* ±60
Buccal tube length	20	24.2	–	18.5 – 25.6	–	22.4 ± 2.3	
Stylet support insertion point	20	14.3	*59.1*	10.7 – 15.2	*57.5 – 59.6*	13.2 ± 1.4	58.8 ± 0.5
Buccal tube external width	20	1.7	*7.0*	1.3 – 1.9	*7.0 – 7.6*	1.6 ± 0.2	*7.3* ± 0.2
Buccal tube internal width	20	1.5	*6.2*	1.1 – 1.7	*5.9 – 6.8*	1.4 ± 0.2	*6.4* ±0.2
Placoid lengths							
Macroplacoid 1	20	4.2	*17.4*	2.9 – 4.5	*15.6 – 17.6*	3.8 ± 0.5	*16.9* ± 0.5
Macroplacoid 2	20	3.1	*12.8*	2.2 – 3.4	*11.8 – 13.4*	2.8 ± 0.5	*12.6*± 0.5
Septulum	14	1.0	*4.1*	0.7 – 1.1	*3.7 – 4.4*	0.9 ± 0.1	*4.0* ± 0.2
Macroplacoid row	20	8.4	*34.7*	5.9 – 9.1	*31.7 – 35.6*	7.6 ± 0.9	*33.9*± 0.9
Placoid row	20	10.1	*41.7*	7.1 – 10.8	*37.2 – 42.2*	8.9 ±1.1	*39.8* ± 1.3
Claw 1 heights							
External base	17	2.9	*12.0*	2.1 – 3.1	*11.3 – 13.0*	2.7 ± 0.4	*12.2* ±0.6
External primary branch	15	5.4	*22.3*	3.9 – 5.7	*21.0 – 23.5*	4.9 ± 0.7	*22.4* ± 0.7
External secondary branch	17	3.6	*14.9*	2.7 – 3.9	*14.2 – 15.5*	3.3 ± 0.4	*14.7* ±0.4
External base/primary branch (*cct*)		53.7	–	52.5 – 57.4	–	54.7 ± 1.5	–
Internal base	16	2.6	*10.7*	1.9 – 2.8	*10.2 – 11.8*	2.5 ± 0.3	*11.1* ± 0.5
Internal primary branch	14	5.1	*21.1*	3.2 – 5.5	*17.2 – 22.6*	4.6 ± 0.8	*20.7* ± 1.5
Internal secondary branch	16	2.9	*12.0*	2.1 – 3.2	*11.1 – 12.5*	2.6 ± 0.3	*11.9* ± 0.4
Internal base/primary branch (*cct*)		51.0	–	49.1 – 59.4	–	53.6 ± 2.9	–
Claw 2 heights							
External base	18	3.1	*12.8*	2.3 – 3.2	*12.2 – 13.0*	2.8 ± 0.3	*12.5* ± 0.2
External primary branch	17	5.9	*24.4*	3.9 – 5.9	*21.0 – 25.1*	5.1 ± 0.6	*22.9* ± 0.9
External secondary branch	18	4.0	*16.5*	2.8 – 4.1	*14.9 – 16.7*	3.5 ± 0.4	*15.8* ± 0.6
External base/primary branch (*cct*)		52.5	–	51.0 – 59.0	–	54.9 ± 1.8	–
Internal base	17	2.7	*11.2*	2.0 – 2.9	*10.8 – 12.1*	2.5 ± 0.3	*11.5* ± 0.4
Internal primary branch	17	5.5	*22.7*	3.4 – 5.6	*18.3 – 23.2*	4.8 ± 0.7	*21.5*± 1.2
Internal secondary branch	17	3.2	*13.2*	2.2 – 3.4	*10.8 – 13.6*	2.7 ± 0.3	*12.1* ± 0.9

Internal base/primary branch (*cct*)		49.1	–	49.1 –58.8	–	53.6 ± 2.5	–
Claw 3 heights							
External base	18	3.1	*12.8*	2.2 – 3.3	*11.8 – 13.3*	2.8 ± 0.3	*12.4* ± 0.4
External primary branch	17	6.1	*25.2*	4.1 – 6.2	*22.0 – 25.6*	5.2± 0.6	*23.6* ± 0.9
External secondary branch	18	3.7	*15.3*	2.7 – 3.7	*14.1 – 15.8*	3.3 ± 0.3	*14.8* ± 0.5
External base/primary branch (*cct*)		50.8	–	50.8 – 54.5	–	52.5 ± 1.1	–
Internal base	18	2.8	*11.6*	2.1 – 3.0	*11.3 – 12.3*	2.6 ± 0.3	*11.6* ± 0.3
Internal primary branch	18	5.7	*23.6*	3.6 – 5.7	*19.4 – 23.6*	5.0 ± 0.6	*22.2*± 0.9
Internal secondary branch	18	3.3	*13.6*	2.3 – 3.5	*12.3 – 13.8*	2.9± 0.3	*12.8*± 0.4
Internal base/primary branch (*cct*)		49.1	–	49.1 – 58.3	–	52.4 ± 1.8	–
Claw 4 heights							
Anterior base	19	3.0	*12.4*	2.3 – 3.2	*11.5 – 12.7*	2.7 ± 0.3	*12.2* ± 0.3
Anterior primary branch	19	5.6	*23.1*	3.9 – 5.9	*21.0 – 23.6*	5.1± 0.6	*22.7* ± 0.7
Anterior secondary branch	19	3.7	*15.3*	2.7 – 3.8	*14.5 – 15.3*	3.3 ± 0.3	*14.8* ± 0.3
Anterior base/primary branch (*cct*)		53.6	–	51.8 – 59.0	–	53.5 ± 1.9	–
Posterior base	20	3.4	*14.0*	2.6 – 3.6	*13.5 – 14.6*	3.2 ± 0.3	*14.2* ± 0.3
Posterior primary branch	20	8.1	*33.5*	5.8 – 8.2	*30.5 – 34.0*	7.2 ± 0.8	*32.2*± 0.8
Posterior secondary branch	20	4.2	*17.4*	3.0 – 4.3	*15.9 – 17.7*	3.7± 0.4	*16.7*± 0.5
Posterior base/primary branch (*cct*)		42.0	–	42.0 – 47.8	–	44.1 ± 1.6	–

Table S2. Comparison of *pt* values between *H. henanensis* sp. nov. and other species of *Hypsibius dujardini* morphogroup.

The full name of species in the table: Hh, *H. henanensis*; Hc, *H. conwentzii*; Hd, *H. dujardini*; He, *H. exemplaris*; Hhe, *H. Heardensis*; Hp, *H. pallidoides*; Hsep, *H. septulatus*; Hsey, *H. seychellensis*; Hv, *H. valentinae.*

SPECIES / CHARACTER	Hh	Hc *(166)*	Hd (*12*)	He (*12*)	Hhe *(167)*	Hsep *(168)*	Hsey *(169)*	Hv *(170)*
Body length	*1067 – 1288*	—	*843 – 1372*	*602 – 1028*	*1458*	*1020*	*839 – 1063*	*907 –1158*
Stylet support insertion point	*57.5 – 59.6*	*58.6 – 62.4*	*57.2 – 64.2*	*65.6 – 68.4*	*56.0–63.0*	*64.5*	*62.3 – 63.7*	*61.3 – 62.5*
Buccal tube external width	*7.0 – 7.6*	*8.7 – 11.2*	*6.9 – 10.2*	*7.4 – 9.4*	*8.3*	*9.0*	*6.3 – 6.4*	*7.4–7.8*
Buccal tube internal width	*5.9 – 6.8*	*3.1 – 4.7*	*1.9 – 5.7*	*3.2 – 5.3*	—	—	—	—
Macroplacoid 1	*15.6 – 17.6*	*14.4 – 17.8*	*13.2 – 19.9*	*15.6 – 19.5*	*22.9*	*21.2*	*18.3 – 19.3*	*20.6–22.1*
Macroplacoid 2	*11.8 – 13.4*	*11.8 – 15.4*	*9.3 – 15.2*	*12.1 – 16.8*	*18.8*	*15.9*	*13.4 – 15.3*	*15.7–17.0*
Septulum	*3.7 – 4.4*	*7.6 – 10.2*	*3.3 – 6.5*	*4.9 – 7.5*	*4.2*	*7.8*	*7.1 – 8.1*	*4.4–5.1*
Macroplacoid row	*31.7 – 35.6*	*31.0 – 37.2*	*26.4 – 37.4*	*32.3 – 38.9*	—	*37.6*	*32.3 – 35.8*	*35.9– 44.5*
Claw 1 heights	—	—	—	—	—	—	—	—
External base	*11.3 – 13.0*	*16.1 – 20.4*	*12.6 – 20.0*	*10.3 – 14.9*	—	—	—	—
External primary branch	*21.0 – 23.5*	*23.4 – 36.5*	*34.9 – 47.4*	*33.3 – 41.5*	—	—	—	—
External secondary branch	*14.2 – 15.5*	*19.2 – 24.5*	*25.6 – 32.3*	*25.0 – 31.8*	—	—	—	—
Internal base	*10.2 – 11.8*	*13.3 – 17.7*	*7.5 – 18.2*	*8.8 – 11.9*	—	—	—	—
Internal primary branch	*17.2 – 22.6*	*19.5 – 26.7*	*24.0 – 30.8*	*27.9 – 31.7*	—	—	—	—
Internal secondary branch	*11.1 – 12.5*	*14.0 – 18.1*	*16.5 – 22.9*	*16.8 – 22.3*	—	—	—	—
Claw 2 heights	—	—	—	—	—	—	—	—
External base	*12.2 – 13.0*	*17.2 – 22.0*	*13.7 – 22.6*	*9.5 – 15.9*	—	—	—	—
External primary branch	*21.0 – 25.1*	*22.0 – 41.9*	*33.0 – 46.0*	*37.5 – 45.7*	—	—	—	—
External secondary branch	*14.9 – 16.7*	*18.7 – 26.5*	*22.0 – 32.8*	*24.5 – 31.5*	—	—	—	—
Internal base	*10.8 – 12.1*	*14.4 – 18.8*	*12.4 – 18.0*	*8.9 – 12.8*	—	—	—	—
Internal primary branch	*18.3 – 23.2*	*24.4 – 33.5*	*27.2 – 36.1*	*26.6 – 33.7*	—	—	—	—

SPECIES / CHARACTER	**Hh**	**Hc** *(166)*	**Hd** (*12*)	**He** (*12*)	**Hhe** *(167)*	**Hsep** *(168)*	**Hsey** *(169)*	**Hv** *(170)*
Internal secondary branch	*10.8 – 13.6*	*16.3 – 24.1*	*17.6 – 24.3*	*18.1 – 25.6*	—	—	—	—
Claw 3 heights	—	—	—	—	—	—	—	—
External base	*11.8 – 13.3*	*17.5 – 23.1*	*15.3 – 22.7*	*10.6 – 16.0*	—	—	—	—
External primary branch	*22.0 – 25.6*	*24.9 – 43.1*	*32.4 – 45.6*	*35.1 – 43.4*	—	—	—	—
External secondary branch	*14.1 – 15.8*	*18.7 – 28.8*	*25.3 – 32.9*	*25.5 – 32.3*	—	—	—	—
Internal base	*11.3 – 12.3*	*14.4 – 19.6*	*13.2 – 18.6*	*8.4 – 12.4*	—	—	—	—
Internal primary branch	*19.4 – 23.6*	*24.7 – 35.5*	*28.0 – 35.4*	*24.5 – 32.1*	—	—	—	—
Internal secondary branch	*12.3 – 13.8*	*15.8 – 23.5*	*19.3 – 26.8*	*19.8 – 25.6*	—	—	—	—
Claw 4 heights	—	—	—	—	—	—	—	—
Anterior base	*11.5 – 12.7*	*13.9 – 22.4*	*13.4 – 20.2*	*8.6 – 13.5*	—	—	—	—
Anterior primary branch	*21.0 – 23.6*	*22.4 – 30.7*	*27.6 – 35.2*	*30.4 – 37.2*	—	—	—	—
Anterior secondary branch	*14.5 – 15.3*	*14.4 – 25.2*	*20.3 – 26.7*	*20.0 – 26.0*	—	—	—	—
Posterior base	*13.5 – 14.6*	*15.3 – 22.7*	*15.6 – 26.0*	*12.2 – 17.7*	—	—	—	—
Posterior primary branch	*30.5 – 34.0*	*30.1 – 47.8*	*40.9 – 56.3*	*45.0 – 54.7*	—	—	—	—
Posterior secondary branch	*15.9 – 17.7*	*20.6 – 28.6*	*26.4 – 34.0*	*27.1 – 35.1*	—	—	—	—
Cuticular bars at base of claw IV	Between	Between	Between	Between	Between	Between	Between	Between
Cuticular bars at base of claw I–III	Absent	Inner	Absent	Absent	Inner	Between Inner	Absent	Absent

Table S3. Sequences of four markers used for genotyping. The sequences for all four DNA markers were of a very good quality. All markers were represented by a single haplotype.

Marker	GenBank accession number	Length (bp)
18S rRNA	OR557238	1730
28S rRNA	OR557239	788
ITS-2	OR557240	447
COI	OR554247	633

Table S4. List of GenBank accession numbers for sequences used for molecular analyses.

Subfamily	Species	18S rRNA	28S rRNA	COI	ITS–2	Analysis
Diphasconinae	*Diphascon greveni* AQ.149	OR693184	OR693199	–	–	Phylogeny
	Diphascon pingue ES	FJ435736	FJ435776	FJ435793	–	Phylogeny
	Diphascon cf. pingue RU	OQ351320	OQ357549	–	–	Phylogeny
	Kararehius gregorii NZ	OP191647	OP191639	OP208046	OP191671	Phylogeny
	Kopakaius sp. NZ	OP191642	OP191651	OP208063	OP191662	Phylogeny
Hypsibiinae	*Cryobiotus klebelsbergi* AT	KT901828	KT901829	KT901833	–	Phylogeny
	Hypsibius convergens ES	FJ435726	FJ435771	FJ435798	–	Phylogeny, p–distances Species delimitation
	Hypsibius dujardini FR.055	MG777532	MG777533	MG818723	MG777531	Phylogeny, p–distances Species delimitation
	Hypsibius exemplaris GB.003	MG800327	MG800337	MG818724	MG800336	Phylogeny, p–distances Species delimitation
	Hypsibius repentinus SE	MN927183	MW549063	MW549048	MW549061	Phylogeny, p–distances Species delimitation
	Hypsibius sp	EU266939		EF632522		Species delimitation
	Hypsibius sp. DNA–DT–39	MN927184	MW549064	MW549049	MW549062	Species delimitation
	Hypsibius cf. *exemplaris* 2.2 KZ–2020			MW010374		Species delimitation
	Hypsibius cf. *exemplaris* 2.1 KZ–2020			MW010373		Species delimitation
Itaquasconinae	*Adropion scoticum* GB.054	MT126752	MT126770	MT107465	OR711205	Phylogeny
	Adropion sp. PL	MT126748	MT126766	–	OR711207	Phylogeny
	Adropion sp. NO	MT126749	MT126767	MT107462	OR711208	Phylogeny
	Adropion sp. TW.008	OR693186	OR693201	OR689304	–	Phylogeny
	Arctodiphascon tenue NO	OQ351311	OQ357540	OQ352269	OQ357877	Phylogeny
	Astatumen bartosi FR.001	MT126754	MT126772	MT107467	OR711209	Phylogeny
	Astatumen sp. HU.002	MT126755	MT126773	MT107468	OR711210	Phylogeny
	Astatumen sp. PL.120	MT126756	MT126774	MT107469	–	Phylogeny
	Astatumen sp. RU	OQ351318	OQ357547	–	–	Phylogeny
	Astatumen sp. GB.059	MT126757	MT126775	MT107470	OR711211	Phylogeny
	Astatumen sp. ES	FJ435733	FJ435775	FJ435792	–	Phylogeny
	Astatumen sp. TW.009	OR693187	OR693202	OR689305	OR711212	Phylogeny

Subfamily	Species	18S rRNA	28S rRNA	COI	ITS–2	Analysis
	Guidettion prorsirostre GB.062	MT126751	MT126769	MT107464	OR711214	Phylogeny
	Guidettion sp. RU	OQ351310	OQ357539	–	–	Phylogeny
	Insulobius orientalis ID.842	MT126764	MT126783	–	–	Phylogeny
	Itaquascon serratulum UG.004	MT126759	MT126778	MT107473	OR711215	Phylogeny
	Mesocrista revelata PL.001	KU528627	KU528628	KU495935	KU528629	Phylogeny
	Mesocrista spitzbergensis NO.021	KX347532	KX347533	KX347535	KX347534	Phylogeny
	Mesocrista sp. TW.008	OR693188	OR693203	OR689306	OR711216	Phylogeny
	Platicrista angustata NO.018	MT126762	MT126781	MT107476	OR711219	Phylogeny
	Platicrista borneensis MY.100	OR693191	OR693206	OR689309	–	Phylogeny
	Platicrista carpathica PL.088	MT126760	MT126779	MT107474	OR711220	Phylogeny
	Platicrista horribilis ME.008	MT126763	MT126782	MT107477	OR711221	Phylogeny
	Platicrista nivea TW.006	OR693192	OR693207	OR689310	–	Phylogeny
	Platicrista sp. FR.001	MT126761	MT126780	MT107475	OR711222	Phylogeny
	Platicrista sp. PE.001	OR693193	OR693208	OR689311	OR711223	Phylogeny
	Platicrista sp. RU	OQ351317	OQ357546	–	–	Phylogeny
	Raribius minutissimus GB.059	MT126758	MT126777	MT107472	OR711224	Phylogeny
Pilatobiinae	*Notahypsibius pallidoides* RU	MK973069	MK967963	MN919385	MN927181	Phylogeny
	Pilatobius cf. bullatus RU	OM304862	OM304869	OP013277	–	Phylogeny
	Pilatobius glacialis GL	MW012733	MW012744	MW009692	–	Phylogeny
	Pilatobius islandicus IS	MH682258	MH682257	MH734939	–	Phylogeny
	Pilatobius nuominensis CN	MT330115	MT330116	MT328915	–	Phylogeny
	Pilatobius oculatus GB.004	OR693194	OR693209	OR689312	OR711225	Phylogeny
	Pilatobius recamieri NO.022	KX347526	KX347527	KX347529	KX347528	Phylogeny
(Outgroup)	*Ramazzottius varieornatus*	AP013352	AP013352	MG432813	MG432816	Phylogeny

Table S5. Pairwise p-distances (%) of the marker sequence between each pair of 5 species in the genus *Hypsibius*.

Species 1	Species 2	COI	ITS-2
Hypsibius henanensis **sp. nov.**	*Hypsibius convergens* ES	17.9	–
Hypsibius henanensis **sp. nov.**	*Hypsibius dujardini* FR.055	6.6	1.9
Hypsibius henanensis **sp. nov.**	*Hypsibius exemplaris* GB.003	21.5	13.0
Hypsibius henanensis **sp. nov.**	*Hypsibius repentinus* SE	23.7	12.0
Hypsibius convergens ES	*Hypsibius dujardini* FR.055	17.6	–
Hypsibius convergens ES	*Hypsibius exemplaris* GB.003	25.1	–
Hypsibius convergens ES	*Hypsibius repentinus* SE	23.3	–
Hypsibius dujardini FR.055	*Hypsibius exemplaris* GB.003	23.1	14.0
Hypsibius dujardini FR.055	*Hypsibius repentinus* SE	23.5	12.8
Hypsibius exemplaris GB.003	*Hypsibius repentinus* SE	21.5	3.3

Table S6. Comparison with published genome assembly of tardigrades. The data of the other tardigrades are from the reference. BUSCO, Benchmarking Universal Single-Copy Orthologs. *BUSCO re-analysis was based on eukaryote lineage gene sets (eukaryota_odb10).

	R. varieornatus **(Rv1.1) (*8*)**	***H. exemplaris*** **(*9*, *13*)**	***P. metropolitanus*** ***(11)***	***E. testudo*** ***(10)***	***H. henanensis*** **sp. nov. (this study)**
Genome Size (Mb)	55.83	102.01	170.48	153.72	112.60
Number of scaffolds	199	982	684	30095	14
Longest scaffold length (Mb)	9.33	24.85	4.48	0.041	19.91
N50 contig length (Mb)	0.13	0.05	1.03	0.006	4.60
N50 scaffold length (Mb)	4.74	18.94	1.03	0.007	19.07
GC proportion (%)	47.51	45.46	43.46	46.26	40.65
Gap proportion (%)	0.75	2.06	0.0000639	NA	0.004
Repeat element content (%)	18.12	26.03	29.75	NA	34.16
BUSCO complete (%)*	83.92	83.92	83.53	82.35	83.92
BUSCO partial (%)*	90.98	91.76	90.59	89.02	90.98

Table S7. Summary of upregulated genes in 75 well-supported HGT genes.

Gene ID	Gene name/description	RNA 200_Up	RNA 2000_Up	Protein 200_Up	Protein 2000_Up
H.Henanensis.Chr4.1382	DODA1	√	√		√
H.Henanensis.Chr4.2062	Hypothetical protein BOTBODRAFT_59412			√	√
H.Henanensis.Chr5.358	BryA			√	√
H.Henanensis.Chr2.1194	Hypothetical protein PLEOSDRAFT_1113427		√		
H.Henanensis.Chr2.682	DUF2807 domain-containing protein		√		
H.Henanensis.Chr3.1327	MscL		√		
H.Henanensis.Chr2.2189	MPPED1		√		
H.Henanensis.Chr2.169	AzoB		√		
H.Henanensis.Chr4.1911	Gated mechanosensitive channel		√		
H.Henanensis.Chr4.155	Hypothetical protein Barrevirus9_4		√		
H.Henanensis.Chr6.1561	Hypothetical protein mv_R860			√	
H.Henanensis.Chr4.1968	TauD				√
H.Henanensis.Chr2.2531	KatE				√

Table S8. The *de novo* assembled transcriptome or EST sequence and the publication and database information.

Class	Order	Family	Genus and species	Transcriptome type	Publication	Latest accessible version
Eutardigrada	Parachela	Hypsibiidae	*Hypsibius exemplaris*	De novo assembled transcriptome	(*171*)	TSA: GBZR01000001:GBZR01012734
			Hypsibius exemplaris	De novo assembled transcriptome	(*18*)	TSA: GFGW01000001:GFGW01030638
		Macrobiotidae	*Mesobiotus philippinicus*	De novo assembled transcriptome	(*172*)	https://doi.org/10.7910/DVN/CFNUGF
			Paramacrobiotus richtersi	De novo assembled transcriptome	(*18*)	TSA: GFGY01000001:GFGY01025776
		Richtersiusidae	*Richtersius* aff. *coronifer* (*Richtersius.* cf. *coronifer*)	De novo assembled transcriptome	(*14*)	https://doi.org/10.17894/ucph.9d3a898c-37bb-4cd1-909f-e7fcb07e58d9
			Richtersius coronifer	De novo assembled transcriptome	(*162*)	https://doi.org/10.6084/m9.figshare.8797184.
		Ramazzottiidae	*Ramazzottius varieornatus*	De novo assembled transcriptome	(*173*)	ftp://ftp.ebi.ac.uk/pub/databases/ena/tsa/public/hbx/HBXH01.fasta.gz
	Apochela	Milnesiidae	*Milnesium inceptum* (*Milnesium tardigradum*)	De novo assembled transcriptome	(*18*)	TSA: GFGZ01000001:GFGZ01038811
			Milnesium inceptum (*Milnesium tardigradum*)	EST	(*15*)	GenBank accession numbers: https://static-content.springer.com/esm/art%3A10.1186%2F1471-2164-11-168/MediaObjects/12864_2009_2762_MOESM1_ESM.XLS
Heterotardigrada	Echiniscoidea	Echiniscidae	*Echiniscus testudo*	EST	(*174*)	TSA: GDAL01000001:GDAL01006146

				De novo assembled transcriptome	(*172*)	https://doi.org/10.7910/DVN/CFNUGF
		Echiniscoididae	*Echiniscoides sigismundi*	De novo assembled transcriptome	(*14*)	https://doi.org/10.17894/ucph.9d3a898c-37bb-4cd1-909f-e7fcb07e58d9

Note: *Richtersius* aff. *coronifer* was previously misidentified as *Richtersius* cf. *coronifer (162)* and *Milnesium inceptum* was previously misidentified as *Milnesium tardigradum* (*163*).

Table S9. Summary of DOPA 4,5-dioxygenase genes.

Organism	Gene name	Gene ID	GenBank accession number	RNA_trend (200/0-2000/0)	Protein_ trend (200/0-2000/0)
Homo sapiens	/	/	/	/	/
Mus musculus	/	/	/		
Drosophila melanogaster	/	/	/		
Caenorhabditis elegans	/	/	/		
Hypsibius henanensis **sp. nov.**	*DODA1*	H.Henanensis.Chr4.1382	/	Up-Up	NA-Up
	DODA2	H.Henanensis.Chr4.1376	/	No_change-No_change	NA
	DODA3	H.Henanensis.Chr4.1380	/	No_change-No_change	NA
	DODA4	H.Henanensis.Chr4.1389	/	No_change-No_change	NA
	DODA5	H.Henanensis.Chr4.493	/	No_change-No_change	Up-Up
Hypsibius exemplaris	*DODA1*	gene-BV898_10867	OQV14963.1	/	/
	DODA2	gene-BV898_10868	OQV14964.1		
	DODA3	gene-BV898_10869	OQV14965.1		
	DODA4	gene-BV898_10855	OQV14951.1		
	DODA5	gene-BV898_19903	OWA55519.1		
	DODA6	gene-BV898_09493	OQV16348.1		

Table S10. Summary of tyrosine hydroxylase/tyrosine 3-monooxygenase genes.

Organism	Gene name	Gene ID	UniProt accession number	RNA_trend (200/0-2000/0)	Protein_ trend (200/0-2000/0)
Homo sapiens	*TH/TYH*	7054	P07101	/	/
Mus musculus	*Th*	21823	P24529		
Drosophila melanogaster	*Ple/TH*	38746	P18459		
Caenorhabditis elegans	*cat-2*	173411	P90986		
Hypsibius henanensis **sp. nov.**	*TH1*	H.Henanensis.Chr5.1336	/	No_change-No_change	NA-NA
	TH2	H.Henanensis.Chr6.391	/	No_change-No_change	NA-NA
Hypsibius exemplaris	*TH*	BV898_06636	A0A1W0WW39	/	/

Table S11. MRM detection methods of betalamic acid and 10 betalains in the extracts of HeLa cells.

	Name	Chemical formula	Parent Ion	MRM transition	Declusterig Potential (volts)	Entrance Potential (volts)	Collision Energy (volts)	Collision Cell Exit Potential (volts)
1	Betalamic acid	$C_9H_9NO_5$	$[M+H]^+$	212.0 > 166.1, 212.0 > 148.1	100, 100	10, 10	15, 22	15, 15
2	Dopaxanthin	$C_{18}H_{18}N_2O_8$	$[M+H]^+$	391.0 > 345.2, 391.0 > 301.1	100, 100	10, 10	35, 33	15, 15
3	Threonine-betaxanthin	$C_{13}H_{16}N_2O_7$	$[M+H]^+$	313.0 > 118.1, 313.0 > 119.1, 313.0 > 120.1, 313.0 > 179.2	100, 100, 100, 100	10, 10, 10, 10	36, 36, 34, 24	15, 15, 15, 15
4	Phenylalanine-betaxanthin	$C_{18}H_{18}N_2O_6$	$[M+H]^+$	359.0 > 313.2, 359.0 > 223.2	100, 100	10, 10	27, 33	15, 15
5	Valine-betaxanthin	$C_{14}H_{18}N_2O_6$	$[M+H]^+$	311.0 > 265.1, 311.0 > 219.2	100, 100	10, 10	26, 32	15, 15
6	Arginine-betaxanthin	$C_{15}H_{21}N_5O_6$	$[M+H]^+$	368.0 > 324.2, 368.0 > 236.3	100, 100	10, 10	12, 17	15, 15
7	Proline-betaxanthin	$C_{14}H_{16}N_2O_6$	$[M+H]^+$	309.0 > 263.1, 309.0 > 217.2	100, 100	10, 10	28, 38	15, 15
8	Glycine-betaxanthin	$C_{11}H_{12}N_2O_6$	$[M+H]^+$	269.0 > 223.2, 269.0 > 177.2	100, 100	10, 10	22, 30	15, 15
9	Gamma-aminobutyric acid-betaxanthin	$C_{13}H_{16}N_2O_6$	$[M+H]^+$	297.0 > 251.2, 297.0 > 187.2	100, 100	10, 10	30, 30	15, 15
10	Phenethylamine-betaxanthin	$C_{17}H_{18}N_2O_4$	$[M+H]^+$	315.0 > 271.2, 315.0 > 105.1	100, 100	10, 10	19, 33	15, 15
11	Lysine-betaxanthin	$C_{15}H_{21}N_3O_6$	$[M+H]^+$	340.0 > 106.1, 340.0 > 296.3, 340.0 > 252.3	100, 100, 100	10, 10, 10	31, 15, 17	15, 15, 15

Table S12. MRM transitions for 11 compounds used in the extracts of *H. henanensis* sp. nov., at least two fragments were monitored for each compound.

	Compounds	Q1 Mass (Da)	Q3 Mass (Da)	Entrance Potential (volts)	Collision Energy (volts)	Collision Cell Exit Potential (volts)
1	Phenylalanine-betaxanthin	359.0	313.1	10	29	10
2	Phenylalanine-betaxanthin	359.0	223.0	10	35	10
3	Dopaxanthin	391.0	255.0	10	35	10
4	Dopaxanthin-	391.0	345.0	10	29	10
5	Betalamic acid	212.0	148.0	10	21	10
6	Betalamic acid	212.0	65.0	10	47	10
7	Threonine-betaxanthin	313.0	179.1	10	34	10
8	Threonine-betaxanthin	313.0	118.0	10	26	10
9	Threonine-betaxanthin	313.0	133.1	10	38	10
10	Threonine-betaxanthin	313.0	106.0	10	36	10
11	Threonine-betaxanthin	313.0	94.0	10	30	10
12	Valine-betaxanthin	311.0	219.2	10	35	10
13	Valine-betaxanthin	311.0	174.8	10	32	10
14	Proline-betaxanthin	309.0	263.2	10	32	10
15	Proline-betaxanthin	309.0	217.2	10	36	10
16	Arginine-betaxanthin	368.0	324.2	10	12	10
17	Arginine-betaxanthin	368.0	236.3	10	17	10
18	Phenethylamine-betaxanthin	315.0	271.2	10	19	10
19	Phenethylamine-betaxanthin	315.0	105.1	10	33	10
20	Glycine-betaxanthin	269.0	223.2	10	30	10
21	Glycine-betaxanthin	269.0	177.2	10	31	10
22	Lysine-betaxanthin	340.0	106.1	10	31	10
23	Lysine-betaxanthin	340.0	296.3	10	15	10
24	Lysine-betaxanthin	340.0	252.3	10	17	10
25	Gamma-aminobutyric acid-betaxanthin	297.0	187.2	10	30	10
26	Gamma-aminobutyric acid-betaxanthin	297.0	251.2	10	30	10

Table S13. Comparison of ^{1}H NMR data of proline-betaxanthin in our study and published data.

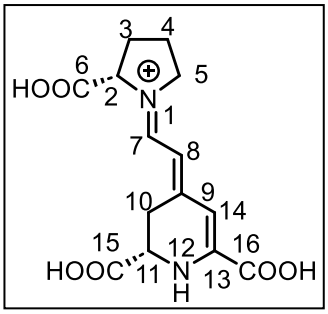

Proline-betaxanthin

Atom	Reference (*175*) δ(H)	Reference (*176*) δ(H)	Our study δ(H)
2	4.63 (dd, J = 3.5, 8.4)	4.62 (dd, J = 2.9. 9.7)	4.65-4.59 (m)
3a	2.32	2.35	2.38-2.27 (m)
3b	2.19	2.18	2.14-2.07(m)
4a	2.03-2.10	2.03 (m)	2.05-1.90 (m)
4b	2	2.03 (m)	2.05-1.90 (m)
5a	3.62-3.71	3.60-3.69	3.69 (td, J = 13.2, 12.7, 6.5)
5b	3.62-3.71	3.60-3.69	3.69 (td, J = 13.2, 12.7, 6.5)
7	8.19 (d, J = 12.2)	8.29 (d, J = 12.1)	8.31 (d, J = 12.3)
8	6.02 (d, J = 12.2)	6.02 (d, J = 12.1)	6.02 (d, J = 12.2)
10a	3.28	3.27	3.09 (dq, J = 16.7, 7.6 Hz)
10b	3.04	3.00	3.09 (dq, J = 16.7, 7.6 Hz)
11	4.43 (t, J = 6.5)	4.43 (t, J = 6.3)	4.43 (t, J = 6.6)
14	6.15 (s)	6.10 (s)	6.14 (d, J = 17.1)

Table S14. Summary of *BCS1* in *H. henanensis* sp. nov.

Gene name	Gene ID	Length (AA)	Domains position		Transmembrane region (AA)
			BCS1_N (AA)	AAA (AA)	
BCS1a	H.Henanensis.Chr1.760	494	79-250	281-428	22-44
BCS1b	H.Henanensis.Chr1.757	286	1-42	73-220	/
BCS1c	H.Henanensis.Chr1.761	492	79-248	279-426	22-44
BCS1d	H.Henanensis.Chr3.1631	483	76-238	269-417	20-41
BCS1e	H.Henanensis.Chr1.158	480	63-232	263-408	15-34
BCS1f	H.Henanensis.Chr3.1437	491	78-244	275-425	13-35
BCS1g	H.Henanensis.Chr1.161	501	73-243	274-409	22-44

Table S15. List of important primers and siRNA sequences used in this study.

Plamsid Names	Plasmid Vector	Primers Sequences	
		Forward (5'-3')	Reverse (5'-3')
GST-HhDODA	pGEX-6p-1	TCCAGGGGCCCCTGGACATGCCGAGCGACACAC	TCGAGTCGACCCGGGTTAGAGGCGAGATAAATCTAGAGGAAGTTG
His-HhDODA	pET28a	GCCGCGCGGCAGCCAAATGCCGAGCGACACACAA	CGGAGCTCGAATTCGTTAGAGGCGAGATAAATCTAGAGGAAGTTGTCT
His-GdDODA	pET28a	GCCGCGCGGCAGCCAAATGACCCCCGTGCCCG	CGGAGCTCGAATTCGTCAGATTGGGGTGGCGCCG
pLVX-HhDODA1-WT-FLAG	pLVX-IRES-puro	TAGAGGATCTATTTCCGGTGGCCACCATGCCGAGCGACACAC	TCGTCATCCTTGTAATCGGAGAGGCGAGATAAATCTAGAGGAAGT
HhDODA1-H16A	pET28a	GTAGACATGTCCGGCAAAACCGCGAGGACGTTCC	GGAACGTCCTCGCGGTTTTGCCGGACATGTCTAC
HhDODA1-H18A	pET28a	GCGTCGAAGTAGACAGCTCCGTGAAAACCGCGAG	CTCGCGGTTTTCACGGAGCTGTCTACTTCGACGC
HhDODA1-H67A	pET28a	ACATTCCAGTGGGAGCTGGACCGATTGGGTAGGG	CCCTACCCAATCGGTCCAGCTCCCACTGGAATGT
HhDODA1-H100A	pET28a	GATCATTTCCAGATAGAACAGCGACCAGAACAGAGAGATCAC	GTGATCTCTCTGTTCTGGTCGCTGTTCTATCTGGAAATGATC
HhDODA1-D106A	pET28a	GGGTGTGGTCGTACAGAGCATTTCCAGATAGAACA	TGTTCTATCTGGAAATGCTCTGTACGACCACACCC
HhDODA1-H110A	pET28a	CAAAGCGCTCCTTGGGTGGCGTCGTACAGATCATTTCC	GGAAATGATCTGTACGACGCCACCCAAGGAGCGCTTTG
TRID1-WT-pLVX	pLVX-IRES-puro	TAGAGGATCTATTTCCGGTGATGGACGAGCTCCGG	TCGTCATCCTTGTAATCGCCATGGCCCATTTGGAGC
TRID1-ΔPrLD-pLVX	pLVX-IRES-puro	TAGAGGATCTATTTCCGGTGGCCACCATGGACGAGCTCCGG	TCGTCATCCTTGTAATCGAAATGGCCCATTTGGAGC
GFP(A206K)	/	CCTGAGCACCCAGTCCAAGCTGAGCAAAGACCCCA	TGGGGTCTTTGCTCAGCTTGGACTGGGTGCTCAGG
TRID1-WT-GFP(A206K)-GST	pGEX-6p-1	TCCAGGGGCCCCTGGACATGGACGAGCTCCGGC (TRID1)	CTCACCATATGGCCCATTTGGAGCAAG (TRID1)
		TGGGCCATATGGTGAGCAAGGGCG (GFP)	TCGAGTCGACCCGGGTTACTTGTACAGCTCGTCCATGCC (GFP)
TRID1-ΔPrLD-GFP(A206K)-GST	pGEX-6p-1	TCCAGGGGCCCCTGGACATGGACGAGCTCCGGC (TRID1 N-terminal)	ACTGCAGGACGCGTCACCATCTTC (TRID1 N-terminal)
		GACGCGTCCTGCAGTGGTGACG (TRID1 C-terminal + GFP)	TCGAGTCGACCCGGGTTACTTGTACAGCTCGTCCATG (TRID1 C-terminal + GFP)
TRID1-WT-GFP	pEGFP-N1	CGAGCTCAAGCTTCGAAGCCACCATGGACGAGCTCCGG	TGGTGGCGACCGGTGGATGGCCCATTTGGAGC
TRID1-ΔPrLD-GFP	pEGFP-N1	CGAGCTCAAGCTTCGAAGCCACCATGGACGAGCTCCGG	TGGTGGCGACCGGTGGATGGCCCATTTGGAGC
NDUFB8-pLVX	pLVX-IRES-puro	TAGAGGATCTATTTCCGGTGGCCACCATGTCGCTTCATTTTTTCAACAAG	TCGTCATCCTTGTAATCGCCGAGATAGCGAACTTTAGTTTCCG
qPCR Primer Names		**Forward (5'-3')**	**Reverse (5'-3')**
DODA1		AATCGGTCCACATCCCACTG	CCTTGGGTGTGGTCGTACAG
TRID1		AAGTGTCGTTGCCGATGAGT	AAGGAACGGAAAGTCGACGG

β-Tubulin1	CGTCGGAGTGGTCAGTTTCA	GACACTGTCGGTTCACCAGT
siRNA Names	**Sense**	**Antisence**
siDODA1	GAAAUGAUCUGUACGACCA (dT)(dT)	UGGUCGUACAGAUCAUUUC (dT)(dT)
siTRID1	CGAUUUACGCGCGAAUGAA (dT)(dT)	UUCAUUCGCGCGUAAAUCG (dT)(dT)

Table S16. Key materials for the research.

Materials	Source	Identifier
Antibody		
Mouse Monoclonal anti-DDDDK antibody	MBL	Cat#M185-3; RRID: AB_10950447
Mouse Monoclonal anti-GAPDH antibody	Santa Cruz Biotechnology	Cat#sc-365062; RRID: AB_10847862
Mouse Monoclonal anti-Tubulin antibody	Proteintech	Cat#66031-1-Ig; RRID: AB_11042766
Rabbit Monoclonal anti-γH2AX antibody	Cell Signaling Technology	Cat#9718P; RRID: AB_2118009
Mouse Monoclonal anti-tyrosine hydroxylase antibody	Santa Cruz Biotechnology	Cat#sc-25269; RRID: AB_628422
Peroxidase-AffiniPure goat anti-rabbit IgG antibody	Peroxidase-AffiniPure goat anti-mouse IgG	Cat#111-035-003; RRID: AB_2313567
Peroxidase-AffiniPure goat anti-mouse IgG antibody	Peroxidase-AffiniPure goat anti-mouse IgG	Cat#115-035-003; RRID: AB_10015289
Goat anti-mouse Alexa Fluor 488 antibody	Invitrogen	Cat#A-11001; RRID: AB_2534069
Goat anti-rabbit Alexa Fluor 594 antibody	Invitrogen	Cat#A-11037; RRID: AB_2534095
XRCC5/Ku80 Polyclonal antibody	Proteintech	Cat#16389-1-AP; RRID: AB_2257509
MRE11 Polyclonal antibody	Proteintech	Cat#10744-1-AP; RRID: AB_2145118
RNF168 Polyclonal antibody	Proteintech	Cat#21393-1-AP; RRID: AB_10733883
EXO1 Polyclonal antibody	Proteintech	Cat#16253-1-AP; RRID: AB_2278140
PARP1 Polyclonal antibody	Proteintech	Cat#13371-1-AP; RRID: AB_2160459
NBN/NBS1 Polyclonal antibody	Proteintech	Cat#55025-1-AP; RRID: AB_10858928
53BP1 Antibody	Novus	Cat#NB100-305; RRID: AB_10001695
Rad50 antibody	GeneTex	Cat#GTX70228; RRID: AB_372854
Anti-PAR Polymer Monoclonal Antibody	R&D Systems	Cat#4335-MC-100; RRID: AB_2572318
Anti-NDUFS1 rabbit polyclonal antibody	Sangon Biotech	Cat#D222747-0100; RRID: AB_3105851
Anti-UQCRFS1(Rieske) mouse monoclonal antibody	Sangon Biotech	Cat#D197250-0100; RRID: AB_3105852
Anti-SDHA rabbit polyclonal antibody	Sangon Biotech	Cat#D223104-0100; RRID: AB_3105853
Anti-COX4I1 mouse monoclonal antibody	Sangon Biotech	Cat#D191070-0100; RRID: AB_3105855
UQCRC2 Polyclonal antibody	Proteintech	Cat#14742-1-AP; RRID: AB_2241442
Mouse anti-β-actin	Santa Cruz	Cat# sc-1616; RRID: AB_630836
Cell lines		
HEK293T	ATCC	Cat#CRL-3216; RRID: CVCL_0063
HeLa	ATCC	Cat#CCL-2; RRID: CVCL_0030
U2OS	ATCC	Cat#HTB-96; RRID: CVCL_0042
Chemicals		
TRIzol reagent	Invitrogen	Cat#15596026

TsingZol Total RNA Extractlon Reagent	TSINGKE	Cat#TSP401
Golden Star T6 Super PCR Mix	TSINGKE	Cat#TSE101
L-DOPA	Solarbio	Cat#ID0360
Levodopa	J&K scientific	Cat#115511
L-DOPA-ring-D3, L-DOPA-2,5,6-d3	MREDA	Cat#M100103
Ascorbic acid	Solarbio	Cat#S9440
Coomassie brilliant blue R-250	Solarbio	Cat#C8430
4,6-diamidino-2-phenylindole dihydrochloride (DAPI)	Solarbio	Cat#C0065
Isopropyl-1-thio-β-D-galactopyranoside (IPTG)	Solarbio	Cat#I1020
Cytochrome c	Solarbio	Cat#C8130
Penicillin-Streptomycin	CellWorld	Cat#C0160-611
SYBR Gold Nucleic Acid Gel Stain	Invitrogen	Cat#S11494
Protease inhibitor	Roche	Cat#11697498001
The SuperSignal West Pico PLUS chemiluminescent Detection Reagent	Thermo Fisher Scientific	Cat#34577
His-tag purification resin	Beyotime	Cat#P2210
GST-tag purification resin	Beyotime	Cat#P2251
anti-FLAG(DYKDDDDK)-G1 Affinity Resin	Genscript	Cat#L00432-10
FLAG peptide	Genscript	Cat#RP10586CN
PreScission protease	Beyotime	Cat#P2302
Puromycin	Invivogen	Cat#ant-pr-1
Hoechst 33342	Solarbio	Cat#IH0070
1,6-hexanediol	Macklin	Cat#629-11-8
4-Aminobutanoic acid	J&K scientific	Cat#207891
L-Ascorbic acid	J&K scientific	Cat#231406
L-Ascorbic Acid Sodium Salt	Solarbio	Cat#S9440
L-Valine	Solarbio	Cat#V0010
L-Arginine	Solarbio	Cat#A0013
L-Lysine	Solarbio	Cat#L0010
L-Threonine	Solarbio	Cat#T0012
L-Phenylalanine	Solarbio	Cat#P0010
L-Proline	Solarbio	Cat#P0011
L-Glycine	Solarbio	Cat#YZ-1295800
2-phenylethylamine	Adamas-beta	Cat#73421G
Rotenone	Sigma	Cat#45656
Oligomycin	Sigma	Cat#495455
MitoTEMPO	Sigma	Cat#SML0737
Antimycin A	Biorab	Cat#QN0022-JOB
2,2,2-tribromoethanol	Sigma	Cat#T48402-5G
D-Sorbitol	Sigma	Cat#S1876
EGTA	Sigma	Cat#E4378
BSA	AMRESCO	Cat#0332

Digitonin	Sigma	Cat#D141
Regular Agarose G-10	Biowest	Cat#BY-RO100
Critical Commercial Assays		
Quick-gDNA MicroPrep kit	Zymo Research	Cat#D3020
RNA MicroPrepwere kit	Zymo Research	Cat#R2060
RNA MicroPrepwere kit	Zymo Research	Cat#R2062
Taq Pro Universal SYBR qPCR Master Mix	Vazyme	Cat#Q712-02
ReverTra Ace qPCR RT Master Mix	TOYOBO	Cat#FSQ-201
MagAttract HMW DNA Kit	QIAGEN	Cat#67563
First Strand cDNA Synthesis Kit	TOYOBO	Cat#FSK-101
BCA protein assay kit	Solarbio	Cat#
Gel filtration calibration kit HMW (high molecular weight)	Healthcare	Cat#28-4038-42
Reactive Oxygen Species Assay Kit	Beyotime	Cat#S0033S
DNA Content Quantitation Assay	Solarbio	Cat#CA1510
Mitochondria Isolation Kit for Cultured Cells	Thermo Fisher Scientific	Cat#89874
CheKine™ Micro Mitochondrial complexI Activity Assay Kit	Abbkine	Cat#KTB1850
CheKine™ Micro Mitochondrial complex III Activity Assay Kit	Abbkine	Cat#KTB1870
CM-H2DCFDA	Thermo Fisher Scientific	Cat#C6827
Cell Titer-Glo® 2.0 Assay	Promega	Cat#G7571
MitoSOX™ Red Mitochondrial Superoxide Indicators	Thermo Fisher Scientific	Cat#M36008
Other		
The green alga *Chlorococcum humicola*	Freshwater Algae Culture Collection at the Institute of Hydrobiology (http://algae.ihb.ac.cn/)	Cat#FACHB-21
Ultra centrifugal filter unit (10 K MWCO)	Merck Millipore	Cat#UFC5010
Glass Bottom cell Culture Dish	NEST	Cat#801002

Movie S1. *H. henanensis* sp. nov. in the culturing system.

H. henanensis **sp. nov.** is terrestrial eutardigrade. They have flexible bodies. The culturing system for *H. henanensis* **sp. nov.** has been successfully established in 2020 in our laboratory. *H. henanensis* **sp. nov.** is herbivorous, fed on green alga *Chlorococcum humicola.*

Movie S2. Ingesting green alga of *H. henanensis* sp. nov.

An active adult of *H. henanensis* **sp. nov.** is shown. Its stylets serve as a miniature needle and straw to puncture the cell and suck the cellular content from it. The pharynx serves as a pump to draw fluids in through the stylets. Note the food (green alga) within the midgut. A pair of eyespots are embedded in the dorsolateral lobes of the brain.

Movie S3. Molting of *H. henanensis* sp. nov.

Like its relatives in the Arthropoda, the tardigrade requires a series of molts as they grow. Body length increases at every molting until maximum size is reached. During molting, the old cuticle, claws, and the cuticle lining internal organs, i.e., the sclerified parts of the buccal-pharyngeal apparatus and rectum, are shed, so the tardigrade cannot feed during molting. The salivary glands are responsible for production of new pharynx elliptical. The molt also includes the cuticular part of the legs, which are reformed by so-called claw glands. This molting process usually requires 5~10 days. Sexual maturity is reached with the second or third molting.

Movie S4. Laying eggs during molting of *H. henanensis* sp. nov.

The *H. henanensis* **sp. nov.** in our laboratory are parthenogenetic. The eggs were laid through the female reproductive pores in exuvia during molting. They can be laid singly or numerously (generally producing 4-6 eggs per clutch). The eggshells are smooth. The time (minute: second) was shown.

Movie S5. *H. henanensis* sp. nov. emerging from its exuvia during molting.

After a period of time (3-7 days) after laying eggs, *H. henanensis* **sp. nov.** emerging from its exuvia, with the regenerated stylet (produced by salivary gland) puncturing the exuvia. The eggs were deposited in exuvia for further development.

Movie S6. 3D reconstruction of immunofluorescence images showing the localization of TRID1 droplets and γH2AX foci (Related to fig. S27F).

Analysis of γH2AX foci in HeLa cells expressing TRID1 under 2 Gy X-ray irradiation, the TRID1 droplet (green) and γH2AX foci (red) were independently distributed in the nucleus without physical contact.

Data S1. Raw morphometric data for the identification of the new species *Hypsibius henanensis* **sp. nov.**

Data S2. Genome annotation of *H. henanensis* **sp. nov.** (Related to fig. S5).

Data S3. Gene annotation of the *H. henanensis* **sp. nov.** including gene length, gene age, disorder, functional annotations and homologous protein information.

Data S4. Synteny blocks of *H. henanensis* **sp. nov.** and three other tardigrades (Related to fig. S6).

Data S5. Transcriptomic and proteomic data of *H. henanensis* **sp. nov.** (Including the results of differential analysis).

Data S6. Identification of HGT genes in *H. henanensis* **sp. nov.**

Data S7. Omics data of other species under radiation or dehydration states.

Data S8. Gene family expansion and contraction in tardigrades (Related to fig. S28).

Data S9. The known stress related genes in *H. henanensis* **sp. nov.** and their differential expression after irradiation.

Data S10. Raw data of the analysis (Related to the other figures not mentioned in data S1to S9).

References and Notes

1. R. O. Schill, Ed., *Water Bears: The Biology of Tardigrades* (Springer, 2018).

2. S. J. McInnes, A. Jørgensen, Ł. Michalczyk, 20 years of *Zootaxa*: Tardigrada (Ecdysozoa: Panarthropoda). *Zootaxa* **4979**, 23–24 (2021). doi:10.11646/zootaxa.4979.1.5 Medline

3. K. Arakawa, Examples of extreme survival: Tardigrade genomics and molecular anhydrobiology. *Annu. Rev. Anim. Biosci.* **10**, 17–37 (2022). doi:10.1146/annurev-animal-021419-083711 Medline

4. K. I. Jönsson, I. Holm, H. Tassidis, Cell biology of the tardigrades: Current knowledge and perspectives. *Results Probl. Cell Differ.* **68**, 231–249 (2019). doi:10.1007/978-3-030-23459-1_10 Medline

5. J. D. Hibshman, J. S. Clegg, B. Goldstein, Mechanisms of desiccation tolerance: Themes and variations in brine shrimp, roundworms, and tardigrades. *Front. Physiol.* **11**, 592016 (2020). doi:10.3389/fphys.2020.592016 Medline

6. K. I. Jönsson, Radiation tolerance in tardigrades: Current knowledge and potential applications in medicine. *Cancers* **11**, 1333 (2019). doi:10.3390/cancers11091333 Medline

7. T. Hashimoto, T. Kunieda, DNA protection protein, a novel mechanism of radiation tolerance: Lessons from tardigrades. *Life (Basel)* **7**, 26 (2017). doi:10.3390/life7020026 Medline

8. T. Hashimoto, D. D. Horikawa, Y. Saito, H. Kuwahara, H. Kozuka-Hata, T. Shin-I, Y. Minakuchi, K. Ohishi, A. Motoyama, T. Aizu, A. Enomoto, K. Kondo, S. Tanaka, Y. Hara, S. Koshikawa, H. Sagara, T. Miura, S. I. Yokobori, K. Miyagawa, Y. Suzuki, T. Kubo, M. Oyama, Y. Kohara, A. Fujiyama, K. Arakawa, T. Katayama, A. Toyoda, T. Kunieda, Extremotolerant tardigrade genome and improved radiotolerance of human cultured cells by tardigrade-unique protein. *Nat. Commun.* **7**, 12808 (2016). doi:10.1038/ncomms12808 Medline

9. Y. Yoshida, G. Koutsovoulos, D. R. Laetsch, L. Stevens, S. Kumar, D. D. Horikawa, K. Ishino, S. Komine, T. Kunieda, M. Tomita, M. Blaxter, K. Arakawa, Comparative genomics of the tardigrades *Hypsibius dujardini* and *Ramazzottius varieornatus*. *PLOS Biol.* **15**, e2002266 (2017). doi:10.1371/journal.pbio.2002266 Medline

10. Y. Murai, M. Yagi-Utsumi, M. Fujiwara, S. Tanaka, M. Tomita, K. Kato, K. Arakawa, Multiomics study of a heterotardigrade, *Echinisicus testudo*, suggests the possibility of convergent evolution of abundant heat-soluble proteins in Tardigrada. *BMC Genomics* **22**, 813 (2021). doi:10.1186/s12864-021-08131-x Medline

11. Y. Hara, R. Shibahara, K. Kondo, W. Abe, T. Kunieda, Parallel evolution of trehalose production machinery in anhydrobiotic animals via recurrent gene loss and horizontal transfer. *Open Biol.* **11**, 200413 (2021). doi:10.1098/rsob.200413 Medline

12. P. Gąsiorek, D. Stec, W. Morek, Ł. Michalczyk, An integrative redescription of *Hypsibius dujardini* (Doyère, 1840), the nominal taxon for Hypsibioidea (Tardigrada: Eutardigrada). *Zootaxa* **4415**, 45–75 (2018). doi:10.11646/zootaxa.4415.1.2 Medline

13. C. Hoencamp, O. Dudchenko, A. M. O. Elbatsh, S. Brahmachari, J. A. Raaijmakers, T. van Schaik, Á. Sedeño Cacciatore, V. G. Contessoto, R. G. H. P. van Heesbeen, B. van den Broek, A. N. Mhaskar, H. Teunissen, B. G. St Hilaire, D. Weisz, A. D. Omer, M. Pham,

Z. Colaric, Z. Yang, S. S. P. Rao, N. Mitra, C. Lui, W. Yao, R. Khan, L. L. Moroz, A. Kohn, J. St. Leger, A. Mena, K. Holcroft, M. C. Gambetta, F. Lim, E. Farley, N. Stein, A. Haddad, D. Chauss, A. S. Mutlu, M. C. Wang, N. D. Young, E. Hildebrandt, H. H. Cheng, C. J. Knight, T. L. U. Burnham, K. A. Hovel, A. J. Beel, P.-J. Mattei, R. D. Kornberg, W. C. Warren, G. Cary, J. L. Gómez-Skarmeta, V. Hinman, K. Lindblad-Toh, F. Di Palma, K. Maeshima, A. S. Multani, S. Pathak, L. Nel-Themaat, R. R. Behringer, P. Kaur, R. H. Medema, B. van Steensel, E. de Wit, J. N. Onuchic, M. Di Pierro, E. Lieberman Aiden, B. D. Rowland, 3D genomics across the tree of life reveals condensin II as a determinant of architecture type. *Science* **372**, 984–989 (2021). doi:10.1126/science.abe2218 Medline

14. M. Kamilari, A. Jørgensen, M. Schiøtt, N. Møbjerg, Comparative transcriptomics suggest unique molecular adaptations within tardigrade lineages. *BMC Genomics* **20**, 607 (2019). doi:10.1186/s12864-019-5912-x Medline

15. B. Mali, M. A. Grohme, F. Förster, T. Dandekar, M. Schnölzer, D. Reuter, W. Wełnicz, R. O. Schill, M. Frohme, Transcriptome survey of the anhydrobiotic tardigrade *Milnesium tardigradum* in comparison with *Hypsibius dujardini* and *Richtersius coronifer*. *BMC Genomics* **11**, 168 (2010). doi:10.1186/1471-2164-11-168 Medline

16. C. Wang, M. A. Grohme, B. Mali, R. O. Schill, M. Frohme, Towards decrypting cryptobiosis—Analyzing anhydrobiosis in the tardigrade *Milnesium tardigradum* using transcriptome sequencing. *PLOS ONE* **9**, e92663 (2014). doi:10.1371/journal.pone.0092663 Medline

17. Y. Yoshida, T. Satoh, C. Ota, S. Tanaka, D. D. Horikawa, M. Tomita, K. Kato, K. Arakawa, Time-series transcriptomic screening of factors contributing to the cross-tolerance to UV radiation and anhydrobiosis in tardigrades. *BMC Genomics* **23**, 405 (2022). doi:10.1186/s12864-022-08642-1 Medline

18. T. C. Boothby, H. Tapia, A. H. Brozena, S. Piszkiewicz, A. E. Smith, I. Giovannini, L. Rebecchi, G. J. Pielak, D. Koshland, B. Goldstein, Tardigrades use intrinsically disordered proteins to survive desiccation. *Mol. Cell* **65**, 975–984.e5 (2017). doi:10.1016/j.molcel.2017.02.018 Medline

19. C. M. Clark-Hachtel, J. D. Hibshman, T. De Buysscher, E. R. Stair, L. M. Hicks, B. Goldstein, The tardigrade *Hypsibius exemplaris* dramatically upregulates DNA repair pathway genes in response to ionizing radiation. *Curr. Biol.* **34**, 1819–1830.e6 (2024). doi:10.1016/j.cub.2024.03.019 Medline

20. Y. Yoshida, D. D. Horikawa, T. Sakashita, Y. Yokota, Y. Kobayashi, M. Tomita, K. Arakawa, RNA sequencing data for gamma radiation response in the extremotolerant tardigrade *Ramazzottius varieornatus*. *Data Brief* **36**, 107111 (2021). doi:10.1016/j.dib.2021.107111 Medline

21. M. Anoud, E. Delagoutte, Q. Helleu, A. Brion, E. Duvernois-Berthet, M. As, X. Marques, K. Lamribet, C. Senamaud-Beaufort, L. Jourdren, A. Adrait, S. Heinrich, G. Toutirais, S. Hamlaoui, G. Gropplero, I. Giovannini, L. Ponger, M. Geze, C. Blugeon, Y. Couté, R. Guidetti, L. Rebecchi, C. Giovannangeli, A. De Cian, J.-P. Concordet, Comparative transcriptomics reveal a novel tardigrade-specific DNA-binding protein induced in response to ionizing radiation. *eLife* **13**, RP92621 (2024). doi:10.7554/eLife.92621.3 Medline

22. Y. Yoshida, A. Hirayama, K. Arakawa, Transcriptome analysis of the tardigrade *Hypsibius exemplaris* exposed to the DNA-damaging agent bleomycin. *Proc. Jpn. Acad., Ser. B, Phys. Biol. Sci.* **100**, 414–428 (2024). doi:10.2183/pjab.pjab.100.023 Medline

23. C. Chavez, G. Cruz-Becerra, J. Fei, G. A. Kassavetis, J. T. Kadonaga, The tardigrade damage suppressor protein binds to nucleosomes and protects DNA from hydroxyl radicals. *eLife* **8**, e47682 (2019). doi:10.7554/eLife.47682 Medline

24. C. Ricci, G. Riolo, C. Marzocchi, J. Brunetti, A. Pini, S. Cantara, The tardigrade damage suppressor protein modulates transcription factor and DNA repair genes in human cells treated with hydroxyl radicals and UV-C. *Biology* **10**, 970 (2021). doi:10.3390/biology10100970 Medline

25. E. Shaba, C. Landi, C. Marzocchi, L. Vantaggiato, L. Bini, C. Ricci, S. Cantara, Proteomics reveals how the tardigrade damage suppressor protein teaches transfected human cells to survive UV-C stress. *Int. J. Mol. Sci.* **24**, 11463 (2023). doi:10.3390/ijms241411463 Medline

26. M. Zarubin, T. Azorskaya, O. Kuldoshina, S. Alekseev, S. Mitrofanov, E. Kravchenko, The tardigrade Dsup protein enhances radioresistance in *Drosophila melanogaster* and acts as an unspecific repressor of transcription. *iScience* **26**, 106998 (2023). doi:10.1016/j.isci.2023.106998 Medline

27. C. Del Casino, V. Conti, S. Licata, G. Cai, A. Cantore, C. Ricci, S. Cantara, Mitigation of UV-B radiation stress in tobacco pollen by expression of the tardigrade damage suppressor protein (Dsup). *Cells* **13**, 840 (2024). doi:10.3390/cells13100840 Medline

28. J. Kirke, X.-L. Jin, X.-H. Zhang, Expression of a tardigrade *Dsup* gene enhances genome protection in plants. *Mol. Biotechnol.* **62**, 563–571 (2020). doi:10.1007/s12033-020-00273-9 Medline

29. N. Kasianchuk, P. Rzymski, Ł. Kaczmarek, The biomedical potential of tardigrade proteins: A review. *Biomed. Pharmacother.* **158**, 114063 (2023). doi:10.1016/j.biopha.2022.114063 Medline

30. J. Chen *et al*., Establishment of *Hypsibius dujardini* laboratory culturing system. *Military Medical Sciences* **44**, 6 (2020).

31. S. M. Soucy, J. Huang, J. P. Gogarten, Horizontal gene transfer: Building the web of life. *Nat. Rev. Genet.* **16**, 472–482 (2015). doi:10.1038/nrg3962 Medline

32. A. Wagner, R. J. Whitaker, D. J. Krause, J.-H. Heilers, M. van Wolferen, C. van der Does, S.-V. Albers, Mechanisms of gene flow in archaea. *Nat. Rev. Microbiol.* **15**, 492–501 (2017). doi:10.1038/nrmicro.2017.41 Medline

33. B. J. Arnold, I. T. Huang, W. P. Hanage, Horizontal gene transfer and adaptive evolution in bacteria. *Nat. Rev. Microbiol.* **20**, 206–218 (2022). doi:10.1038/s41579-021-00650-4 Medline

34. J. Van Etten, D. Bhattacharya, Horizontal gene transfer in eukaryotes: Not if, but how much? *Trends Genet.* **36**, 915–925 (2020). doi:10.1016/j.tig.2020.08.006 Medline

35. F. Husnik, J. P. McCutcheon, Functional horizontal gene transfer from bacteria to eukaryotes. *Nat. Rev. Microbiol.* **16**, 67–79 (2018). doi:10.1038/nrmicro.2017.137 Medline

36. Y. Yoshida, R. W. Nowell, K. Arakawa, M. Blaxter, “Horizontal gene transfer in metazoa: Examples and methods” in *Horizontal Gene Transfer: Breaking Borders Between Living Kingdoms*, T. G. Villa, M. Viñas, Eds. (Springer, 2019), pp. 203–226.

37. P. Martínez-Rodríguez, M. A. Guerrero-Rubio, P. Henarejos-Escudero, F. García-Carmona, F. Gandía-Herrero, Health-promoting potential of betalains in vivo and their relevance as functional ingredients: A review. *Trends Food Sci. Technol.* **122**, 66–82 (2022). doi:10.1016/j.tifs.2022.02.020

38. M. G. Miguel, Betalains in some species of the amaranthaceae family: A review. *Antioxidants* **7**, 53 (2018). doi:10.3390/antiox7040053 Medline

39. F. C. Stintzing, R. Carle, Functional properties of anthocyanins and betalains in plants, food, and in human nutrition. *Trends Food Sci. Technol.* **15**, 19–38 (2004). doi:10.1016/j.tifs.2003.07.004

40. X. Lu, Y. Wang, Z. Zhang, Radioprotective activity of betalains from red beets in mice exposed to gamma irradiation. *Eur. J. Pharmacol.* **615**, 223–227 (2009). doi:10.1016/j.ejphar.2009.04.064 Medline

41. J. Cho, S. J. Bing, A. Kim, N. H. Lee, S.-H. Byeon, G.-O. Kim, Y. Jee, Beetroot (*Beta vulgaris*) rescues mice from γ-ray irradiation by accelerating hematopoiesis and curtailing immunosuppression. *Pharm. Biol.* **55**, 306–316 (2017). doi:10.1080/13880209.2016.1237976 Medline

42. G. Polturak, A. Aharoni, “La Vie en Rose”: Biosynthesis, sources, and applications of betalain pigments. *Mol. Plant* **11**, 7–22 (2018). doi:10.1016/j.molp.2017.10.008 Medline

43. J. P. Carreón-Hidalgo, D. C. Franco-Vásquez, D. R. Gómez-Linton, L. J. Pérez-Flores, Betalain plant sources, biosynthesis, extraction, stability enhancement methods, bioactivity, and applications. *Food Res. Int.* **151**, 110821 (2022). doi:10.1016/j.foodres.2021.110821 Medline

44. F. Gandía-Herrero, F. García-Carmona, Biosynthesis of betalains: Yellow and violet plant pigments. *Trends Plant Sci.* **18**, 334–343 (2013). doi:10.1016/j.tplants.2013.01.003 Medline

45. L. E. Contreras-Llano, M. A. Guerrero-Rubio, J. D. Lozada-Ramírez, F. García-Carmona, F. Gandía-Herrero, First betalain-producing bacteria break the exclusive presence of the pigments in the plant kingdom. *mBio* **10**, e00345-19 (2019). doi:10.1128/mBio.00345-19 Medline

46. L. Christinet, F. X. Burdet, M. Zaiko, U. Hinz, J. P. Zrÿd, Characterization and functional identification of a novel plant 4,5-extradiol dioxygenase involved in betalain pigment biosynthesis in *Portulaca grandiflora*. *Plant Physiol.* **134**, 265–274 (2004). doi:10.1104/pp.103.031914 Medline

47. W. P. Roos, A. D. Thomas, B. Kaina, DNA damage and the balance between survival and death in cancer biology. *Nat. Rev. Cancer* **16**, 20–33 (2016). doi:10.1038/nrc.2015.2 Medline

48. M. H. Barcellos-Hoff, C. Park, E. G. Wright, Radiation and the microenvironment – tumorigenesis and therapy. *Nat. Rev. Cancer* **5**, 867–875 (2005). doi:10.1038/nrc1735 Medline

49. K. I. Matsumoto, M. Ueno, Y. Shoji, I. Nakanishi, Heavy-ion beam-induced reactive oxygen species and redox reactions. *Free Radic. Res.* **55**, 450–460 (2021). doi:10.1080/10715762.2021.1899171 Medline

50. I. Sadowska-Bartosz, G. Bartosz, Biological properties and applications of betalains. *Molecules* **26**, 2520 (2021). doi:10.3390/molecules26092520 Medline

51. F. Gandía-Herrero, J. Escribano, F. García-Carmona, The role of phenolic hydroxy groups in the free radical scavenging activity of betalains. *J. Nat. Prod.* **72**, 1142–1146 (2009). doi:10.1021/np900131r Medline

52. J. Escribano, M. A. Pedreño, F. García-Carmona, R. Muñoz, Characterization of the antiradical activity of betalains from *Beta vulgaris* L. roots. *Phytochem. Anal.* **9**, 124–127 (1998). doi:10.1002/(SICI)1099-1565(199805/06)9:3<124:AID-PCA401>3.0.CO;2-0

53. C. Hesgrove, T. C. Boothby, The biology of tardigrade disordered proteins in extreme stress tolerance. *Cell Commun. Signal.* **18**, 178 (2020). doi:10.1186/s12964-020-00670-2 Medline

54. Y. Yoshida, S. Tanaka, Deciphering the biological enigma—genomic evolution underlying anhydrobiosis in the phylum tardigrada and the chironomid *Polypedilum vanderplanki*. *Insects* **13**, 557 (2022). doi:10.3390/insects13060557 Medline

55. J. D. Hibshman, S. Carra, B. Goldstein, Tardigrade small heat shock proteins can limit desiccation-induced protein aggregation. *Commun. Biol.* **6**, 121 (2023). doi:10.1038/s42003-023-04512-y Medline

56. C. Belott, B. Janis, M. A. Menze, Liquid-liquid phase separation promotes animal desiccation tolerance. *Proc. Natl. Acad. Sci. U.S.A.* **117**, 27676–27684 (2020). doi:10.1073/pnas.2014463117 Medline

57. K. Nguyen, S. Kc, T. Gonzalez, H. Tapia, T. C. Boothby, Trehalose and tardigrade CAHS proteins work synergistically to promote desiccation tolerance. *Commun. Biol.* **5**, 1046 (2022). doi:10.1038/s42003-022-04015-2 Medline

58. A. Malki, J.-M. Teulon, A. R. Camacho-Zarco, S. W. Chen, W. Adamski, D. Maurin, N. Salvi, J.-L. Pellequer, M. Blackledge, Intrinsically disordered tardigrade proteins self-assemble into fibrous gels in response to environmental stress. *Angew. Chem. Int. Ed.* **61**, e202109961 (2022). doi:10.1002/anie.202109961 Medline

59. A. Tanaka, T. Nakano, K. Watanabe, K. Masuda, G. Honda, S. Kamata, R. Yasui, H. Kozuka-Hata, C. Watanabe, T. Chinen, D. Kitagawa, S. Sawai, M. Oyama, M. Yanagisawa, T. Kunieda, Stress-dependent cell stiffening by tardigrade tolerance proteins that reversibly form a filamentous network and gel. *PLOS Biol.* **20**, e3001780 (2022). doi:10.1371/journal.pbio.3001780 Medline

60. M. Yagi-Utsumi, K. Aoki, H. Watanabe, C. Song, S. Nishimura, T. Satoh, S. Yanaka, C. Ganser, S. Tanaka, V. Schnapka, E. W. Goh, Y. Furutani, K. Murata, T. Uchihashi, K. Arakawa, K. Kato, Desiccation-induced fibrous condensation of CAHS protein from an anhydrobiotic tardigrade. *Sci. Rep.* **11**, 21328 (2021). doi:10.1038/s41598-021-00724-6 Medline

61. A. Thalhammer, G. Bryant, R. Sulpice, D. K. Hincha, Disordered cold regulated15 proteins protect chloroplast membranes during freezing through binding and folding, but do not

stabilize chloroplast enzymes in vivo. *Plant Physiol.* **166**, 190–201 (2014). doi:10.1104/pp.114.245399 Medline

62. Y. Gao, X. Li, P. Li, Y. Lin, A brief guideline for studies of phase-separated biomolecular condensates. *Nat. Chem. Biol.* **18**, 1307–1318 (2022). doi:10.1038/s41589-022-01204-2 Medline

63. L. Li, L. Shi, S. Yang, R. Yan, D. Zhang, J. Yang, L. He, W. Li, X. Yi, L. Sun, J. Liang, Z. Cheng, L. Shi, Y. Shang, W. Yu, SIRT7 is a histone desuccinylase that functionally links to chromatin compaction and genome stability. *Nat. Commun.* **7**, 12235 (2016). doi:10.1038/ncomms12235 Medline

64. H. H. Y. Chang, N. R. Pannunzio, N. Adachi, M. R. Lieber, Non-homologous DNA end joining and alternative pathways to double-strand break repair. *Nat. Rev. Mol. Cell Biol.* **18**, 495–506 (2017). doi:10.1038/nrm.2017.48 Medline

65. E. J. Wurtmann, S. L. Wolin, RNA under attack: Cellular handling of RNA damage. *Crit. Rev. Biochem. Mol. Biol.* **44**, 34–49 (2009). doi:10.1080/10409230802594043 Medline

66. N. Wagener, M. Ackermann, S. Funes, W. Neupert, A pathway of protein translocation in mitochondria mediated by the AAA-ATPase Bcs1. *Mol. Cell* **44**, 191–202 (2011). doi:10.1016/j.molcel.2011.07.036 Medline

67. D. A. Stroud, E. E. Surgenor, L. E. Formosa, B. Reljic, A. E. Frazier, M. G. Dibley, L. D. Osellame, T. Stait, T. H. Beilharz, D. R. Thorburn, A. Salim, M. T. Ryan, Accessory subunits are integral for assembly and function of human mitochondrial complex I. *Nature* **538**, 123–126 (2016). doi:10.1038/nature19754 Medline

68. L. Kater, N. Wagener, O. Berninghausen, T. Becker, W. Neupert, R. Beckmann, Structure of the Bcs1 AAA-ATPase suggests an airlock-like translocation mechanism for folded proteins. *Nat. Struct. Mol. Biol.* **27**, 142–149 (2020). doi:10.1038/s41594-019-0364-1 Medline

69. W. K. Tang, M. J. Borgnia, A. L. Hsu, L. Esser, T. Fox, N. de Val, D. Xia, Structures of AAA protein translocase Bcs1 suggest translocation mechanism of a folded protein. *Nat. Struct. Mol. Biol.* **27**, 202–209 (2020). doi:10.1038/s41594-020-0373-0 Medline

70. I. Vercellino, L. A. Sazanov, The assembly, regulation and function of the mitochondrial respiratory chain. *Nat. Rev. Mol. Cell Biol.* **23**, 141–161 (2022). doi:10.1038/s41580-021-00415-0 Medline

71. M. H. Broeks, N. W. F. Meijer, D. Westland, M. Bosma, J. Gerrits, H. M. German, J. Ciapaite, C. D. M. van Karnebeek, R. J. A. Wanders, F. J. T. Zwartkruis, N. M. Verhoeven-Duif, J. J. M. Jans, The malate-aspartate shuttle is important for de novo serine biosynthesis. *Cell Rep.* **42**, 113043 (2023). doi:10.1016/j.celrep.2023.113043 Medline

72. M. Kang, S. Park, S. H. Park, H. G. Lee, J. H. Park, A double-edged sword: The two faces of PARylation. *Int. J. Mol. Sci.* **23**, 9826 (2022). doi:10.3390/ijms23179826 Medline

73. B. Zhu, M.-M. Lou, G.-L. Xie, G.-Q. Zhang, X.-P. Zhou, B. Li, G.-L. Jin, Horizontal gene transfer in silkworm, *Bombyx mori*. *BMC Genomics* **12**, 248 (2011). doi:10.1186/1471-2164-12-248 Medline

74. B. F. Sun, J. H. Xiao, S. M. He, L. Liu, R. W. Murphy, D. W. Huang, Multiple ancient horizontal gene transfers and duplications in lepidopteran species. *Insect Mol. Biol.* **22**, 72–87 (2013). doi:10.1111/imb.12004 Medline

75. C. F. Wang, W. Sun, Z. Zhang, Functional characterization of the horizontally transferred 4,5-DOPA extradiol dioxygenase gene in the domestic silkworm, *Bombyx mori*. *Insect Mol. Biol.* **28**, 409–419 (2019). doi:10.1111/imb.12558 Medline

76. Y. Li, Z. Liu, C. Liu, Z. Shi, L. Pang, C. Chen, Y. Chen, R. Pan, W. Zhou, X. X. Chen, A. Rokas, J. Huang, X.-X. Shen, HGT is widespread in insects and contributes to male courtship in lepidopterans. *Cell* **185**, 2975–2987.e10 (2022). doi:10.1016/j.cell.2022.06.014 Medline

77. M. Mínguez-Toral, B. Cuevas-Zuviría, M. Garrido-Arandia, L. F. Pacios, A computational structural study on the DNA-protecting role of the tardigrade-unique Dsup protein. *Sci. Rep.* **10**, 13424 (2020). doi:10.1038/s41598-020-70431-1 Medline

78. W. A. da Silveira, H. Fazelinia, S. B. Rosenthal, E. C. Laiakis, M. S. Kim, C. Meydan, Y. Kidane, K. S. Rathi, S. M. Smith, B. Stear, Y. Ying, Y. Zhang, J. Foox, S. Zanello, B. Crucian, D. Wang, A. Nugent, H. A. Costa, S. R. Zwart, S. Schrepfer, R. A. L. Elworth, N. Sapoval, T. Treangen, M. MacKay, N. S. Gokhale, S. M. Horner, L. N. Singh, D. C. Wallace, J. S. Willey, J. C. Schisler, R. Meller, J. T. McDonald, K. M. Fisch, G. Hardiman, D. Taylor, C. E. Mason, S. V. Costes, A. Beheshti, Comprehensive multi-omics analysis reveals mitochondrial stress as a central biological hub for spaceflight impact. *Cell* **183**, 1185–1201.e20 (2020). doi:10.1016/j.cell.2020.11.002 Medline

79. P.-C. Fan, Y. Zhang, Y. Wang, W. Wei, Y.-X. Zhou, Y. Xie, X. Wang, Y.-Z. Qi, L. Chang, Z.-P. Jia, Z. Zhou, H. Guan, H. Zhang, P. Xu, P.-K. Zhou, Quantitative proteomics reveals mitochondrial respiratory chain as a dominant target for carbon ion radiation: Delayed reactive oxygen species generation caused DNA damage. *Free Radic. Biol. Med.* **130**, 436–445 (2019). doi:10.1016/j.freeradbiomed.2018.10.449 Medline

80. T. Yamamori, H. Yasui, M. Yamazumi, Y. Wada, Y. Nakamura, H. Nakamura, O. Inanami, Ionizing radiation induces mitochondrial reactive oxygen species production accompanied by upregulation of mitochondrial electron transport chain function and mitochondrial content under control of the cell cycle checkpoint. *Free Radic. Biol. Med.* **53**, 260–270 (2012). doi:10.1016/j.freeradbiomed.2012.04.033 Medline

81. D. Stec, R. Smolak, Ł. Kaczmarek, Ł. Michalczyk, An integrative description of *Macrobiotus paulinae* sp. nov. (Tardigrada: Eutardigrada: Macrobiotidae: *hufelandi* group) from Kenya. *Zootaxa* **4052**, 501–526 (2015). doi:10.11646/zootaxa.4052.5.1 Medline

82. J. Zhang, P. Kapli, P. Pavlidis, A. Stamatakis, A general species delimitation method with applications to phylogenetic placements. *Bioinformatics* **29**, 2869–2876 (2013). doi:10.1093/bioinformatics/btt499 Medline

83. Z. Yang, The BPP program for species tree estimation and species delimitation. *Curr. Zool.* **61**, 854–865 (2015). doi:10.1093/czoolo/61.5.854

84. A. Luo, C. Ling, S. Y. W. Ho, C. D. Zhu, Comparison of methods for molecular species delimitation across a range of speciation scenarios. *Syst. Biol.* **67**, 830–846 (2018). doi:10.1093/sysbio/syy011 Medline

85. N. Puillandre, S. Brouillet, G. Achaz, ASAP: Assemble species by automatic partitioning. *Mol. Ecol. Resour.* **21**, 609–620 (2021). doi:10.1111/1755-0998.13281 Medline

86. D. Stec, M. Vecchi, M. Dudziak, P. J. Bartels, S. Calhim, Ł. Michalczyk, Integrative taxonomy resolves species identities within the *Macrobiotus pallarii* complex (Eutardigrada: Macrobiotidae). *Zoological Lett.* **7**, 9 (2021). doi:10.1186/s40851-021-00176-w Medline

87. T. Chen, X. Chen, S. Zhang, J. Zhu, B. Tang, A. Wang, L. Dong, Z. Zhang, C. Yu, Y. Sun, L. Chi, H. Chen, S. Zhai, Y. Sun, L. Lan, X. Zhang, J. Xiao, Y. Bao, Y. Wang, Z. Zhang, W. Zhao, The Genome Sequence Archive Family: toward explosive data growth and diverse data types. *Genomics Proteomics Bioinformatics* **19**, 578–583 (2021). doi:10.1016/j.gpb.2021.08.001 Medline

88. CNCB-NGDC Members and Partners, Database resources of the National Genomics Data Center, China National Center for Bioinformation in 2023. *Nucleic Acids Res.* **51**, D18–D28 (2023). doi:10.1093/nar/gkac1073 Medline

89. M. Chen, Y. Ma, S. Wu, X. Zheng, H. Kang, J. Sang, X. Xu, L. Hao, Z. Li, Z. Gong, J. Xiao, Z. Zhang, W. Zhao, Y. Bao, Genome Warehouse: A public repository housing genome-scale data. *Genomics Proteomics Bioinformatics* **19**, 584–589 (2021). doi:10.1016/j.gpb.2021.04.001 Medline

90. J. Ma, T. Chen, S. Wu, C. Yang, M. Bai, K. Shu, K. Li, G. Zhang, Z. Jin, F. He, H. Hermjakob, Y. Zhu, iProX: An integrated proteome resource. *Nucleic Acids Res.* **47**, D1211–D1217 (2019). doi:10.1093/nar/gky869 Medline

91. T. Chen, J. Ma, Y. Liu, Z. Chen, N. Xiao, Y. Lu, Y. Fu, C. Yang, M. Li, S. Wu, X. Wang, D. Li, F. He, H. Hermjakob, Y. Zhu, iProX in 2021: Connecting proteomics data sharing with big data. *Nucleic Acids Res.* **50**, D1522–D1527 (2022). doi:10.1093/nar/gkab1081 Medline

92. D. D. Horikawa, T. Kunieda, W. Abe, M. Watanabe, Y. Nakahara, F. Yukuhiro, T. Sakashita, N. Hamada, S. Wada, T. Funayama, C. Katagiri, Y. Kobayashi, S. Higashi, T. Okuda, Establishment of a rearing system of the extremotolerant tardigrade *Ramazzottius varieornatus*: A new model animal for astrobiology. *Astrobiology* **8**, 549–556 (2008). doi:10.1089/ast.2007.0139 Medline

93. R. McNuff, Laboratory culture of *Hypsibius exemplaris*. *Cold Spring Harb. Protoc.* **2018**, pdb.prot102319 (2018). doi:10.1101/pdb.prot102319 Medline

94. B. Goldstein, The emergence of the tardigrade *Hypsibius exemplaris* as a model system. *Cold Spring Harb. Protoc.* **2018**, pdb.emo102301 (2018). doi:10.1101/pdb.emo102301 Medline

95. W. Morek, D. Stec, P. Gąsiorek, R. O. Schill, Ł. Kaczmarek, Ł. Michalczyk, An experimental test of eutardigrade preparation methods for light microscopy. *Zool. J. Linn. Soc.* **178**, 785–793 (2016). doi:10.1111/zoj.12457

96. Ł. Kaczmarek, Ł. Michalczyk, The *Macrobiotus hufelandi* group (Tardigrada) revisited. *Zootaxa* **4363**, 101–123 (2017). doi:10.11646/zootaxa.4363.1.4 Medline

97. K. G. Field, G. J. Olsen, D. J. Lane, S. J. Giovannoni, M. T. Ghiselin, E. C. Raff, N. R. Pace, R. A. Raff, Molecular phylogeny of the animal kingdom. *Science* **239**, 748–753 (1988). doi:10.1126/science.3277277 Medline

98. P. Gąsiorek, B. Blagden, W. Morek, Ł. Michalczyk, What is a 'strong' synapomorphy? Redescriptions of Murray's type species and descriptions of new taxa challenge the systematics of Hypsibiidae (Eutardigrada: Parachela). *Zool. J. Linn. Soc.* **202**, zlad151 (2023). doi:10.1093/zoolinnean/zlad151

99. P. Gąsiorek, D. Stec, W. Morek, K. Zawierucha, Ł. Kaczmarek, D. Lachowska-Cierlik, Ł. Michalczyk, An integrative revision of *Mesocrista* Pilato, 1987 (Tardigrada: Eutardigrada: Hypsibiidae). *J. Nat. Hist.* **50**, 2803–2828 (2016). doi:10.1080/00222933.2016.1234654

100. R. Bertolani, L. Rebecchi, I. Giovannini, M. Cesari, DNA barcoding and integrative taxonomy of *Macrobiotus hufelandi* CAS Schultze 1834, the first tardigrade species to be described, and some related species. *Zootaxa* **2997**, 19–36 (2011). doi:10.11646/zootaxa.2997.1.2

101. K. Tamura, G. Stecher, S. Kumar, MEGA11: Molecular Evolutionary Genetics Analysis Version 11. *Mol. Biol. Evol.* **38**, 3022–3027 (2021). doi:10.1093/molbev/msab120 Medline

102. K. Katoh, D. M. Standley, MAFFT multiple sequence alignment software version 7: Improvements in performance and usability. *Mol. Biol. Evol.* **30**, 772–780 (2013). doi:10.1093/molbev/mst010 Medline

103. K. Katoh, K. Misawa, K. Kuma, T. Miyata, MAFFT: A novel method for rapid multiple sequence alignment based on fast Fourier transform. *Nucleic Acids Res.* **30**, 3059–3066 (2002). doi:10.1093/nar/gkf436 Medline

104. S. Capella-Gutiérrez, J. M. Silla-Martínez, T. Gabaldón, trimAl: A tool for automated alignment trimming in large-scale phylogenetic analyses. *Bioinformatics* **25**, 1972–1973 (2009). doi:10.1093/bioinformatics/btp348 Medline

105. D. Zhang, F. Gao, I. Jakovlić, H. Zou, J. Zhang, W. X. Li, G. T. Wang, PhyloSuite: An integrated and scalable desktop platform for streamlined molecular sequence data management and evolutionary phylogenetics studies. *Mol. Ecol. Resour.* **20**, 348–355 (2020). doi:10.1111/1755-0998.13096 Medline

106. R. Lanfear, P. B. Frandsen, A. M. Wright, T. Senfeld, B. Calcott, PartitionFinder 2: New methods for selecting partitioned models of evolution for molecular and morphological phylogenetic analyses. *Mol. Biol. Evol.* **34**, 772–773 (2017). Medline

107. L. T. Nguyen, H. A. Schmidt, A. von Haeseler, B. Q. Minh, IQ-TREE: A fast and effective stochastic algorithm for estimating maximum-likelihood phylogenies. *Mol. Biol. Evol.* **32**, 268–274 (2015). doi:10.1093/molbev/msu300 Medline

108. S. Hengherr, F. Brümmer, R. Schill, Anhydrobiosis in tardigrades and its effects on longevity traits. *J. Zool.* **275**, 216–220 (2008). doi:10.1111/j.1469-7998.2008.00427.x

109. E. Beltrán-Pardo, K. I. Jönsson, M. Harms-Ringdahl, S. Haghdoost, A. Wojcik, Tolerance to gamma radiation in the tardigrade *Hypsibius dujardini* from embryo to adult correlate

inversely with cellular proliferation. *PLOS ONE* **10**, e0133658 (2015). doi:10.1371/journal.pone.0133658 Medline

110. F. A. Simão, R. M. Waterhouse, P. Ioannidis, E. V. Kriventseva, E. M. Zdobnov, BUSCO: Assessing genome assembly and annotation completeness with single-copy orthologs. *Bioinformatics* **31**, 3210–3212 (2015). doi:10.1093/bioinformatics/btv351 Medline

111. H. Li, Minimap2: Pairwise alignment for nucleotide sequences. *Bioinformatics* **34**, 3094–3100 (2018). doi:10.1093/bioinformatics/bty191 Medline

112. W. N. Gabriel, R. McNuff, S. K. Patel, T. R. Gregory, W. R. Jeck, C. D. Jones, B. Goldstein, The tardigrade *Hypsibius dujardini*, a new model for studying the evolution of development. *Dev. Biol.* **312**, 545–559 (2007). doi:10.1016/j.ydbio.2007.09.055 Medline

113. X. Wang, L. Wang, GMATA: An integrated software package for genome-scale SSR mining, marker development and viewing. *Front. Plant Sci.* **7**, 1350 (2016). doi:10.3389/fpls.2016.01350 Medline

114. G. Benson, Tandem repeats finder: A program to analyze DNA sequences. *Nucleic Acids Res.* **27**, 573–580 (1999). doi:10.1093/nar/27.2.573 Medline

115. J. A. Bedell, I. Korf, W. Gish, MaskerAid: A performance enhancement to RepeatMasker. *Bioinformatics* **16**, 1040–1041 (2000). doi:10.1093/bioinformatics/16.11.1040 Medline

116. J. Keilwagen, M. Wenk, J. L. Erickson, M. H. Schattat, J. Grau, F. Hartung, Using intron position conservation for homology-based gene prediction. *Nucleic Acids Res.* **44**, e89 (2016). doi:10.1093/nar/gkw092 Medline

117. T. D. Wu, C. K. Watanabe, GMAP: A genomic mapping and alignment program for mRNA and EST sequences. *Bioinformatics* **21**, 1859–1875 (2005). doi:10.1093/bioinformatics/bti310 Medline

118. B. J. Haas, S. L. Salzberg, W. Zhu, M. Pertea, J. E. Allen, J. Orvis, O. White, C. R. Buell, J. R. Wortman, Automated eukaryotic gene structure annotation using EVidenceModeler and the Program to Assemble Spliced Alignments. *Genome Biol.* **9**, R7 (2008). doi:10.1186/gb-2008-9-1-r7 Medline

119. S. Tang, A. Lomsadze, M. Borodovsky, Identification of protein coding regions in RNA transcripts. *Nucleic Acids Res.* **43**, e78 (2015). doi:10.1093/nar/gkv227 Medline

120. M. Stanke, M. Diekhans, R. Baertsch, D. Haussler, Using native and syntenically mapped cDNA alignments to improve de novo gene finding. *Bioinformatics* **24**, 637–644 (2008). doi:10.1093/bioinformatics/btn013 Medline

121. Y. Wang, H. Tang, J. D. Debarry, X. Tan, J. Li, X. Wang, T. H. Lee, H. Jin, B. Marler, H. Guo, J. C. Kissinger, A. H. Paterson, MCScanX: A toolkit for detection and evolutionary analysis of gene synteny and collinearity. *Nucleic Acids Res.* **40**, e49 (2012). doi:10.1093/nar/gkr1293 Medline

122. C. Boschetti, A. Carr, A. Crisp, I. Eyres, Y. Wang-Koh, E. Lubzens, T. G. Barraclough, G. Micklem, A. Tunnacliffe, Biochemical diversification through foreign gene expression in bdelloid rotifers. *PLOS Genet.* **8**, e1003035 (2012). doi:10.1371/journal.pgen.1003035 Medline

123. M. N. Price, P. S. Dehal, A. P. Arkin, FastTree: Computing large minimum evolution trees with profiles instead of a distance matrix. *Mol. Biol. Evol.* **26**, 1641–1650 (2009). doi:10.1093/molbev/msp077 Medline

124. E. Paradis, J. Claude, K. Strimmer, APE: Analyses of Phylogenetics and Evolution in R language. *Bioinformatics* **20**, 289–290 (2004). doi:10.1093/bioinformatics/btg412 Medline

125. K. P. Schliep, phangorn: Phylogenetic analysis in R. *Bioinformatics* **27**, 592–593 (2011). doi:10.1093/bioinformatics/btq706 Medline

126. H. Thorvaldsdóttir, J. T. Robinson, J. P. Mesirov, Integrative Genomics Viewer (IGV): High-performance genomics data visualization and exploration. *Brief. Bioinform.* **14**, 178–192 (2013). doi:10.1093/bib/bbs017 Medline

127. R. Patro, G. Duggal, M. I. Love, R. A. Irizarry, C. Kingsford, Salmon provides fast and bias-aware quantification of transcript expression. *Nat. Methods* **14**, 417–419 (2017). doi:10.1038/nmeth.4197 Medline

128. J. Cox, M. Mann, MaxQuant enables high peptide identification rates, individualized p.p.b.-range mass accuracies and proteome-wide protein quantification. *Nat. Biotechnol.* **26**, 1367–1372 (2008). doi:10.1038/nbt.1511 Medline

129. B. Buchfink, C. Xie, D. H. Huson, Fast and sensitive protein alignment using DIAMOND. *Nat. Methods* **12**, 59–60 (2015). doi:10.1038/nmeth.3176 Medline

130. T. Domazet-Lošo, J. Brajković, D. Tautz, A phylostratigraphy approach to uncover the genomic history of major adaptations in metazoan lineages. *Trends Genet.* **23**, 533–539 (2007). doi:10.1016/j.tig.2007.08.014 Medline

131. T. Domazet-Lošo, D. Tautz, A phylogenetically based transcriptome age index mirrors ontogenetic divergence patterns. *Nature* **468**, 815–818 (2010). doi:10.1038/nature09632 Medline

132. A. S. Trigos, R. B. Pearson, A. T. Papenfuss, D. L. Goode, Altered interactions between unicellular and multicellular genes drive hallmarks of transformation in a diverse range of solid tumors. *Proc. Natl. Acad. Sci. U.S.A.* **114**, 6406–6411 (2017). doi:10.1073/pnas.1617743114 Medline

133. C. Gao, C. Ma, H. Wang, H. Zhong, J. Zang, R. Zhong, F. He, D. Yang, Intrinsic disorder in protein domains contributes to both organism complexity and clade-specific functions. *Sci. Rep.* **11**, 2985 (2021). doi:10.1038/s41598-021-82656-9 Medline

134. J. Hanson, K. Paliwal, Y. Zhou, Accurate single-sequence prediction of protein intrinsic disorder by an ensemble of deep recurrent and convolutional architectures. *J. Chem. Inf. Model.* **58**, 2369–2376 (2018). doi:10.1021/acs.jcim.8b00636 Medline

135. J. Gsponer, M. E. Futschik, S. A. Teichmann, M. M. Babu, Tight regulation of unstructured proteins: From transcript synthesis to protein degradation. *Science* **322**, 1365–1368 (2008). doi:10.1126/science.1163581 Medline

136. E. M. Zdobnov, R. Apweiler, InterProScan—An integration platform for the signature-recognition methods in InterPro. *Bioinformatics* **17**, 847–848 (2001). doi:10.1093/bioinformatics/17.9.847 Medline

137. J. Huerta-Cepas, D. Szklarczyk, D. Heller, A. Hernández-Plaza, S. K. Forslund, H. Cook, D. R. Mende, I. Letunic, T. Rattei, L. J. Jensen, C. von Mering, P. Bork, eggNOG 5.0: A hierarchical, functionally and phylogenetically annotated orthology resource based on 5090 organisms and 2502 viruses. *Nucleic Acids Res.* **47**, D309–D314 (2019). doi:10.1093/nar/gky1085 Medline

138. S. Alberti, S. Saha, J. B. Woodruff, T. M. Franzmann, J. Wang, A. A. Hyman, A user's guide for phase separation assays with purified proteins. *J. Mol. Biol.* **430**, 4806–4820 (2018). doi:10.1016/j.jmb.2018.06.038 Medline

139. F. Gandía-Herrero, F. García-Carmona, Characterization of recombinant *Beta vulgaris* 4,5-DOPA-extradiol-dioxygenase active in the biosynthesis of betalains. *Planta* **236**, 91–100 (2012). doi:10.1007/s00425-012-1593-2 Medline

140. G. F. Trezzini, J.-P. Zrÿb, Characterization of some natural and semi-synthetic betaxanthins. *Phytochemistry* **30**, 1901–1903 (1991). doi:10.1016/0031-9422(91)85036-Y

141. M. A. Guerrero-Rubio, R. López-Llorca, P. Henarejos-Escudero, F. García-Carmona, F. Gandía-Herrero, Scaled-up biotechnological production of individual betalains in a microbial system. *Microb. Biotechnol.* **12**, 993–1002 (2019). doi:10.1111/1751-7915.13452 Medline

142. P. Martínez-Rodríguez, M. A. Guerrero-Rubio, S. Hernández-García, P. Henarejos-Escudero, F. García-Carmona, F. Gandía-Herrero, Characterization of betalain-loaded liposomes and its bioactive potential in vivo after ingestion. *Food Chem.* **407**, 135180 (2023). doi:10.1016/j.foodchem.2022.135180 Medline

143. G. Speit, A. Rothfuss, The comet assay: A sensitive genotoxicity test for the detection of DNA damage and repair. *Methods Mol. Biol.* **920**, 79–90 (2012). doi:10.1007/978-1-61779-998-3_6 Medline

144. M. Pachitariu, C. Stringer, Cellpose 2.0: How to train your own model. *Nat. Methods* **19**, 1634–1641 (2022). doi:10.1038/s41592-022-01663-4 Medline

145. K. S. Lee, Z. Landry, F. C. Pereira, M. Wagner, D. Berry, W. E. Huang, G. T. Taylor, J. Kneipp, J. Popp, M. Zhang, J.-X. Cheng, R. Stocker, Raman microspectroscopy for microbiology. *Nat. Rev. Methods Primers* **1**, 80 (2021). doi:10.1038/s43586-021-00075-6

146. P. Lasch, Spectral pre-processing for biomedical vibrational spectroscopy and microspectroscopic imaging. *Chemom. Intell. Lab. Syst.* **117**, 100–114 (2012). doi:10.1016/j.chemolab.2012.03.011

147. R. Wang, Y. Li, D. Li, W. Zhang, X. Wang, X. Wen, Z. Liu, Y. Feng, X. Zhang, Identification of the extracellular nuclease influencing soaking RNA interference efficiency in *Bursaphelenchus xylophilus*. *Int. J. Mol. Sci.* **23**, 12278 (2022). doi:10.3390/ijms232012278 Medline

148. M. Du, Z. J. Chen, DNA-induced liquid phase condensation of cGAS activates innate immune signaling. *Science* **361**, 704–709 (2018). doi:10.1126/science.aat1022 Medline

149. Q. Hu, D. Wu, M. Walker, P. Wang, R. Tian, W. Wang, Genetically encoded biosensors for evaluating NAD^+/NADH ratio in cytosolic and mitochondrial compartments. *Cell Rep. Methods* **1**, 100116 (2021). doi:10.1016/j.crmeth.2021.100116 Medline

150. Y. Zhao, A. Wang, Y. Zou, N. Su, J. Loscalzo, Y. Yang, *In vivo* monitoring of cellular energy metabolism using SoNar, a highly responsive sensor for NAD^+/NADH redox state. *Nat. Protoc.* **11**, 1345–1359 (2016). doi:10.1038/nprot.2016.074 Medline

151. R. Guo, S. Zong, M. Wu, J. Gu, M. Yang, Architecture of human mitochondrial respiratory megacomplex $I_2III_2IV_2$. *Cell* **170**, 1247–1257.e12 (2017). doi:10.1016/j.cell.2017.07.050 Medline

152. I. Wittig, H.-P. Braun, H. Schägger, Blue native PAGE. *Nat. Protoc.* **1**, 418–428 (2006). doi:10.1038/nprot.2006.62 Medline

153. W. Liu, R. Wu, J. Guo, C. Shen, J. Zhao, G. Mao, H. Mou, L. Zhang, G. Du, High turnover and rescue effect of XRCC1 in response to heavy charged particle radiation. *Biophys. J.* **121**, 1493–1501 (2022). doi:10.1016/j.bpj.2022.03.011 Medline

154. K. W. Caldecott, XRCC1 protein; Form and function. *DNA Repair* **81**, 102664 (2019). doi:10.1016/j.dnarep.2019.102664 Medline

155. C. J. Whitehouse, R. M. Taylor, A. Thistlethwaite, H. Zhang, F. Karimi-Busheri, D. D. Lasko, M. Weinfeld, K. W. Caldecott, XRCC1 stimulates human polynucleotide kinase activity at damaged DNA termini and accelerates DNA single-strand break repair. *Cell* **104**, 107–117 (2001). doi:10.1016/S0092-8674(01)00195-7 Medline

156. J. R. Walker, R. A. Corpina, J. Goldberg, Structure of the Ku heterodimer bound to DNA and its implications for double-strand break repair. *Nature* **412**, 607–614 (2001). doi:10.1038/35088000 Medline

157. J. Jumper, R. Evans, A. Pritzel, T. Green, M. Figurnov, O. Ronneberger, K. Tunyasuvunakool, R. Bates, A. Žídek, A. Potapenko, A. Bridgland, C. Meyer, S. A. A. Kohl, A. J. Ballard, A. Cowie, B. Romera-Paredes, S. Nikolov, R. Jain, J. Adler, T. Back, S. Petersen, D. Reiman, E. Clancy, M. Zielinski, M. Steinegger, M. Pacholska, T. Berghammer, S. Bodenstein, D. Silver, O. Vinyals, A. W. Senior, K. Kavukcuoglu, P. Kohli, D. Hassabis, Highly accurate protein structure prediction with AlphaFold. *Nature* **596**, 583–589 (2021). doi:10.1038/s41586-021-03819-2 Medline

158. L. A. Mueller, U. Hinz, J.-P. Zrÿd, Characterization of a tyrosinase from Amanita muscaria involved in betalain biosynthesis. *Phytochemistry* **42**, 1511–1515 (1996). doi:10.1016/0031-9422(96)00171-9

159. M. A. Guerrero-Rubio, F. García-Carmona, F. Gandía-Herrero, First description of betalains biosynthesis in an aquatic organism: Characterization of 4,5-DOPA-extradiol-dioxygenase activity in the cyanobacteria *Anabaena cylindrica*. *Microb. Biotechnol.* **13**, 1948–1959 (2020). doi:10.1111/1751-7915.13641 Medline

160. N. Speeckaert, N. M. Adamou, H. A. Hassane, F. Baldacci-Cresp, A. Mol, G. Goeminne, W. Boerjan, P. Duez, S. Hawkins, G. Neutelings, T. Hoffmann, W. Schwab, M. El Jaziri, M. Behr, M. Baucher, Characterization of the UDP-glycosyltransferase UGT72 family in poplar and identification of genes involved in the glycosylation of monolignols. *Int. J. Mol. Sci.* **21**, 5018 (2020). doi:10.3390/ijms21145018 Medline

161. C. Song, K. Härtl, K. McGraphery, T. Hoffmann, W. Schwab, Attractive but toxic: Emerging roles of glycosidically bound volatiles and glycosyltransferases involved in their formation. *Mol. Plant* **11**, 1225–1236 (2018). doi:10.1016/j.molp.2018.09.001 Medline

162. D. Stec, Ł. Krzywański, K. Arakawa, Ł. Michalczyk, A new redescription of *Richtersius coronifer*, supported by transcriptome, provides resources for describing concealed species diversity within the monotypic genus *Richtersius* (Eutardigrada). *Zoological Lett.* **6**, 2 (2020). doi:10.1186/s40851-020-0154-y Medline

163. W. Morek, A. C. Suzuki, R. O. Schill, D. Georgiev, M. Yankova, N. J. Marley, Ł. Michalczyk, Redescription of *Milnesium alpigenum* Ehrenberg, 1853 (Tardigrada: Apochela) and a description of *Milnesium inceptum* sp. nov., a tardigrade laboratory model. *Zootaxa* **4586**, 53–64 (2019). doi:10.11646/zootaxa.4586.1.2 Medline

164. J. Chao, Z. Li, Y. Sun, O. O. Aluko, X. Wu, Q. Wang, G. Liu, MG2C: A user-friendly online tool for drawing genetic maps. *Mol. Hortic.* **1**, 16 (2021). doi:10.1186/s43897-021-00020-x Medline

165. S. C. Daubner, T. Le, S. Wang, Tyrosine hydroxylase and regulation of dopamine synthesis. *Arch. Biochem. Biophys.* **508**, 1–12 (2011). doi:10.1016/j.abb.2010.12.017 Medline

166. Ł. Kaczmarek, I. Parnikoza, M. Gawlak, J. Esefeld, H.-U. Peter, I. Kozeretska, M. Roszkowska, Tardigrades from *Larus dominicanus* Lichtenstein, 1823 nests on the Argentine Islands (maritime Antarctic). *Polar Biol.* **41**, 283–301 (2018). doi:10.1007/s00300-017-2190-4

167. W. R. Miller, S. J. McInnes, D. M. Bergstrom, Tardigrades of the Australian Antarctic: *Hypsibius heardensis* (Eutardigrada: Hypsibiidae: dujardini group) a new species from sub-Antarctic Heard Island. *Zootaxa* **1022**, 57–64 (2005). doi:10.11646/zootaxa.1022.1.3

168. G. Pilato, M. G. Binda, A. Napolitano, E. Moncada, Remarks on some species of tardigrades from South America with the description of two new species. *J. Nat. Hist.* **38**, 1081–1086 (2002). doi:10.1080/00222930310000715 41

169. G. Pilato, M. G. Binda, O. Lisi, Three new species of eutardigrades from the Seychelles. *N. Z. J. Zool.* **33**, 39–48 (2006). doi:10.1080/03014223.2006.9518429

170. G. Pilato, Y. Kiosya, O. Lisi, G. Sabella, New records of Eutardigrada from Belarus with the description of three new species. *Zootaxa* **3179**, 39–60 (2012). doi:10.11646/zootaxa.3179.1.2

171. M. Levin, L. Anavy, A. G. Cole, E. Winter, N. Mostov, S. Khair, N. Senderovich, E. Kovalev, D. H. Silver, M. Feder, S. L. Fernandez-Valverde, N. Nakanishi, D. Simmons, O. Simakov, T. Larsson, S.-Y. Liu, A. Jerafi-Vider, K. Yaniv, J. F. Ryan, M. Q. Martindale, J. C. Rink, D. Arendt, S. M. Degnan, B. M. Degnan, T. Hashimshony, I. Yanai, The mid-developmental transition and the evolution of animal body plans. *Nature* **531**, 637–641 (2016). doi:10.1038/nature16994 Medline

172. M. A. Mapalo, K. Arakawa, C. M. Baker, D. K. Persson, D. Mirano-Bascos, G. Giribet, The unique antimicrobial recognition and signaling pathways in tardigrades with a comparison across Ecdysozoa. *G3* **10**, 1137–1148 (2020). doi:10.1534/g3.119.400734 Medline

173. A. Møbjerg, M. Kodama, J. Ramos-Madrigal, R. C. Neves, A. Jørgensen, M. Schiøtt, M. T. P. Gilbert, N. Møbjerg, Extreme freeze-tolerance in cryophilic tardigrades relies on controlled ice formation but does not involve significant change in transcription. *Comp. Biochem. Physiol. A Mol. Integr. Physiol.* **271**, 111245 (2022). doi:10.1016/j.cbpa.2022.111245 Medline

174. J. Borner, P. Rehm, R. O. Schill, I. Ebersberger, T. Burmester, A transcriptome approach to ecdysozoan phylogeny. *Mol. Phylogenet. Evol.* **80**, 79–87 (2014). doi:10.1016/j.ympev.2014.08.001 Medline

175. F. C. Stintzing, F. Kugler, R. Carle, J. Conrad, First ^{13}C-NMR assignments of betaxanthins. *Helv. Chim. Acta* **89**, 1008–1016 (2006). doi:10.1002/hlca.200690077

176. H. Sekiguchi, Y. Ozeki, N. Sasaki, In vitro synthesis of betaxanthins using recombinant DOPA 4,5-dioxygenase and evaluation of their radical-scavenging activities. *J. Agric. Food Chem.* **58**, 12504–12509 (2010). doi:10.1021/jf1030086 Medline